Studies on Quality Improvement of Treatment Plan and Quality Assurance of Linear Accelerator using high energy Bremsstrahlung X-rays

Thesis submitted to the University of Calicut
in partial fulfillment of the requirements
for the award of the degree of

Doctor of Philosophy

in

Physics

Niyas P

Department of Physics

Farook College

Kozhikode - 673632

Kerala

October 2018

CERTIFICATE

Certified that the work presented in this thesis entitled 'Studies on Quality Improvement of Treatment Plan and Quality Assurance of Linear Accelerator using high energy Bremsstrahlung X-rays' is a bonafide work done by Mr. Niyas P, under my guidance in the Department of Physics, Farook College and this work has not been included in any other thesis submitted previously for the award of any degree.

Farook College

October 2018

Dr. K. K. Abdullah

(Supervising Guide)

CERTIFICATE

This is to certify that the thesis titled 'Studies on Quality Improvement of Treatment Plan and Quality Assurance of Linear Accelerator using high energy Bremsstrahlung X-rays' has been checked for plagiarism, using the URKUND software, at the CHMK library, University of Calicut. Also, all the changes suggested by the thesis referees after evaluation are incorporated, and therefore, there are no further corrections to be made in this thesis.

Farook College   Dr. K. K. Abdullah

May 2019   (Supervising Guide)

DECLARATION

I hereby declare that the work presented in this thesis entitled 'Studies on Quality Improvement of Treatment Plan and Quality Assurance of Linear Accelerator using high energy Bremsstrahlung X-rays' is based on the original work done by me under the guidance of Dr. K. K. Abdullah, Department of Physics, Farook College and has not been included in any other thesis submitted previously for the award of any degree.

Farook College

October 2018   Niyas P

Acknowledgements

Foremost, I would like to express my sincere gratitude to my research guide Dr. K.K. Abdullah for the continuous support of my Ph.D study and related research, for his patience, motivation, immense knowledge and experience in the field. His guidance helped me in all the time of research and writing of this thesis. I could not have imagined having a better advisor and mentor for my Ph.D study. I thankfully remember the way he ignited and triggered my research work, which has culminated in this thesis. I recollect with overwhelming gratitude the consolation and affection he rendered me during moments of distress and tribulation in the course of my research.

I am also extremely indebted to Dr. P.A. Subha, Head of the Department of Physics, Farook college for providing me valuable suggestions in various stages of the work. She has supported me to overcome many difficulties during the time of research. I also express my deepest sense of appreciation to her for her deep involvement and continuous encouragement.

I express my special thanks to Prof. E.P. Imbichikoya and Dr. K.M. Naseer, the former and the present principals of Farook College, for their support and encouragement. I would also like to thank my colleagues and faculties in the Department of Physics, Farook College, for their keen interest and encouragement in my research work.

I am really thankful to Prof. T. Sankaran Nair, Chief Medical physicist and Dr. P.R. Sasindran, Head-Radiation Oncology division of Baby Memorial Hos-

Contents

List of papers published/under review

1. Quality Assurance of Linear Accelerator: A Comprehensive system using Electronic Portal Imaging Device. **P. Niyas***, K.K. Abdullah, M.P. Noufal, R. Vysakh. Journal of Radiotherapy in Practice, 2019, 18(2), 138-149

2. Comparison of treatment plans: a retrospective study by the method of radiobiological evaluation. **P. Niyas***, K.K. Abdullah, M.P. Noufal, N. singh, E.C. Jumanath, K.U. Jamshad. Polish Journal of Medical Physics and Engineering, 2016, 22(3): 61-68.

3. Effect of fluence smoothing on the quality of intensity-modulated radiation treatment plans. **P. Niyas***, K.K. Abdullah, M.P. Noufal, T.S. Nair. Radiological Physics and Technology, 2016, 9(2): 202-213.

4. A simple approach to study the performance of electron Monte Carlo algorithm in cancer treatment using medical Linear Accelerator. **P. Niyas***, K.K. Abdullah, M.P. Noufal. International Journal of Applied and Pure Science and Agriculture, 2015, 1(11): 55-64.

5. Validation of Dolphin dosimetry in three dimensional patient-specific Quality Assurance program. **P. Niyas***, K.K. Abdullah, M. Dinesh, K. Arun, CP Ranjith, R. vysakh. Reports of Practical Oncology and Radiotherapy (under review).

List of conference presentations

1. Impact of dose calculation algorithms in inhomogeneous medium. Annual conference of Medical physicists of India-2012, Manipal.

2. Study of performance of electron monte carlo algorithm in high energy electron beams from a medical linear accelerator. 19th National Symposium on Radiation Physics-2012, Chennai.

3. A comparative study of treatment plans by method of radiobiological response evaluation. Annual conference of Medical physicists of India-2013, Kolkata.

4. Effect of fluence smoothing on quality of cancer treatment by intensity modulated radiation therapy. 27th Kerala Science Congress-2015, Alappuzha.

5. Evaluation of structural shielding adequacy of a medical linear accelerator. 21st National Symposium on Radiation Physics-2017, Indore.

6. Imaging methods for treatment verification. International Oncology Conference-2018, Kozhikode.

Preface

X-rays are electromagnetic radiation which is capable of ionizing the matter. Radiation therapy uses high-energy ionizing radiation to kill or destroy tumour cells. The mostly used form of radiation in the treatment of cancer is photons and electrons of energies in the order of Million electron Volts. The primary tool for delivery of radiation therapy is a medical Linear Accelerator (LINAC) that uses high frequency electromagnetic waves to accelerate electrons into high energy through a linear tube. The high energy electron beam itself is used for treating superficial tumours or it can be made to collide a heavy metal target to produce high energy X- rays for treating deep seated tumours.

There are different delivery techniques available in radiation therapy. Among this, Intensity Modulated Radiation Therapy (IMRT) offers highly conformal dose shaping in three dimensions and saves normal tissues as much as possible. The state of the art techniques of modern radiation therapy are delivered by varying the intensity of radiation beam. These techniques are very effective, however, are complex and need high degree of accuracy. Quality Assurance (QA) program in radiation therapy consists of a set of procedures for ensuring the accurate administration of radiation dose to the patient with minimal exposure to others. QA is essential to minimize uncertainties in treatment planning and dose delivery and thereby to improve the results of radiation therapy.

In the present work, we have studied and formulated a few innovative methods for improving the quality of treatment planning and delivery. The thesis is divided into six chapters. Chapter-I briefly explains the production of X-rays, their applications in radiation therapy and associated radiation dosimetry. An

overview of the thesis highlighting the need for carrying out this work is also included in this chapter. A brief review of literature related to work is described in every chapter. We have taken keen interest to minimize the total beam-on time of an IMRT delivery without compromising the quality of treatment plans. Therefore the effect of smoothing function on quality of treatment plans has been investigated in different IMRT plans prepared in Eclipse (Varian Medical Systems, Palo Alto, CA) Treatment Planning System, which is detailed in chapter-II. Ranking of treatment plans based on radiobiological methods of plan evaluation is discussed in chapter-III. The radiobiological technique together with conventional evaluation methods provide higher confidence in IMRT plan evaluation. One of the practical concern of implementing QA in routine practice is the large time requirement of QA procedure. A quick and effective method for a comprehensive QA program in LINAC has been developed and described in chapter-IV.

The advancement of radiation therapy by use of highly conformal delivery techniques demands a novel method for patient-specic QA. In Chapter-V, the commissioning and clinical use of a three dimensional dosimetry system is extensively reported. This dosimetry system is capable of reconstructing 3D doses in pre-treatment verification of treatment plans. Electron beam is also used in radiation therapy, though not as frequent as photons. We have therefore introduced a quality improvement technique for checking the performance of dose calculation algorithm of electron beam, which is discussed in chapter-VI.

As a future perspective of the study, the method of fluence smoothing can also be employed in other commercially available Treatment Planning Systems. The protocols adopted in the present study for QA of photon beam can also be extended to electron beam.

Abbreviations

- AAA - Anisotropic Analytical Algorithm

- AAPM - American Association of Physicists in Medicine

- CT - Computed Tomography

- d_{max}- depth of maximum dose

- D_{max}- maximum dose

- dMLC - dynamic Multi-leaf Collimator

- DMPO - Direct Machine Parameter Optimization

- DTA - Distance To Agreement

- DVH- Dose Volume Histogram

- DVO - Dose Volume Optimizer

- eMC - electron Monte Carlo

- EPID- Electronic Portal Imaging Device

- EUD - Equivalent Uniform Dose

- FWHM - Field Width at Half Maximum

- HN - Head & Neck

- IEC - International Electrotechnical Commission

- IMB - Intensity Modulated Beam

- IMRT - Intensity Modulated Radiation Therapy

- KeV - Kilo electron Volt

- LINAC - Linear Accelerator

- LMC - Leaf Motion Calculator

- MC - Monte Carlo

- MeV - Million electron Volt

- MLC - Multi-leaf Collimator

- MU- Monitor Unit

- NTCP - Normal Tissue Complication Probability

- OAR - Organs At Risk

- O.F - Output Factor

- PDD - Percentage Depth Dose

- PTV - Planning Target Volume

- QA - Quality Assurance

- QUANTEC - Quantitative Analysis of Normal Tissue Effects in the Clinic

- RF - Radio Frequency

- RMSE - Root Mean Square Error

- RTOG - Radiation Therapy Oncology Group

- SAD - Source to Axis Distance

- SBRT - Stereotactic Body Radiotherapy

- SDD - Source to Detector Distance

- SRS - Stereotactic Radio Surgery

- SSD - Source to Surface Distance

- TCP- Tumour Control Probability

- TG - Task Group

- TPS - Treatment Planning System

- VMAT - Volumetric Modulated Arc Therapy

- XVMC - X-ray Voxel Monte Carlo

- 2D - Two Dimensional

- 3D - Three Dimensional

- 3DCRT - Three Dimensional Conformal Radiation Therapy

Chapter 1

Introduction and Thesis Outline

1.1 High energy X-rays and its applications

X-rays are a form of electromagnetic radiations having ability of penetration through matter. High energy X-rays are with varying energies from several hundreds of Kilo electron Volt (KeV) to a few Million electron Volt (MeV). Based on the origin of production, X-rays are classified as bremsstrahlung and characteristic X-rays. The process of bremsstrahlung is a result of inelastic scattering between high energy electron and high atomic number nucleus. The deceleration or deflection of electron from its path while passing near a nucleus by the action of coulomb forces of attraction between nucleus and electron, results in loss of energy. As an outcome, a spectrum of X-rays with a continuous emission of energies up to that of the incident electron is produced. The energy loss per atom depends on the square of the atomic number (Z^2) and hence the probability of bremsstrahlung varies with Z^2 of the target [1]. Characteristic X-rays are produced when an energetic electron interacts with a bound electron of an atom. The target electron is ejected from the inner orbits of the atom by leaving vacant energy level in the inner orbit of the atom. Outer-orbit electrons then fall into the inner orbit, emitting X-rays with an energy equivalent to the energy difference between the outer and inner orbits. Each orbit of any element has a
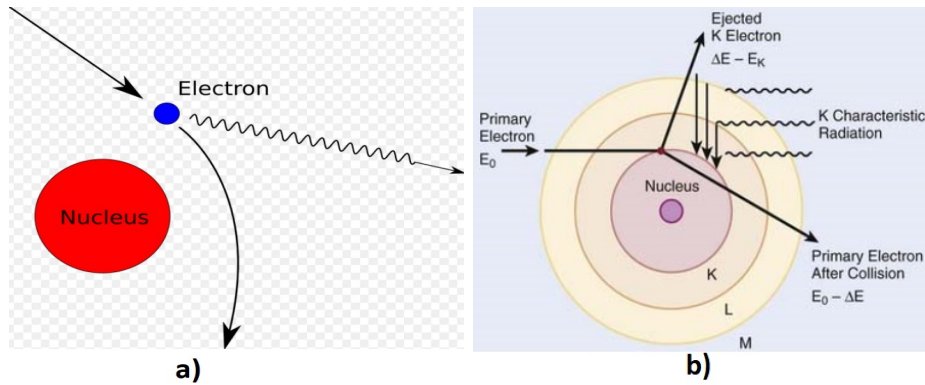
Figure 1.1: Schematic diagram of production of a) bremsstrahlung and b) characteristic X-rays.

unique set of energy levels, and thus the transition between any two pair of orbits results in the X-rays, which are characteristic to each element. The schematic diagram of production of bremsstrahlung and characteristic X-rays is depicted in Figure 1.1.

X-rays are used for a number of applications in industry, security, research and medicine. The non-destructive tests of industrial radiography is used to verify the interior structure and integrity of the object under study. X-rays are essential for the security checks of cargo, luggage and passengers. X-rays are also used in X-ray diffraction and other research studies in various disciplines of physics, chemistry, biology and pharmacy. The primary application of X-ray is in medicine, in which it is classified under diagnosis and therapy. X-ray imaging procedures are: 1) fast, non-invasive and painless methods for diagnosing diseases and 2) guiding medical personnel to insert catheters or stents into the body, remove blood clots or other blockages. A typical X-ray tube used for medical diagnosis is shown in Figure 1.2, which is an evacuated glass tube with two electrodes. Its therapeutic application is in cancer treatment to control or kill tumour cells using Mega Voltage (MV) X-rays.
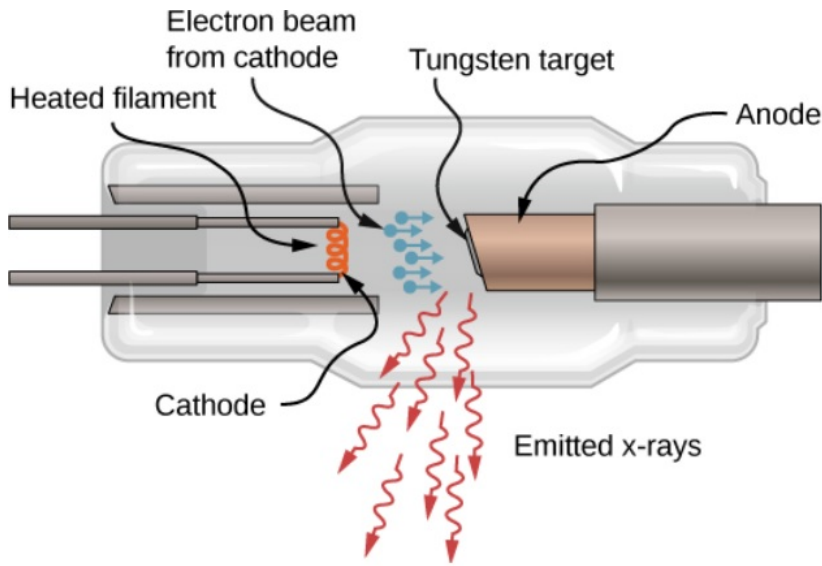
Figure 1.2: Diagram of a typical diagnostic X-ray tube and its components.

1.2 Radiation therapy and dosimetry

A mass of cells having uncontrolled cell growth and cell division is referred to as a tumour, and is sometimes cancerous when invasive to surrounding healthy normal tissues. Radiation therapy uses high-energy ionizing radiation to kill or destroy the growth and functioning of tumour cells. Ionizing radiation is capable of causing irreparable damage to DNA of cells and thus can be used to inhibit the function and multiplication of tumour cells. The mostly used form of ionizing radiation in the treatment of cancer is photons and electrons of energies in the order of MeV. The radiation therapy, typically, begins with a Computed Tomography (CT) scan of the patient in a fixed setup that can be reproduced at the time of treatment delivery. The three-dimensional (3D) anatomical information is then imported into a computerized Treatment Planning System (TPS) for treatment planning. The treatment plan is prepared by medical physicist with the help of dose calculation algorithms available in the TPS. TPS is capable of doing delineation of tumors and normal structures, iterative optimization, dose calculation, dose evaluation and treatment plan approval. Plan evaluation is usually performed by viewing dose values in transverse, sagittal and coronal

sections of patient CT scans and using the Dose Volume Histogram (DVH) data. DVH is a powerful tool incorporated with the TPS, which relates the amount of dose received and volume of the tissues. Figure 1.3 represents DVH of a treatment plan made by Eclipse (Varian Medical Systems, Palo Alto, CA, USA) TPS. Once a suitable plan has been approved by a physician, patients are positioned appropriately at the treatment unit and the planned radiation fields are delivered. In an earlier era of radiation therapy, the treatments were given with one or two beams, which resulted in a high dose to the normal tissue close to the tumor, as well as to the tumor. Later, Three Dimensional Conformal Radiation Therapy (3DCRT) was developed with several beams from different angles along with shielding to provide dose conformity with the aim of normal tissue sparing. However, better dose shaping in three dimensions has been achieved with the help of a technique called Intensity Modulated Radiation Therapy (IMRT). IMRT generally uses an inverse treatment planning with an optimization algorithm to reach the prescribed dose distribution to the Planning Target Volume (PTV) and a less dose to the surrounding Organs At Risk (OARs). A more recent technique, Volumetric-Modulated Arc Therapy (VMAT) yields dose distribution similar to IMRT and enables patient treatment in shorter time [2]. Stereotactic Body Radiotherapy (SBRT) and Stereotactic Radio Surgery (SRS) are the other two novel techniques used for delivering high dose in small number of fractions for extra and intra-cranial tumors. These techniques are very useful when the PTV and the OAR situate nearer or overlapping each other.

Radiation absorbed dose (or dose) is a measure of energy deposited by ionizing radiation per unit mass of the interacting medium. Its unit is Grey (Gy), represented as J/Kg, which means one Joule of energy is absorbed per one kilogram of matter. Radiation dosimetry deals with the measurement, calculation and evaluation of the radiation absorbed dose. The accuracy in the delivery of radiation therapy is very essential for achieving maximum tumor control. The overall uncertainty during radiation therapy is estimated as 5% [3]. It is important to ensure the accurate dosimetry by measuring and analysing the dosimetric
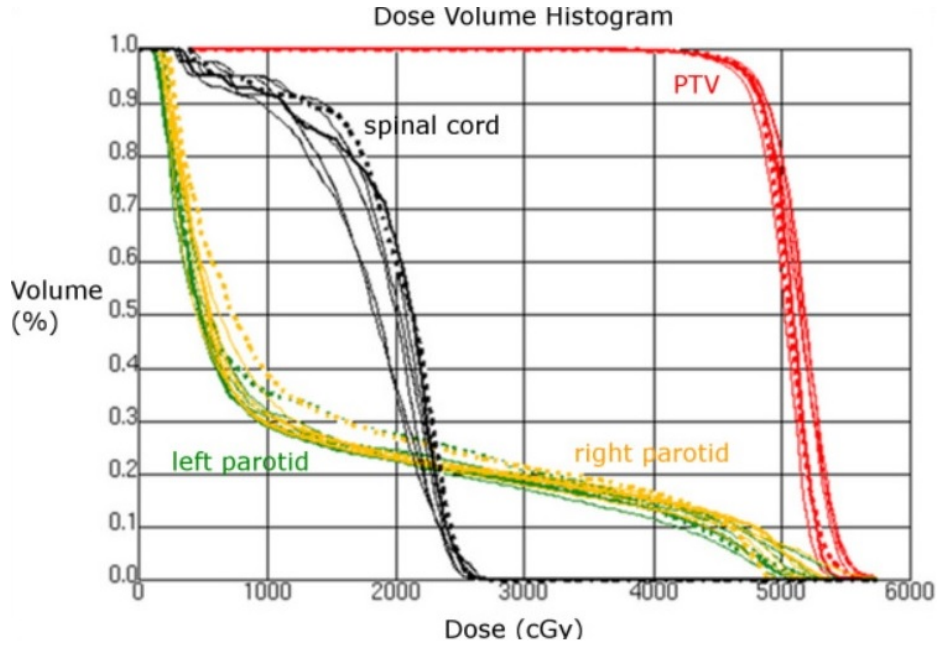
Figure 1.3: Dose volume histogram of an intensity modulated radiation treatment plan.

parameters of radiation field and planned dose of individual treatment. Water phantom is generally used as the medium of measurement as it is very common and analogous to human tissue in terms of interaction of radiation. Solid water phantoms are also available for dosimetry, which is very convenient for routine measurements [4]. Radiation dosimeters are the devices used for measurement and evaluation of dose. Different types of dosimeters are available commercially; in which, ionization chambers, diode detector, two dimensional (2D) array detectors and Electronic Portal Imaging Device (EPID) are used in this study. Small volume ionization chambers manufactured by IBA dosimetry system, a farmer type chamber of 0.65 cm^3 volume (FC65) and thimble chamber of 0.13 cm^3 volume (CC13), are the dosimeters used for point dose measurements. For small field measurements, silicon diode detector (Razor detector) from IBA is used. MatriXX 2D and Dolphin are the two array detectors used for planar dose measurements. MatriXX 2D array consists of 1020 air-vented ionization chambers (volume of each chamber is 0.08 cm^3) and Dolphin is made up of 1513 air-vented ionization chambers with individual chamber volume of 0.016 cm^3. Portal Vi-

5

sion aS1000 is a flat panel EPID consisting of amorphous silicon diode. It has an active imaging area of 40 x 30 cm^2. Diagrams of these radiation dosimeters are shown in Figure 1.4.
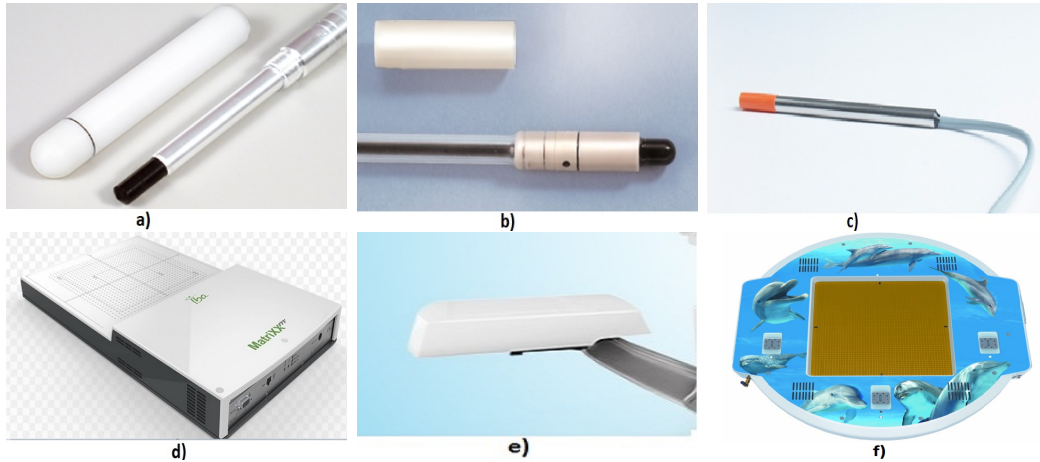
Figure 1.4: Diagrams of dosimeters used in the study. a) FC65 ionization chamber, b) CC13 ionization chamber, c) Razor diode, d) MatriXX 2D array detector, e) EPID and f) Dolphin detector.

1.3   Medical Linear Accelerator

The primary tool for delivery of radiation therapy is a medical Linear Accelerator (LINAC) that rotates on a gantry around the patient, emitting uniform or modulated beams of X-rays. LINAC uses high frequency electromagnetic waves to accelerate electron to high energy through a linear tube, accelerating wave guide. The high energy electron beam itself is used for treating superficial tumours or it can be made to collide a heavy metal target to produce high energy X- rays for treating deep seated tumours. Different types of LINACs are available from various vendors. Clinac-iX (Varian Medical Systems, Palo Alto, CA, USA) and Versa-HD (Elekta, Stockholm, Sweeden) are the two LINACs, which are shown in Figure 1.5 were used in our study. A typical LINAC consists of the four major components, they are: 1) modulator cabinet, 2) drive stand, 3) gantry and 4) patient couch. Figure 1.6 represents the schematic diagram of LINAC with its main components.

Figure 1.5: Photographs of a) Clinac-iX and b) Versa-HD medical Linear Accelerators.

1.3.1 Modulator cabinet

This is located inside the treatment room. It has a fan control, auxiliary power distribution and primary power distribution system. The modulator converts the incoming alternating current into pulses of flat topped direct current and these are fed to the electron gun and to the microwave power source.

1.3.2 Drive stand

Drive stand provides assistance for driving the gantry. There are four major components in the stand; Radio Frequency (RF) power source, RF power transmission waveguide, circulator and water cooling system.

The high frequency electromagnetic radiation used to accelerate electrons in the accelerating waveguide is produced by RF power source. There are two types, 1) Magnetron and 2) Klystron. The former is preferred for lower energies and the latter is used in the acceleration of higher energy electron beams. The magnetron is in cylindrical shape with central cathode and outer anode (Figure 1.7). The resonant cavities are made up of solid piece of copper and the space between the cathode and anode is evacuated. A magnetic field is applied perpendicular to the cross sectional plane of the cavities and a pulsed DC electric field is applied between anode and cathode. The electrons emitted from the cathode are accelerated towards the anode by the action of electric field. As the electrons pass the cavity, they induce a resonant RF field in the cavity, which can then be extracted out. Klystron is a RF power amplifier, which amplifies the low power RF waves generated by an RF driver. A schematic diagram of Klystron is shown in Figure 1.8. The low power RF signal excites the input (buncher) cavity, set up an alternating electric field across the cavity and electrons produced by the cathode are accelerated or decelerated by the buncher cavity. This results in bunching of electrons, which generates a retarding electric field and the kinetic energy of electrons converted in to high power RF wave in output cavity.

RF power transmission waveguide transmits the RF power from magnetron

8
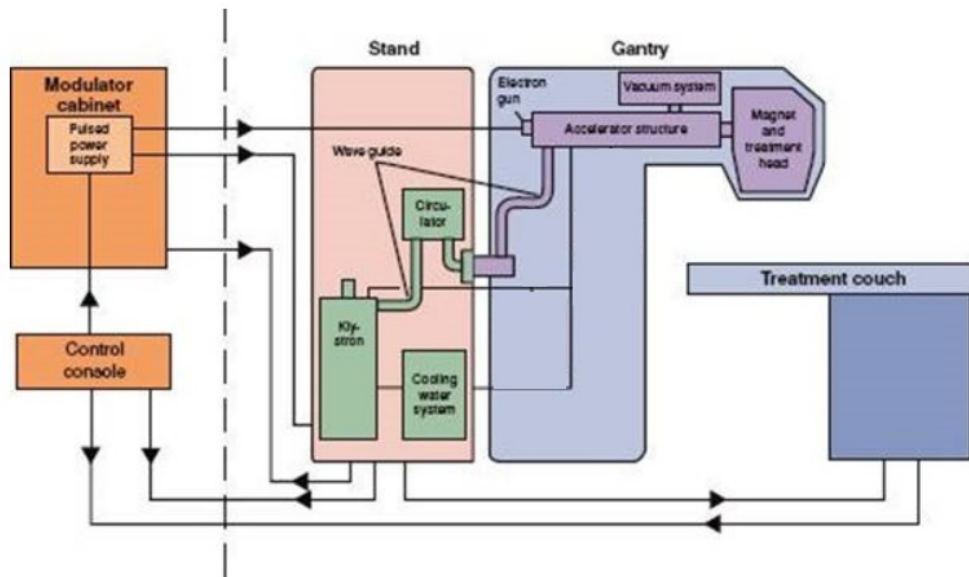
Figure 1.6: Schematic diagram of LINAC with its main components.

or klystron to the accelerating wave guide. Circulator connects RF power source to RF wave guide. Water cooling system provides thermal stability for many components in drive stand and in gantry.

1.3.3 Gantry

Gantry directs the X-ray and electron beams to the patient by rotating 360 degrees around the patient and enables the treatment. Electron gun, accelerating waveguide and treatment head are the major components of gantry.

Electron gun

The electron gun produces electron by thermionic emission of heated cathode. These electrons are accelerated towards the perforated anode, coupled with RF wave from transmission wave guide and entered into the accelerating wave guide.

Accelerating waveguide

It is an evacuated metallic circular structure for accelerating electrons with the help of micro wave power. The cavities of the waveguide provide a suitable
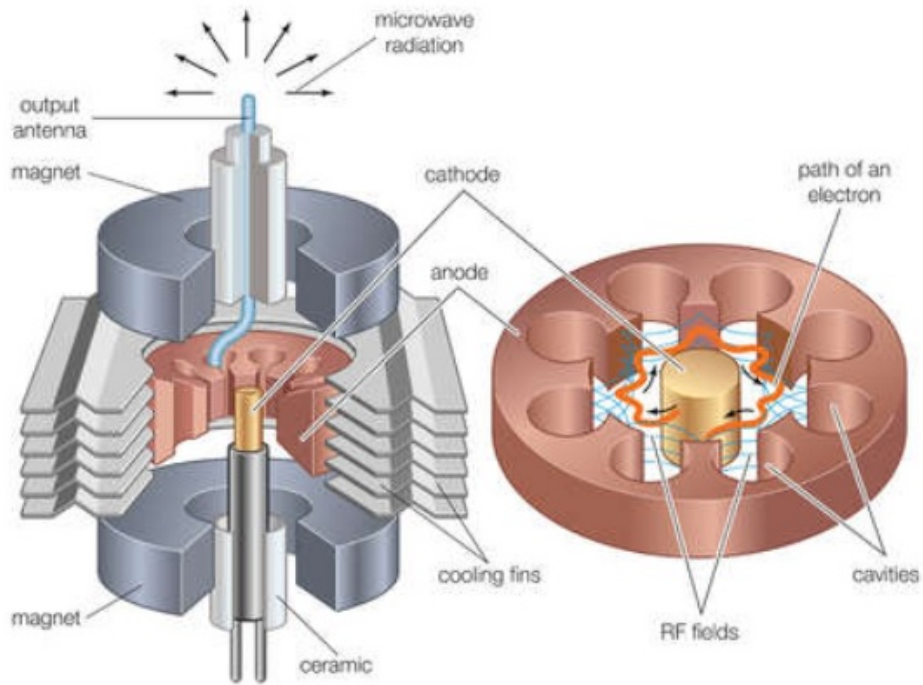
Figure 1.7: Schematic diagram of magnetron.
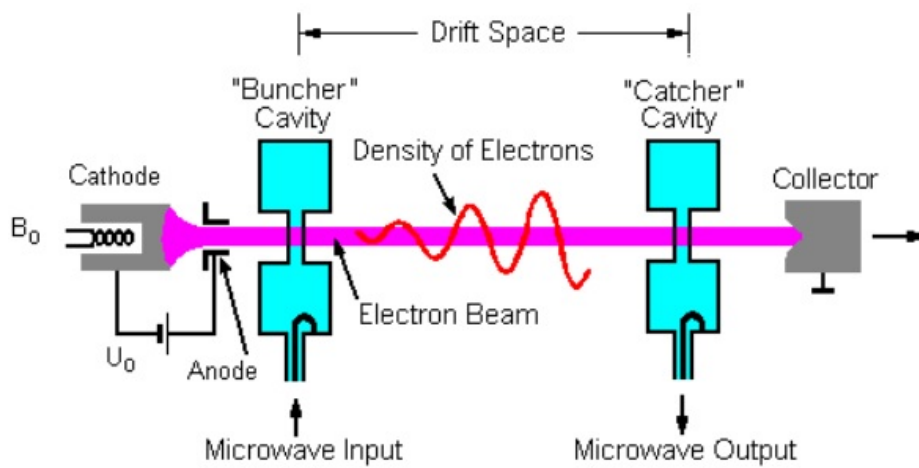
Figure 1.8: Schematic diagram of klystron.
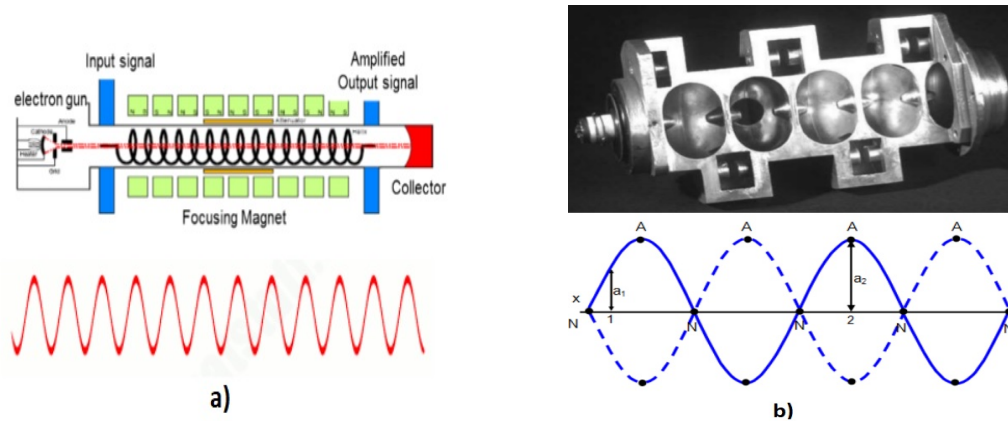
Figure 1.9: a) Travelling waveguide and wave pattern and b) Standing waveguide and wave pattern.

electric field pattern for the electron acceleration and also help to couple and distribute the microwave power between the adjacent cavities. It is mounted in the gantry horizontally or vertically. Two types, 1) travelling and 2) standing wave guides have been developed, which is illustrated in Figure 1.9. In the travelling waveguide, microwaves enter on the gun side and propagate towards the other end of the waveguide. Microwaves are absorbed at the distal surface and thus forms a travelling wave pattern. However, in the standing structure, each end of the waveguide is terminated with a conducting disc to reflect the microwave power and hence results in formation of standing waves in the waveguide. In this configuration, every second cavity carries no electric field, acts as coupling cavities and can be effectively shorten the accelerating waveguide by 50%. There are two additional structures, steering coils and focussing coils. Two quadra pole magnets placed in the steering coils control the path of the electron beam and focusing coil helps to focus the electron into thin beam when it hits the target. At the exit of the accelerating waveguide, the electron beam passes through a bending magnet system and are directed towards the treatment head.

Treatment head

The components of treatment head is shown in Figure 1.10, which consists of an X-ray target, beam flattening filter, scattering foils, monitor chambers and col-

limators. Treatment head is shielded with high density shielding material such as lead and tungsten against radiation leakage. The high energy electrons, in the form of a narrow pencil beam, exiting from the end window of the accelerator falls on the Tungsten target placed in the path of the beam, generates a forward peaking shaped X-rays. There is a fixed primary collimator made up of high atomic number elements to minimise the leakage and absorb the scattered X-rays. It collimates the X-ray beam and defines the maximum size of the beam. The forward peaking X-ray beam is allowed to pass through a flattening filter placed after the primary collimator to obtain a flattened, symmetrical and uniform beam. The flattening filter is a conical shaped metal absorber made up of tungsten, steel, lead and aluminium. If the LINAC is operated in electron mode, the narrow pencil beam of electron hits on thin scattering foil instead of striking the target. Different scattering foils are fabricated with aluminium or copper for each electron energy. The scattering foils are so thin that most of the electrons are scattered instead of undergoing bremsstrahlung process.

The radiations coming out of the flattening filter or scattering foil are passed through dual monitor ionization chamber. It monitors dose, dose rate and symmetry of the delivered radiation beam. The radiation output of the LINAC is represented in terms of Monitor Unit (MU) and the LINAC is calibrated to deliver 1.0 cGy/MU. Monitor chambers read 1 MU, when an absorbed dose of 1 cGy is delivered to a point at depth of maximum dose (d_{max}) and field size of 10 x 10 cm^2 in a water phantom, when the phantom surface is positioned at 100 cm from the target. After passing through the ion chambers, the radiation beam is further collimated by a secondary collimator system. It consists of upper and lower collimator jaws, made up of lead or tungsten. The jaws define rectangular or square shaped X-ray beams, typically from 2 x 2 cm^2 to 40 x 40 cm^2 at iso-centre. Another type of collimator system, Multi-leaf Collimator (MLC), is attached in the LINAC head, which can generate irregular shaped fields also.
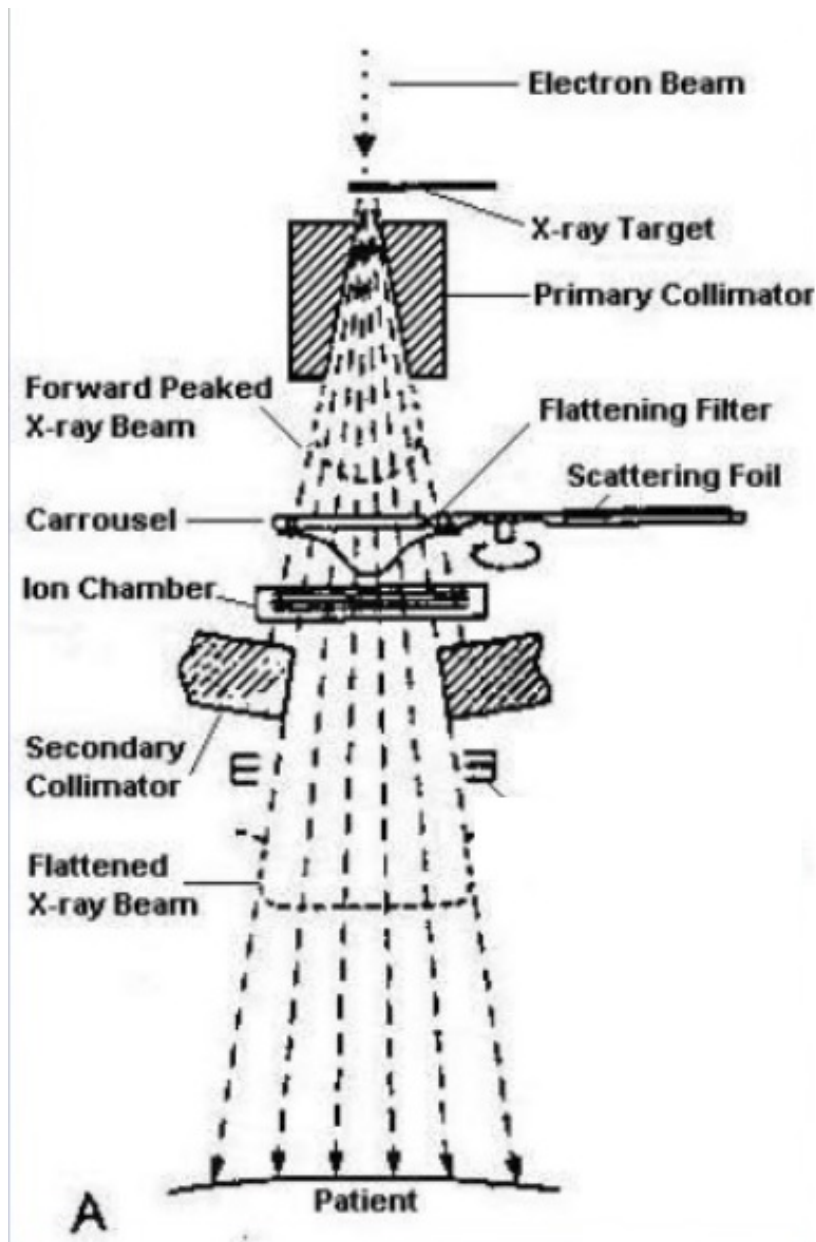
Figure 1.10: Components of treatment head.
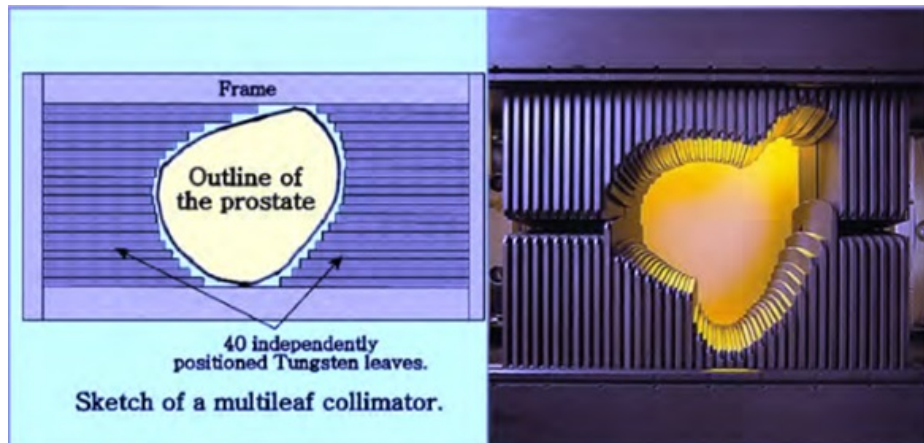
Figure 1.11: Diagram of Multi-leaf Collimator.

Multi-leaf Collimator

MLC is a field shaping device, consisting of large number of leaves made up of heavy metal alloy. Its computer-controlled leaves act as a filter, move independently and transmit radiation in the form of small beamlets in order to conform the radiation field to the shape of the tumor as depicted in Figure 1.11. The primary role of MLC is to create any irregular shaped fields for sparing the normal structures near to the treatment volume. It has massive role in the intensity modulation of X-rays in IMRT and VMAT. MLC is attached in the treatment head by either replacing the upper or lower jaws of secondary collimator or adding as a tertiary collimator. The width, speed, radiation attenuation and maximum travelling distance are the different key parameters of the leaves, which vary with the different vendors. The LINACs in our study were equipped with 120 leaf millennium MLC (Varian Medical Systems, Palo Alto, CA, USA) & 160 leaf Agility MLC (Elekta, Stockholm, Sweeden). Width of the leaf is specified at iso-centre of the LINAC. Iso-centre is a point in space at 100 cm from target through which the central axis of radiation beam passes. It is the intersection point of axes of rotation of gantry, collimator and couch.

1.3.4   Treatment couch

Treatment couch or table is the place where the patient lies down for the treatment. It has the freedom for movement in longitudinal, lateral, vertical and rotational about an axis passing through the iso-centre. Robotic couches with more rotational degree of freedom are also available now.

1.4   Quality Assurance

Quality Assurance (QA) in radiotherapy includes all procedures that ensure the accurate administration of radiation dose to the target volume, together with least dose to normal tissue and minimal exposure to others. QA minimizes uncertainties in treatment planning and dose delivery and thereby improves the results of radiation therapy. The state of the art facilities of modern radiation therapy machine cannot be fully utilized unless a high degree of accuracy is obtained through effective QA programs. In addition to this, QA allows inter-comparison of planning, machine and treatment data among different radiation therapy centres for ensuring more accurate dosimetry. There are various recommendations for general QA tests pertaining to the LINAC and TPS [5-8]. Pre-treatment QA is also recommended for advanced treatment techniques, such as IMRT and VMAT. [9-10]. Unlike the conventional techniques, the Intensity Modulated Radiation Treatment is delivered by varying the intensity of radiation beam with in the treatment field. Intensity modulation is accomplished with the help of MLC or gantry movement. A user can define the number of radiation beam, direction of the beam and dose-volume constraints for treatment planning. Inverse optimization algorithm of TPS executes planning on the above input parameters. A large radiation beam is divided into many small beamlets and TPS adjusts the weights of beamlets to obtain varying intensity according to the planning dose objective. This optimized intensity patterns are converted into a deliverable fluence with different MLC shapes. Thus, any intensity profile shape can be obtained by leaf movement. Because of the higher complexity in

planning and radiation delivery, more rigorous QA for the machine and treatment plan is required. Machine QA involves the checking of radiation beam constancy, beam energy, reproducibility and leakage of MLC, mechanical movement accuracy of various components of LINAC and positional accuracy of iso-centre. QA of treatment plan is to ensure the quality of treatment plan and to confirm that the right treatment plan is delivered to the patient. QA is performed in different periodicity such as daily, weekly, monthly and annually. Medical physicists are responsible for customizing, designing and conducting the QA checks.

1.5 Thesis Outline

Radiation therapy has been a powerful tool for treatment of cancer for more than hundred years. Tremendous advancement in treatment planning and delivery have enabled radiation therapy more effective and precise. The treatment plans and LINAC are to be constantly reviewed and ensured their quality to assure that the intended treatment is being delivered. Medical physicists develop and review the treatment plans and also are responsible for performing QA of treatment delivery. Various publications are available in literatures to guide the physicist for improving the quality of radiation treatment [5-9]. Report of American Association of Physicists in Medicine (AAPM) radiation therapy committee Task Group 40 (TG-40) discusses a comprehensive QA for radiation therapy [5]. Meticulous planning and careful implementation of the treatment are highly essential for achieving good results in radiation therapy. In the present work, we have studied and formulated a few innovative methods for improving the quality of treatment planning and delivery. We have taken keen interest to minimize the total beam-on time of an IMRT delivery without compromising the quality of treatment. We have also studied the ranking of treatment plans based on radiobiological methods of plan evaluation. One of the practical concerns of implementing QA in routine practice is the large time requirement of QA procedure. In the present study, we have developed a quick and effective method

for a comprehensive QA program in LINAC. Evaluation of pre-treatment verification of plans by using a 3D dosimetry system attracts great significance for modern treatments using complex techniques. The study including the commissioning and clinical use of a recently developed 3D dosimetry will be helpful for a full-fledged patient-specific QA. The quality improvement method is also extended to the electron beam radiation therapy by checking the performance of dose calculation algorithm.

The thesis is divided into six chapters. Chapter-I briefly explains the production of X-rays, their applications in radiation therapy and associated radiation dosimetry. An overview of the thesis highlighting the need for carrying out this work is also included in this chapter. A brief review of literature related to work is described in every chapter. In chapter-II, the effect of smoothing function on quality of treatment plans has been investigated in different IMRT plans prepared in Eclipse TPS. In spite of all the methods to deliver maximum dose to tumor and minimum dose to normal tissues, there is a concern of low intensity leakage radiation falling on tissues distant to treatment area. The leakage radiation has influence on secondary cancer induction risk, which was evaluated and reported by some authors [11-13]. The probability of leakage radiation is more in treatments using intensity modulated X-ray beams. Highly conformal intensity modulated beams are planned in TPS by generating complex fluence maps. Increased complexity of fluence will result in large number of MUs per radiation beam and hence, in more leakage radiation. A method for smoothing of fluence maps used for reducing the complexity of plans. Modern treatment planning systems include an interface for adjusting the level of smoothing. It is the common practice to use the default smoothing level recommended by vendor, which gives a moderate level of smoothing without losing the plan quality. We have developed a new fluence smoothing values by studying the effect of different smoothing levels on quality of treatment plans in detail. The Smoothing levels are varied and the change in MUs, plan quality and deliverability were investigated. Plan quality was assessed in terms of DVH data and radiobiological

indices. The 2D fluence of 180 treatment plans was measured using MatriXX 2D ionization array detector and compared with the TPS fluence.

Chapter-III describes radiobiological methods for treatment plan comparison. Selection of good treatment plan is as important as the generation of plans and most often, it is required to compare multiple treatment plans for selection of an optimal plan. Conventional methods of plan evaluation are viewing the 2D dose distribution on CT images and analysing DVHs of tumor and other organs of interest. There is an additional plan evaluation tool using radiobiological parameters such as Equivalent Uniform Dose (EUD), Tumor Control Probability (TCP) and Normal Tissue Complication Probability (NTCP) [14]. The radiobiological plan comparison technique together with conventional evaluation methods provide higher confidence to the physician, especially, for IMRT as it has more complex and heterogeneous dose distribution [15]. However, treatment plan analysis by using all the above methods needs extra time for plan evaluation, hence the visual inspection of dose distribution and comparison of DVH indices are usually carried out in clinical practice. In this chapter, we aimed to study the radiobiological method of plan evaluation by using Niemierko's phenomenological model [16]. DVH data of 30 patients representing typical cases of head and neck, prostate and brain tumors were obtained. Four sets of IMRT plans for each patient were retrospectively studied. The EUD, TCP and NTCP were estimated from the DVH data using a MATLAB program and correlated with physical dose indices for target coverage and dose to OARs. The ranking and selection of the most suitable treatment plan with the help of stated radiobiological quantities and DVH analysis was discussed in detail.

Chapter-IV discusses a comprehensive system for QA of LINAC by using EPID. Initially, EPID was designed for patient treatment setup verification, however, its use as a dosimeter in 2D fluence verification is very significant [17-18]. The extensive QA protocol in radiation therapy demands more human resource and time for QA. This can be resolved by using a fast radiation detector having minimum setup time, simple readout system and good accuracy. EPID, being

a versatile dosimeter, possess good resolution and requires easy setup procedure and less time. However, the usage of EPID is not well established because of the requirement of software solution for interpreting the EPID output. Many institutions do not have the commercially available EPID dosimetry software. We have developed a software solution using MATLAB program (The MathWorks, Inc., Natick, MA, USA) to utilize the full potential of EPID in dosimetry. The flatness, symmetry and radiation beam output are the major beam characteristics, they are to be monitored periodically to ensure the correct delivery of radiation beam [5]. Three years of daily QA data were measured, analysed and correlated with the data from an independent ionization chamber detector. We have also checked the feasibility of EPID for doing QA of MLC. Customized MLC patterns were created with the help of MLC shaper software, irradiated in LINAC and MLC QA was performed with the help of EPID and indigenously developed software. It is recommended to perform verification of treatment plans in phantom before it deliver to patient. EPID is a powerful tool for patient-specific QA and the institutional data of 350 IMRT plans were used for the study. MATLAB program based image comparison tool is developed and aimed to use for patient specific QA.

Currently available dosimetry system for patient-specific QA are film dosimeter, 2D array detectors and EPID. All these detectors have been proven beneficial in 2D fluence comparison in terms of gamma index. However, the advancement of radiation therapy by the use of highly conformal delivery techniques such as IMRT, VMAT and SBRT demands a novel method for patient-specific QA. Chapter-V explains the commissioning and clinical use of a three dimensional dosimetry system for verification of 3D dose of the target and OARs. Dolphin-Compass system is a recently available dosimetry solution from IBA dosimetry, which is capable of reconstructing 3D doses in phantom or CT images of patient. The system consists of Dolphin 2D array detector and Compass software solution. Dolphin detector is made up of 1513 air-vented ionization chambers and can be mounted on the treatment head of LINAC. Hence the detector system

offers increased spatial resolution and improved set-up efficiency. The Compass software is based on collapsed-cone convolution/superposition dose computation algorithm [19], which requires modelling of LINAC head similar to any other TPS. Compass computes the 3D dose by using the modelled data of photon beam from LINAC and patient treatment data from TPS. Also, it performs a measurement based 3D dose reconstruction in patient volume. We have commissioned the Dolphin-Compass dosimetry by measuring the required radiation beam data. The whole process of commissioning and validation of the dosimetry for patient-specific QA is described in this chapter. The accuracy of beam modelling is tested with the help of various fields, MLC patterns and complex treatment plans. This study is extended to 30 treatment plans, generated with complex treatment techniques of IMRT, VMAT and SBRT for evaluating the efficiency of the system for 3D patient-specific QA.

Electron beam is also used in radiation therapy, though not as frequent as photons. We have therefore introduced a quality improvement technique for checking the performance of dose calculation algorithm of electron beam which is detailed in chapter-VI. The electron beam coming out of accelerator head is collimated to the treatment area by electron applicators. There are five types of applicators available in the LINAC. Applicators are capable of providing treatment fields of 6 x 6 cm^2, 10 x 10 cm^2, 15 x 15 cm^2, 20 x 20 cm^2 and 25 x 25 cm^2 at the iso-centre. The output of all electron beam is measured using ionization chamber in each applicator and normalized with the standard 10 x 10 cm^2 applicator, known as ouput factor. In addition to the applicator, customized electron beam cutouts were also used for shaping the irregular treatment fields. Radiation output of electron beam with different cutouts were also measured and the output factors (O.F) of the cutouts were determined. Dose calculation of electron beam is performed by electron Monte Carlo (eMC) algorithm available in the TPS. The accuracy of eMC is checked and verified by several group of people [20-22]. We aimed to test the performance of eMC by using measured O.F of electron applicators and cutouts. A measurement based simple and easy

method was developed to validate the electron dose calculation algorithm.

The investigated method of fluence smoothing yielded a significant reduction in the total MU. No appreciable differences in doses to the target and most of the OARs were noticed. The measured doses indicated improvements in deliverability of the plans with higher smoothing values. Hence, it can be concluded that increased smoothing reduced the total MUs exceptionally well without any considerable changes in OAR doses. The observed progress in plan deliverability in terms of the gamma index strongly supports the recommendation of smoothing levels up to X=70 and Y=60. Radiobiological method of treatment plan evaluation study resulted an effective way of plan comparison. The estimated biological outcome and DVH data showed least differences between plans for IMRT when compared to VMAT. Our retrospective study based on 120 plans, validated the radiobiological method of plan evaluation. The tumour cure or normal tissue complication probabilities were found to be correlated with the corresponding physical dose indices. The comprehensive QA protocol using EPID and indigenously developed MATLAB program is suitable for daily, patient specific and MLC checks. Our study recommends EPID as a versatile dosimetry system in a busy radiation therapy department. The measured data revealed the reliability and consistency of portal detector. In combination with the MATLAB analysis software, EPID has immense potential for different QA checks of LINAC. The Dolphin-Compass dosimetry system was installed for enhancing the patient-specific QA program. The accuracy of beam modelling was validated and a detailed 3D dose comparison was performed. The detector system is found to be efficient for the patient-specific QA of complex treatment techniques such as IMRT, VMAT and SBRT. The study of eMC algorithm indicated its acceptance for clinical use. The O.F and cutout factor calculated by eMC algorithm in various electron beam agreed with the corresponding measured values. Hence the given method was proved to check the performance of eMC in electron dose calculation.

As a future perspective of the present study, optimum levels of fluence

smoothing can be extended to other commercially available TPS. The QA protocol using EPID can be made available into the case of electron beam also. A new quantitative index for interpreting the results of fluence comparison using MATLAB program will be helpful for effective analysis of patient-specific QA.

References

[1] Khan F.M. Physics of Radiation Therapy. 3rd Edition, Lippincott Williams Wilkins, Philadelphia, 2003.

[2] David Palma, Emily Vollans, Kerry James, Sandy Nakano, Vitali Moiseenko, Richard Shaffer, Michael McKenzie, James Morris, Karl Otto. Volumetric Modulated Arc Therapy for Delivery of Prostate Radiotherapy: Comparison with Intensity-Modulated Radiotherapy and Three-Dimensional Conformal Radiotherapy. International Journal of Radiation Oncology*Biology*Physics, 2008, 72(4): 996-1001.

[3] David Thwaites. Accuracy required and achievable in radiotherapy dosimetry: have modern technology and techniques changed our views? J Phys 2013; 444: 012006.

[4] R.F. Hill, S. Brown, C. Baldock. Evaluation of the water equivalence of solid phantoms using gamma ray transmission measurements. Radiation Measurements, 2008, 43(7): 1258 - 1264.

[5] Kutcher GJ, Coia L, Gillin M, et al. Comprehensive QA for radiation oncology: Report of AAPM Radiation Therapy Committee Task Group 40. Med Phys. 1994, 21(4): 581-618.

[6] Klein EE, Hanley J, Bayouth J, et al. Task Group 142 report: quality assurance of medical accelerators. Med Phys. 2009, 36(9): 4197-212.

[7] International Atomic Energy Agency. Commissioning and Quality Assurance of Computerized Planning Systems for Radiation Treatment of Cancer, IAEATRS-430. Vienna: IAEA, 2004.

[8] Fraass B1, Doppke K, Hunt M, Kutcher G, Starkschall G, Stern R, Van Dyke J. American Association of Physicists in Medicine Radiation Therapy Committee Task Group 53: quality assurance for clinical radiotherapy treatment planning. Med Phys. 1998, 25(10): 1773-1829.

[9] Agazaryan N, Solberg TD, DeMarco JJ. Patient specific quality assurance for the delivery of intensity modulated radiotherapy. J Appl Clin Med Phys. 2003, 4(1): 40-50.

[10] Ravichandran R, Bhasi S, Binukumar J P, Davis C A. Need of patient-specific quality assurance and pre-treatment verification program for special plans in radiotherapy. J Med Phys. 2011, 36: 181-183

[11] Kim DW, Chung WK, Shin D, et al. Risk of second cancer from scattered radiation of intensity-modulated radiotherapies with lung cancer. Radiation Oncology (London, England). 2013, 8(47): 8-47.

[12] Berrington de Gonzalez A, Wong J, Kleinerman R, Kim C, Morton L, Bekelman JE. Risk of second cancers according to radiation therapy technique and modality in prostate cancer survivors. Int J Radiat Oncol Biol Phys. 2015, 91(2): 295-302.

[13] Yoon M, Ahn SH, Kim JS. Radiation-induced cancers from modern radiotherapy techniques: Intensity-modulated radiotherapy versus proton therapy. Int J Radiat Biol Phys. 2010, 77: 1477-1485.

[14] Roy S, Badragan I, Ahmed SN, Sia M, Singh J, Bahl G. Integration of radiobiological modeling and indices in comparative plan evaluation: A study comparing VMAT and 3D-CRT in patients with NSCLC. Pract Radiat Oncol. 2018, 8(5): 355-363.

[15] N. Daly-Schveitzer, M. Juliron, Y. Gan Tao, A. Moussier, J. Bourhis. Intensity-modulated radiation therapy (IMRT): Toward a new standard for radiation therapy of head and neck cancer. European Annals of Otorhinolaryngology, Head and Neck Diseases. 2011, 128(5): 241-247.

[16] Niemierko A. Radiobiological models of tissue response to radiation in treatment planning systems. Tumori. 1998, 84: 140-3.

[17] Herman, M. G., Balter, J. M., Jaffray, D. A., McGee, K. P., Munro, P. , Shalev, S. , Van Herk, M. and Wong, J. W. Clinical use of electronic portal imaging: Report of AAPM Radiation Therapy Committee Task Group 58. Med. Phys. 2001, 28: 712-737.

[18] Pasma, K. L., Dirkx, M. L. P., Kroonwijk, M., Visser, A. G. and Heijmen, B. J. M. Dosimetric verification of intensity modulated beams produced with dynamic multileaf collimation using an electronic portal imaging device. Med. Phys. 1999, 26: 2373-2378.

[19] Vikraman S, Manigandan D, Karrthick KP, et al. Quantitative evaluation of 3D dosimetry for stereotactic volumetric-modulated arc delivery using COMPASS. J Appl Clin Med Phys. 2014, 16(1): 5128.

[20] J. F. Aubry, H. Bouchard, I. Bessires, and F. Lacroix. Validation of an electron Monte Carlo dose calculation algorithm in the presence of heterogeneities using EGSnrc and radiochromic film measurements J. Appl. Clin. Med. Phys. 2011, 12: 3392.

[21] T. Arunkumar, C. Varatharaj, M. Ravikumar, K. M. Ganesh, S. Sathiyan, Shwetha B. Commissioning and validation of the electron Monte Carlo dose calculation at extended source to surface distance from a medical linear accelerator. 2016, 4(7): 1155-1163.

[22] Popple RA, Weinber R, Antolak JA, et al. Comprehensive evaluation of a commercial macro Monte Carlo electron dose calculation implementation using a standard verification data set. Med Phys. 2006, 33(6):1540-1551.

Chapter 2

Effect of fluence smoothing on the quality of intensity-modulated radiation treatment plans

2.1 Introduction

Radiation therapy uses ionizing radiation to inhibit the functioning and multiplication of tumor cells. External-beam radiation therapy has been found to be beneficial for 52% of all cancer patients [1] while others resort to surgery and chemotherapy. The objective of radiation therapy is to deliver a prescribed amount of lethal radiation dose to the tumor while minimizing the dose to surrounding normal tissues. This has been achieved with the help of a technique called IMRT, which generally uses inverse planning with an optimization algorithm for the desired dose distribution to reach the PTV and a low dose to the surrounding OARs. After fixing the number of beams and their directions and defining constraints on the doses to the PTVs and the OARs, the computerized TPS creates a large numbers of beamlets. Radiation fluence is defined as the

number of particles (dN) incident on a sphere of cross-sectional area (dA)(Figure 2.1), which is mathematically represented as:

$$\Phi = \frac{dN}{dA} \tag{2.1}$$

The fluences of these beamlets are optimized by use of inverse-planning algo-
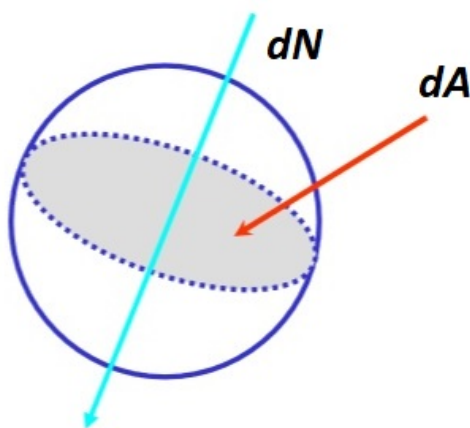
Figure 2.1: Number of particles incident on cross sectional area.

rithms. There are two different approaches for optimization of IMRT planning. In the traditional two-step optimization process, the beamlet fluences are first optimized to produce an "optimal fluence map" by use of iterative reconstruction. The Leaf Motion Calculator (LMC) creates the MLC positions and accounts for physical and mechanical constraints on the MLC such as leaf transmission, maximum leaf speed, and leaf edge shape. Because of these limitations, more complex plans are more difficult to achieve and the LMC creates an "actual fluence map" which is as close to the "optimal fluence map" as possible [2]. In the second approach, Direct Machine Parameter Optimization (DMPO), the MLC constraints are taken into account in the optimization process itself and deliverable treatment plans are optimized in a single step [3, 4]. As there is no conversion of the fluence map at the end of the optimization, the planner has better control over the complexity of plans than is possible with two-step optimization. The term, complexity can be described as the degree of frequency fluctuations and the amplitude in the fluence distribution of the beam [5]. Depending on the geometry of

the PTVs and the OARs, the demands for conformity to the PTV and the tolerance of the surrounding OARs, the fluence maps can be correspondingly complex. If the complexity is reduced, this implies that the quality of the treatment plan may deteriorate because of loss in the conformity or because of unacceptable doses to OARs. However, more complex plans cause greater practical difficulties for the delivery system. Increased complexity of the delivered fluence map will result in a large number of MUs. This addresses challenges such as long-term secondary cancer induction [6], increased skin dose, a longer treatment time and uncertainties during treatment delivery. These potential consequences can be minimized by use of several methods which reduce the complexity of treatment plans. Such methods are known as "smoothing" of the delivered intensity maps [7 - 11].

Two recommended methods of fluence map smoothing are:

1) the use of Intensity-Modulated Beam (IMB) smoothing filters and

2) inclusion of smoothness terms into the objective function of the optimization algorithm.

Both of these methods reduce fluence variations between adjacent beamlets by eliminating noise in the fluence maps. Commercially available treatment-planning systems typically include a smoothing interface by which the user can adjust the smoothing parameters for different levels of fluence smoothing. Most TPS vendors recommend the use of a default set of smoothing parameters within their software, which leads to a moderate level of smoothing. However, it has been observed that a change in default smoothing levels results in a change in both plan quality and treatment efficiency in terms of the integral dose [12]. These effects will vary with treatment sites.

In the present study, we have evaluated the effect of such smoothing functions in Varian Eclipse TPS, version 10.0 (Varian Medical Systems, Palo Alto, CA) for 20 IMRT cases at two complex sites treated in our radiation therapy center. We also have investigated the improvements in the plan quality for these two sites while varying the fluence smoothness and thereby could recommend an optimum

smoothing parameter for the particular anatomic regions.

2.2 Materials and Methods

For understanding the effect of the smoothing parameters in the inverse TPS, it is very important to know how a TPS performs fluence smoothing within its inverse-planning process. In Eclipse (Varian Medical Systems, Palo Alto, CA, USA), fluence smoothing is attained within the objective function of the TPS [13]. A user can define dose-volume constraints, their priorities, and the smoothing values in both the direction of leaf travel (X) and the direction perpendicular to leaf travel (Y). Smoothing is applied at each iteration by addition of a smoothing weighted objective in the cost function and the total objective function becomes a combination of two terms [14]:

$$F(x) = \sum_i w_i(D_i - P_i)^2 + \sum_k w_k(x_{k+1} - x_k)^2 \qquad (2.2)$$

The first term is the usual component for dose-volume constraints. P_i is the prescribed dose of the ith voxel, w_i is the weight (priority) factor given to particular objective and D_i is the computed dose at point i. D_i is expressed as follows:

$$D_i = \sum_i d_{j,i}.x_j \qquad (2.3)$$

where $d_{j,i}$ is the dose to point i from the jth beamlet, and x_j is the jth beamlet weight in the fluence map. The second term in equation (2.2) is related to the smoothing and is used to reduce excessive fluence differences between adjacent bixels in the X or Y direction. The two weights w_k (X and Y smoothing values) determine the relative priority of these goals in the total objective function. For each beamlet, the fluence value differences between adjacent pencil beams are summed together and then multiplied by user-defined X and Y smoothing values, which are then added to the penalty score of the total objective function. Thus,

the fluence-smoothing process increases the total value of the objective function penalty score for plans with broadly varying fluence maps, thereby guiding the optimization, toward smoother fluence maps [12].

Our total of 20 cases consisted of 10 patients with carcinoma of the nasopharynx and 10 patients with carcinoma of the lung. These patients had already completed their treatments in our radiation therapy center with use of a Varian clinac-iX LINAC with a 120 leaf millennium MLC (Varian Medical Systems, Palo Alto, CA). Treatments were delivered by inverse planned dynamic-IMRT techniques. All of the investigated nasopharynx cases were treated with a dose of 212.1 cGy/fraction (total dose = 7000 cGy). The lung patients were treated with 200 cGy/fraction (total dose = 6000 cGy). All of these treatment plans had nine and seven static beam angles for the nasopharynx and lung, respectively. Figure 2.2 shows examples of dose distributions for the nasopharynx and lung plans. The plans were produced in the Varian Eclipse TPS with 6 MV energy beams in two-step optimization by use of vendor-default smoothing values. Each of these approved and verified plans were used as reference plans for evaluation of newly created treatment plans. The reference plans were then copied and modified by use of different X and Y smoothing parameters which varied from 0 to 100. A total of nine plans with smoothing at (X = 0, Y = 0; vendor-defined minimum), (X = 20, Y = 10), (X = 40, Y = 30; vendor-default), (X=50, Y=40), (X = 60, Y = 50), (X = 70, Y = 60), (X = 80, Y = 70), (X = 90, Y = 80) and (X = 100, Y = 100; maximum defined in standard practice [15]) were created for all patients. Even though the range of possible smoothing levels in Eclipse is 0-999, in the present study we have adopted the range and interval used by a previous author, Armoogum [16]. All optimization parameters, except the smoothing values, were held constant at all times. These plans were then re-optimized for 100 iterations as this value is sufficient for a minimum objective function. An Anisotropic Analytical Algorithm (AAA) was used for the final dose calculation with a grid size of 2.5 mm. For these 20 IMRT patients, 20 x 9 combinations of treatment plans were optimized, giving a total of 180 individual dose plans.

A comparative study of treatment plans was done from the treatment plan reports, DVH data, and the calculated radiobiological indices. The deliverability of these plans was also examined by 2D fluence comparisons between the planned and measured fluence. For a better understanding of the results, statistical tests have been carried out. We have used one-way ANOVA, the column analysis method, in which the mean of each column (data for various smoothing levels) has been compared with the mean of every other column, whereby it can be concluded whether the observed variations in different figures are statistically significant. GraphPad prism (Graphpad software, San Diego, CA, USA, version 6.07) was used for the above tests and the deviations were considered significant for p values < 0.05.
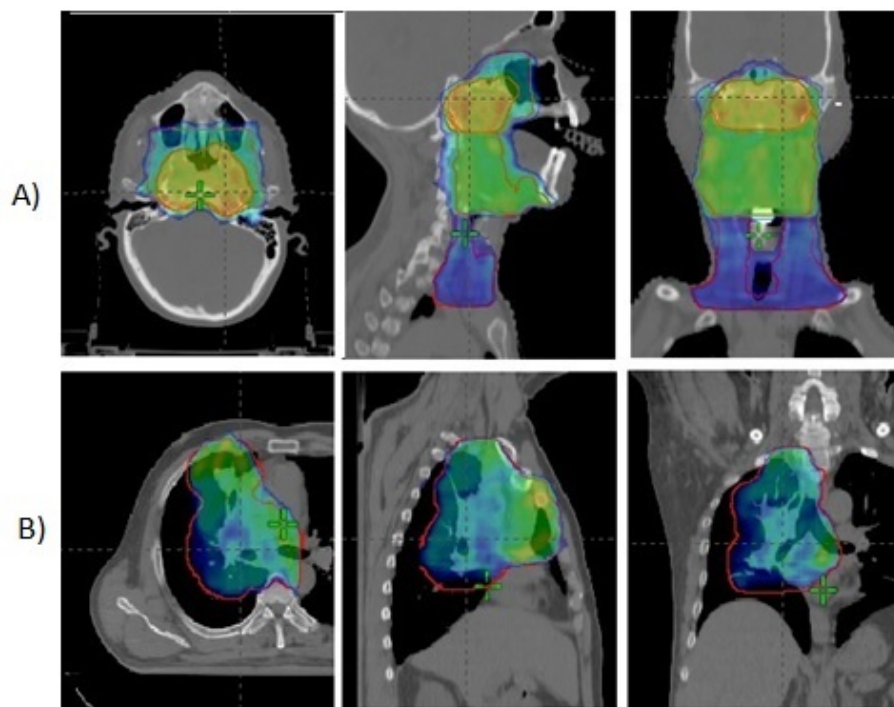
Figure 2.2: Axial, sagittal and coronal views (from left to right) of color washed isodose distributions of a A) nasopharynx and B) lung plans.

2.2.1 Treatment plan reports and Dose Volume Histogram

We have generated treatment plan reports to obtain the total number of MUs. We have performed DVH analysis to determine the near-maximum dose ($D_{2\%}$), the dose to 95% of the volume ($D_{95\%}$) for the PTV. We have also determined the maximum dose (D_{max}) and the doses received by the different volumes of OARs as per the Radiation Therapy Oncology Group (RTOG) protocols. For target coverage, at least 95% of the prescribed dose should receive more than 95% of the PTV. The OAR constraints include volumes $< 1\%$ above 5400 cGy for the optic nerves and chiasm, a maximum dose < 5400 cGy for the brainstem, and a volume of the spinal cord $< 1\%$ above 5000 cGy [17 - 19]. Additional constraints, including a volume of the whole lung receiving 2000 cGy (V_{2000}) < 30-35% for lung and the volume of the heart receiving 4000 cGy (V_{4000}) $< 30\%$ for heart were also taken care of [20, 21].

2.2.2 Radiobiological Indices

Treatment plans can be effectively compared based on EUD-based radiobiological estimates [22]. TCP and NTCP were estimated in this study from the calculated EUD values [23-24]. The variation in these quantities were closely reviewed by changing the fluence smoothing values from X,Y=0 to X,Y=100.

2.2.3 Dose measurements

The fluence complexity has a considerable effect on the accuracy of dose delivery [14]. Therefore, we have also studied the correlation of the fluence complexity with delivery accuracy. The 2D dose distributions for each plan were calculated with a MULTICube phantom in Eclipse and compared with the corresponding measured dose distributions. The MatriXX 2D (IBA Dosimetry, Schwarzenbruck, Germany) array system consisting of 1020 vented parallel ion chambers, arranged in 32 x 32 grids, was used for measurements. The diameter, height

and volume of each detector were 4.5 mm, 5 mm, and 0.08 cm^3, respectively. The inherent water-equivalent build-up thickness was 3.2 mm, and the active measurement area was 24 x 24 cm^2. The spatial resolution of the detector system was 7.6 mm. This low spatial resolution due to the size of a detector and the transport of secondary electrons from the walls into the measuring volume introduces large errors in the gamma analysis of steep dose gradients. The dose points measured by the detector array were interpolated from 7.6 mm to 1.0 mm by use of the linear interpolation method of the IBA OmniPro IMRT verification system (IBA Dosimetry, Schwarzenbruck, Germany). The calculated 2D fluence maps of all of the plans were transferred to the OmniPro IMRT verification system. These plans were delivered to the detector in a fixed set-up with use of the MULTICube phantom. The source-to-detector distance was 100 cm, and the thickness of the build-up and backscatter material was 10.5 cm and 7.5 cm respectively.

The quantitative evaluation in terms of the gamma index (% dose difference and Distance To Agreement [DTA]) [25] of the measured against the TPS-calculated doses was performed for all dynamic IMRT plans. The percentage of the beam area with a gamma value smaller than one (area γ <1 [%]) was obtained and tabulated. The standard passing criterion is 3% for dose difference analysis, and the 3 mm criterion for DTA analysis (3% - 3 mm) [26]. This 3% - 3mm passing criterion and a tighter criterion of 2% - 2mm were evaluated in this study. The mean and standard deviation for the gamma values were calculated and compared. This helped to great extent in understanding of the smoothing values with a higher degree of deliverability.

2.3   Results

A detailed analysis of the treatment plans reports, DVH and fluence measurements results in the following information. The variation of these parameters with respect to different level of fluence smoothing is discussed below.

Table 2.1: Detailed reports of MUs generated by TPS over various fluence levels in both study groups. Abbreviations: Max. = Maximum, Min. = Minimum, Avg. = Average, S.D. = standard deviation.

Smoothing levels	Nasopharynx plans			Lung plans		
	Max. MU	Min. MU	Avg. MU $\pm$ S.D.	Max. MU	Min. MU	Avg. MU $\pm$ S.D.
X=0, Y=0	2433	1743	2079 $\pm$ 265.4	2189	798	1556 $\pm$ 490.3
X=20, Y=10	2360	1693	2004 $\pm$ 244.4	2125	769	1488 $\pm$ 465.7
X=40, Y=30	2049	1399	1696 $\pm$ 212.4	1817	680	1240 $\pm$ 368.7
X=50, Y=40	1683	1169	1416 $\pm$ 149.1	1435	589	1011 $\pm$ 282.8
X=70, Y=60	1604	1089	1306 $\pm$ 150.8	1254	546	944 $\pm$ 246.9
X=80, Y=70	1510	1066	1239 $\pm$ 131.8	1148	536	876 $\pm$ 219.1
X=90, Y=80	1478	1013	1184 $\pm$ 139.2	1081	525	843 $\pm$ 203.9
X=100, Y=100	1415	992	1107 $\pm$ 137.4	1001	499	791 $\pm$ 176.8
p value			<0.0001			<0.0001

2.3.1 Total Monitor Units

We have observed that the averages of the total MUs for both study groups decreased with increasing X-Y smoothing values, as shown in Table 2.1. For the nasopharynx, the total number of MUs came down from 2079 $\pm$ 265.4 at X=0, Y=0 to 1107 $\pm$ 137.4 at X=100, Y=100, whereas for the lung, the corresponding decrease was from 1556 $\pm$ 490.3 to 791 $\pm$ 176.8.

2.3.2 Dose Volume Histogram analysis

$D_{95\%}$ of the PTV obtained from the DVH had a maximum variation of only 0.6% for the nasopharynx and 0.5% for the lung. Similarly, the average $D_{2\%}$ was found to vary by 0.3% and 1.3% for the nasopharynx and lung respectively, when we increased smoothing from X=0, Y=0 to X=100, Y =100. Table 2.2 presents the average dose values (cGy) for 95% and 2% of the PTVs of the respective groups. The maximum dose and the volume dose for various OARs were studied and the detailed DVH data are plotted in Figure 2.3 & Figure 2.4.

2.3.3 Radiobiological Indices

The average EUD and the estimated TCP varied minimally during the process of smoothing. The maximum changes observed in the average EUD and TCP
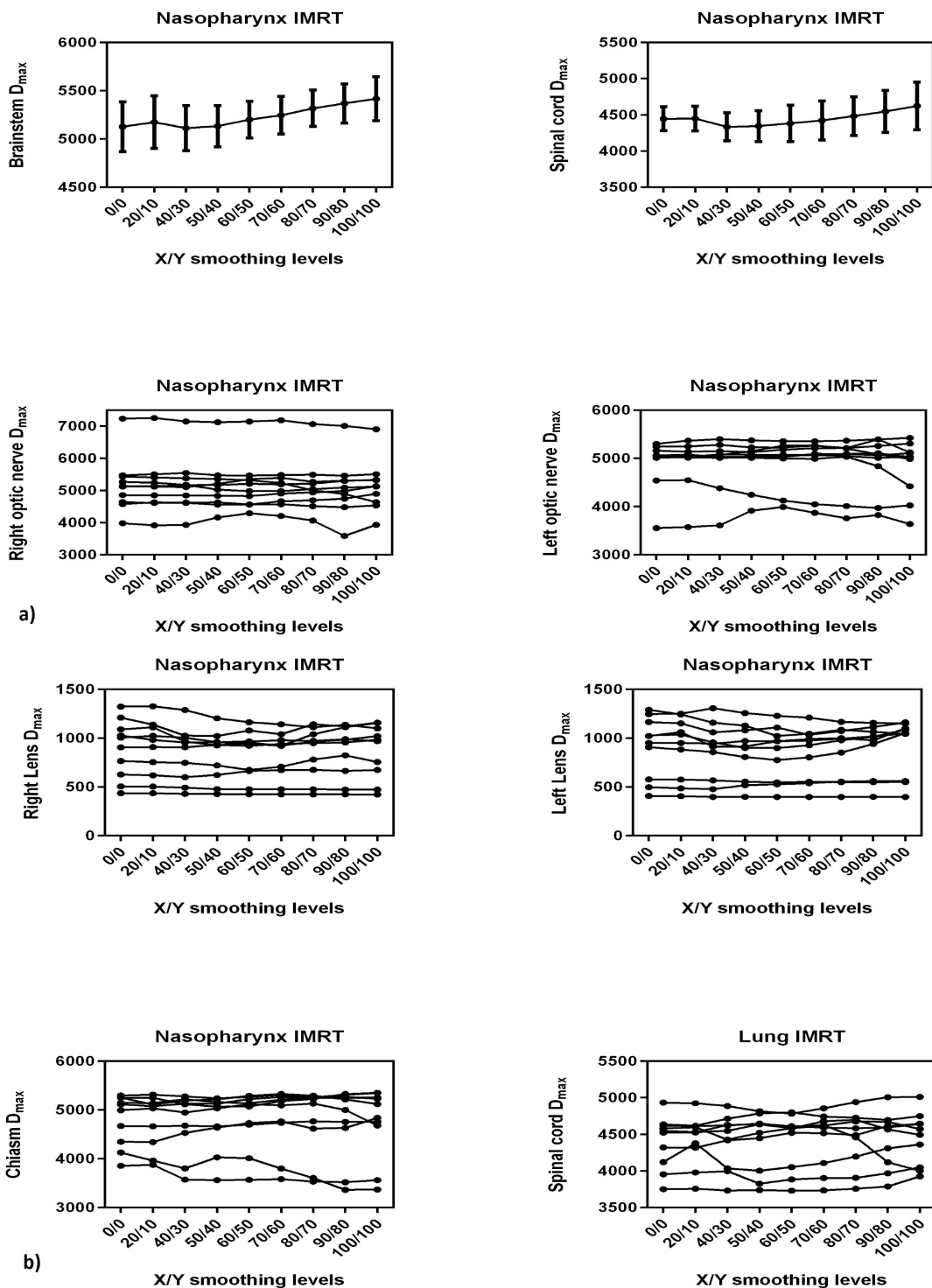
Figure 2.3: Effect of smoothing on the maximum dose in both study groups. D_{max} (cGy) is plotted for brainstem, spinal cord, optic nerves, chiasm, and lenses.
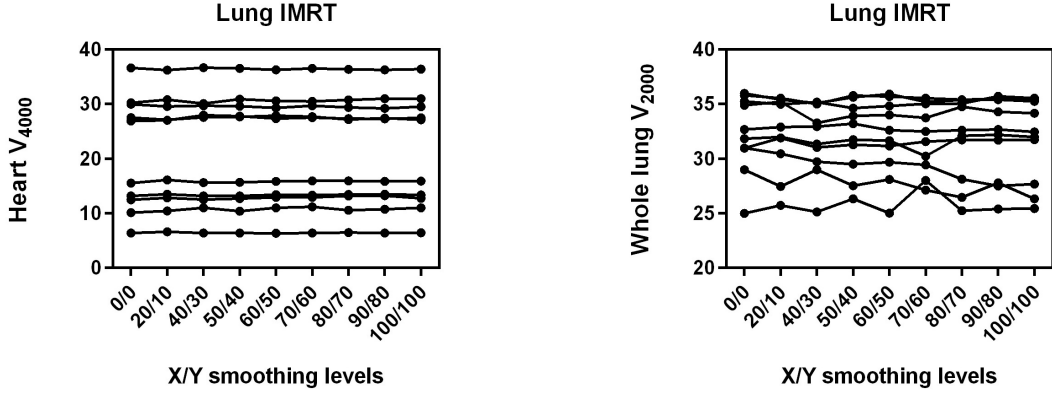
Figure 2.4: Effect of smoothing on the volume dose of heart and lung in lung plans. The percentage of heart and lung volumes that received 4000 cGy and 2000 cGy respectively are plotted.

Table 2.2: Average doses (cGy) to 95 % and 2 % of PTV obtained from DVH of both nasopharynx and lung plans. No statistically signicant variations were observed.

Smoothing levels	$D_{95\%}$ of nasopharynx plans (Avg. $\pm$ SD)	$D_{95\%}$ of lung plans (Avg. $\pm$ SD)	$D_{2\%}$ of nasopharynx plans (Avg. $\pm$ SD)	$D_{2\%}$ of lung plans (Avg. $\pm$ SD)
0/0	6763.3 $\pm$ 69.46	5732.0 $\pm$ 56.79	7347.6 $\pm$ 216.78	6386.7 $\pm$ 196.88
20/10	6769.1 $\pm$ 70.89	5754.7 $\pm$ 67.18	7348.5 $\pm$ 219.02	6404.2 $\pm$ 195.63
40/30	6772.4 $\pm$ 71.66	5729.6 $\pm$ 54.08	7335.1 $\pm$ 187.27	6407.2 $\pm$ 175.48
50/40	6762.6 $\pm$ 59.22	5764.5 $\pm$ 67.41	7338.7 $\pm$ 181.34	6414.4 $\pm$ 179.75
60/50	6749.4 $\pm$ 50.82	5749.6 $\pm$ 57.52	7340.6 $\pm$ 186.35	6427.1 $\pm$ 176.92
70/60	6773.3 $\pm$ 71.37	5744.4 $\pm$ 57.80	7346.1 $\pm$ 189.48	6419.2 $\pm$ 187.67
80/70	6754.2 $\pm$ 63.82	5731.6 $\pm$ 68.43	7363.8 $\pm$ 203.58	6417.4 $\pm$ 192.71
90/80	6734.4 $\pm$ 65.80	5727.4 $\pm$ 68.21	7371.0 $\pm$ 202.41	6423.8 $\pm$ 205.26
100/100	6737.8 $\pm$ 65.75	5725.7 $\pm$ 68.21	7371.4 $\pm$ 173.12	6469.1 $\pm$ 195.15
p value	0.2646	0.1158	0.1622	0.0997
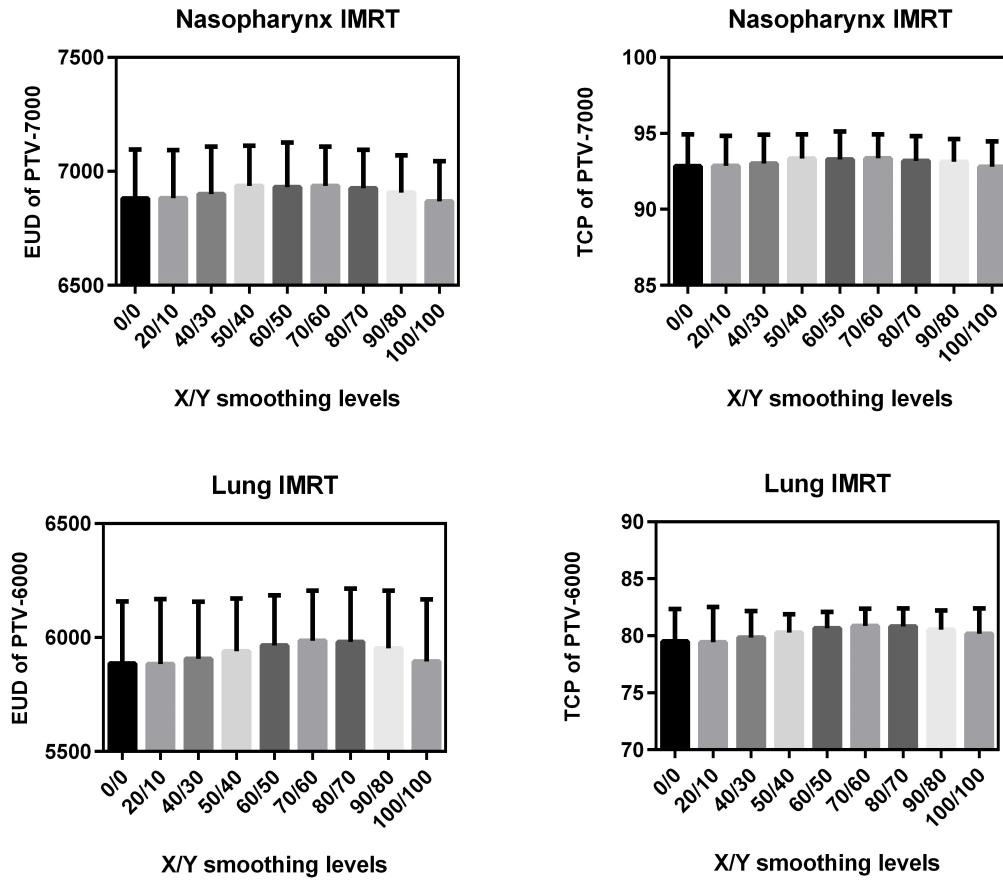
Figure 2.5: Average EUD/TCP variations with increasing smoothing levels in both study groups.

of the nasopharynx plans were from 6935.8 $\pm$ 172.4 to 6868.5 $\pm$ 176.4 and from 93.4 $\pm$ 1.6 to 92.8 $\pm$ 1.7, respectively (p values: 0.1629 and 0.2103). In the case of the lung plans, the corresponding changes were from 5986.5 $\pm$ 218.7 to 5885.8 $\pm$ 272.4 in the average EUD and from 80.9 $\pm$ 1.5 to 79.4 $\pm$ 3.1 in the average TCP (p values: 0.2011 and 0.2993). However, a small but reproducible increase in the EUD and TCP values at medium smoothing levels between X=50, Y=40 and X=80, Y=70 was observed. Figure 2.5 depicts the variations in the average EUD and TCP with increasing smoothing levels. Radiobiological estimation of the NTCP was done for selected normal tissues, and the result is given in Table 2.3.

Table 2.3: Average values of EUD (cGy) and NTCP (%) for different OARs with various degrees of fluence smoothing.

Smoothing levels	Brainstem		Spinal cord (nasopharynx)		Chiasm		Lung		Spinal cord (lung)		Heart	
	EUD	NTCP	EUD	NTCP	EUD	NTCP	EUD	NTCP	EUD	NTCP	EUD	NTCP
0/0	3211.0	0.0291	2750.1	0.0001	3455.1	0.1379	1583.5	6.017	2904.8	0.0005	2918.1	0.8523
20/10	3197.9	0.0286	2745.7	0.0001	3402.1	0.1214	1584.7	5.984	2896.5	0.0005	2914.5	0.8279
40/30	3169.9	0.0244	2713.6	0.0001	3388.6	0.1178	1590.8	6.287	2912.6	0.0005	2916.6	0.8426
50/40	3224.2	0.0350	2708.1	0.0001	3412.5	0.1066	1603.6	6.664	2924.5	0.0005	2931.4	0.8888
60/50	3278.3	0.0360	2762.1	0.0001	3406.0	0.1207	1620.8	7.173	2929.9	0.0006	2939.5	0.8836
70/60	3357.7	0.0467	2801.0	0.0002	3478.0	0.1549	1647.1	7.956	2927.3	0.0006	2951.0	0.8476
80/70	3362.7	0.0635	2864.1	0.0002	3455.7	0.1414	1476.5	8.592	2950.6	0.0007	2946.6	0.8298
90/80	3512.6	0.0792	2931.2	0.0003	3390.1	0.1565	1294.7	9.677	2887.9	0.0007	2921.1	0.7907
100/100	3583.3	0.0990	3005.7	0.0004	3468.0	0.1893	1701.6	10.72	2851.2	0.0007	2896.4	0.7556
p value	0.0016	0.0184	0.0417	0.0289	0.7002	0.5157	0.2928	0.2834	0.5398	0.4845	0.3964	0.6912
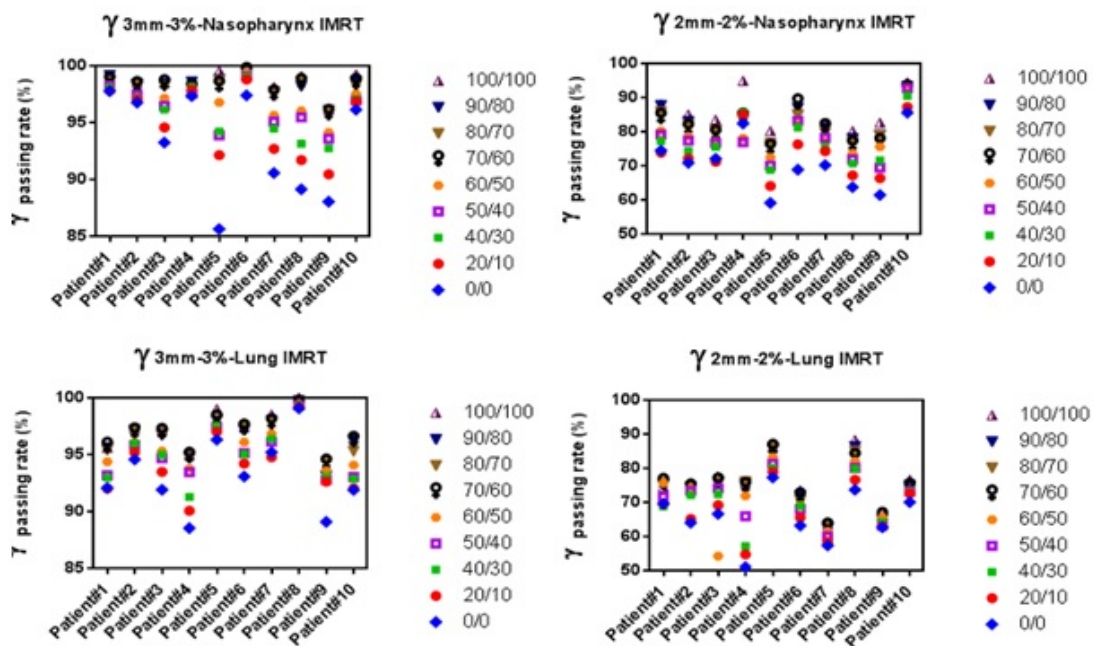
Figure 2.6: Dosimetric comparison of different smoothing plans with their measured distributions. Smoothing improved the agreement between measured and TPS plans in both groups.

2.3.4 Dose map comparison

The results for the gamma passing rate for all measured smoothing levels with respect to their TPS plans for both treatment sites are summarized in Table 2.4. In the nasopharynx plans, the percentage of points within the passing range (γ 3mm - 3%) is only 92.68 ± 4.52 for X=0, Y=0, whereas 98.55 ± 0.98 % points remain in the same range for X=100, Y=100 smoothing. Similarly, in the lung patients, the corresponding improvement in the percentage of points was from 93.15 ± 3.22 to 97.02 ± 1.88 for a change in smoothing from X=0, Y=0 to X=100, Y=100. Gamma passing rates using stricter gamma criteria (γ 2mm - 2%) also exhibited substantial improvements in percentage of points from lower to higher smoothing values. In both cases, the measured plans with smoothing values X=70, Y=60 and above showed an improved agreement with the TPS plans, as is evident in Figure 2.6.

39

2.4 Discussion

In the present study, we have investigated the application of the vendor-supplied fluence-smoothing interface of Eclipse TPS in treatment plan optimization and related changes in the quality of nasopharynx and lung IMRT plans. The examination of 180 individually optimized plans revealed that, as smoothing was increased, the number of maximum, minimum, and average MUs decreased for both groups of patients. MUs are calculated from a term called MU factor which, in turn, is related to the complexity of the plan. A small field requires a larger number of MUs to reach the same dose as that for large fields. The large-scale modulations in complex IMRT plans require a large number of small and irregularly shaped beam segments to achieve high dose conformity. Thus, the complexity of IMRT is reflected in a large number of treatment MUs [5]. Plan complexity and smoothing are always inversely related, and any reduction in fluence complexity is highly correlated with a corresponding decrease in MUs [14]. Our results for sites with numerous critical structures and inhomogeneities agree with previous findings for various other sites [5, 7, 14, 16]. The observed decrease in the average MUs was 46.8% for the nasopharynx and 49.2% for the lung plans over the whole range of smoothing, which was statistically significant. However, the major contributions (37.2% and 39.3%) are from smoothing X=0, Y=0 to X=70, Y=60. Percentages of reduction in MU from vendor-recommended smoothing to X=70, Y=60 plans are 23.0% and 23.9% for the nasopharynx and lung plans, respectively. All of the above differences are statistically significant (p values <0.0001).

Another important aspect of this study is the radiobiological estimation of treatment plans. Radiobiological models were proved to be effective in predicting treatment outcome precisely by use of DVH data when compared to the uncertainty of using physical dose metrics alone for plan evaluation [22]. The results for the 90 plans investigated in each group did not show any major violations of the clinical acceptability of those plans. The estimation of TCP, which had a good correlation with the conformity index [22], also showed little or no varia-

tion with fluence smoothing. However, the observed slight improvements in both EUD and TCP from the X=50, Y=40 to the X=80, Y=70 smoothing interval was noticeable.

Although variations are observed in the $D_{95\%}$ and $D_{2\%}$ of the PTVs (Table 2.2), the given method of DVH analysis may not clearly reflect the small change in the PTV volume dose. A detailed study about various OARs revealed that there was no significant difference in the organ dose values except for the D_{max} of the brainstem and spinal cord in the nasopharynx group. A statistically significant increase of D_{max} in both the brainstem and spinal cord was obtained. This is because of the increase in smoothing, which obstructs the optimizer for achieving harder constraints of the plans. The average maximum doses to the brainstem and spinal cord were increased by 5.9% and 6.7%, respectively for an increase in smoothing from default values to the highest levels (p values: 0.0005 and 0.0255). The major changes in the D_{max} occurred approximately from X=70, Y=60 to the highest values in this study. The observed increase in the D_{max} of the brainstem and spinal cord from vendor-recommended values to X = 70, Y=60 was 2.6% and 2.0%, respectively (p values: 0.0023 and 0.1722). The estimated EUD and NTCP of these structures showed a similar behavior. However, the analyzed dose figures for the optic nerve, optic chiasm and lenses in the nasopharynx patients and those of the spinal cord, lung, and heart in the lung patients did not show any trend or reproducibility over the entire smoothing range.

The measurements and evaluation processes with the MatriXX 2D system can be used for quantifying the degree of deliverability of the TPS-generated plans. The results of a 2D dose comparison show gradual improvements in the percentage of points satisfying the passing criterion with respect to the increased fluence smoothing. This is clearly shown in Figure 2.7 for a particular patient in each of the groups (four levels of successive smoothing are given). Low smoothing parameters in Eclipse make the fluences appear more complex and the gamma passing rate decreases with increasing complexity of the plan. Another interesting observation is the similarity of the gamma results for the fluence levels of

Table 2.4: Gamma results summary of comparison between TPS fluence and that measured with MatriXX 2D array system.

Smoothing levels	% of pixels passed ($\gamma <1$) in nasopharynx plans		% of pixels passed ($\gamma <1$) in lung plans	
	3%-3mm	2%-2mm	3%-3mm	2%-2mm
00/00	92.68 ± 4.52	70.41 ± 8.48	93.15 ± 3.22	65.51 ± 7.72
20/10	94.67 ± 3.04	73.70 ± 7.58	94.05 ± 2.66	67.34 ± 7.62
40/30	95.78 ± 2.25	77.06 ± 6.84	94.93 ± 2.45	69.39 ± 7.89
50/40	96.15 ± 1.83	77.32 ± 6.84	95.08 ± 2.14	71.02 ± 6.89
60/50	96.85 ± 1.48	78.63 ± 5.59	95.68 ± 1.86	71.03 ± 8.88
70/60	98.13 ± 0.97	81.77 ± 5.56	96.80 ± 1.56	74.54 ± 6.90
80/70	98.12 ± 0.87	81.89 ± 4.73	96.66 ± 1.66	74.50 ± 7.56
90/80	98.25 ± 0.93	82.46 ± 5.28	96.68 ± 1.85	74.77 ± 7.51
100/100	98.55 ± 0.98	85.47 ± 5.35	97.02 ± 1.88	75.66 ± 7.49

X=70, Y= 60 or above (except for X=100, Y=100) in any combinations, which can be well understood from Table 2.4.

In a number of studies, the use of fluence-smoothing function of commercial IMRT planning systems has been investigated. A study performed by Armoogum [16] examined the effect of fluence smoothing with an inverse-planning IMRT software (Helios, Eclipse version 8.9.09, Varian Medical Systems) for a cohort of prostate and of head and neck patients. The average leaf-pair opening (LPO), MU factor and total number of MUs were studied with different fluence-smoothing values. The study showed that an increase in smoothing results in a significant reduction in MUs and a definite increase in average LPO due to the reduced plan complexity. Another study by Anker et al. [12] compared the behavior of these smoothing functions in three inverse TPSs (Eclipse-Varian Medical Systems, Palo Alto, CA; BrainScan, BrainLAB AG, Feldkirchen, Germany; and CORVUS, Best Nomos, Pittsburg, PA) for four different IMRT plans. This analysis was essentially done for understanding of each TPSs smoothing algorithm by discussing them in parallel. Within the wide range of fluence smoothing from X,Y=0 to X,Y=999, they found a significant degradation in plan conformality at $X \geq 150$, $Y \geq 150$ smoothing levels. All OARs showed a higher D_{max} at X = 200, Y = 200 and they have recommended for considering the increasing of smoothing levels, by keeping $X \leq 80$ and $Y \leq 60$, to achieve the benefit of de-
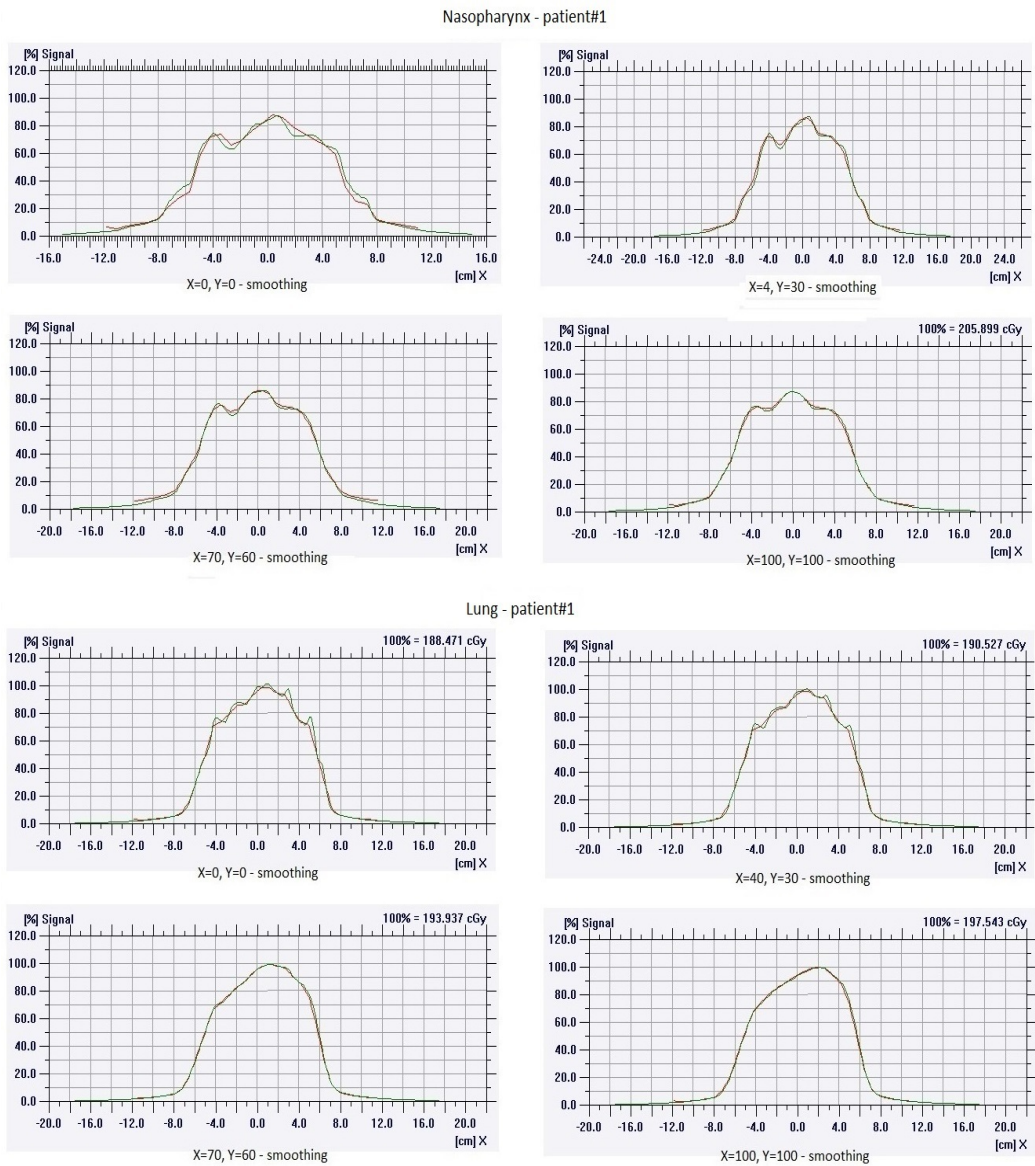
Figure 2.7: Comparison between TPS fluence and that measured with the MatriXX 2D array system for a nasopharynx and lung IMRT plan with 4 different levels of smoothing. A better correlation is observed toward maximum smoothing.

creasing complexity without compromising PTV coverage or OAR sparing. The behavior of smoothing functions in our study is in good agreement with their findings. We have done our studies on two particular sites (nasopharynx and lung), which were chosen because of their relatively highly complex and heterogeneous dose distribution. In contrast to those purely computational studies, the present study verifies the deliverability of treatment plans by actual measurement based on a larger set of data (180 plans). Our study not only is limited to physical dose evaluation, but also investigates the impact of fluence complexity on radiobiology based plan quality parameters. The effect of smoothing on more popular prostate groups was done by the above authors. The behavior of the prostate plans was consistent with that of other sites. A more noticeable decrease in the MUs was observed with an increase in smoothing [16]. However, the quality degradation of these plans started for smoothing values above X = 60, Y = 45 [12].

A recommendation for good IMRT practice is always to minimize the treatment MUs as far as possible. For every patient, there may be an optimum complexity level needed for achieving an acceptable plan. Obviously, this complexity will be decided by the required dose distribution leading to tumor lethality and the chosen constraints for the OAR. However, any additional complexity resulting in noise in the fluence map causes a significant increase in MUs, with little or no plan refinement. It is essential to determine the optimum values of smoothing for routine planning without sacrificing the quality of the treatment plans, especially for complex and irregular anatomic regions.

Even though it may not be possible to suggest the exact smoothing values for Varian Eclipse TPS, our studies can give recommendations for changing the standard smoothing values to some higher values. Interestingly, all smoothing combinations of the current study, starting from X=40, Y=30, produced a clinically acceptable plan in terms of both tumor control and normal-tissue complications. However, an optimum smoothing value of X=70, Y=60 can be recommended based on the observations of outstanding differences in MUs, along

with the slight improvements in the EUD and a lesser deviation of the D_{max} of certain critical structures from the default plans. The noted differences of about 23.0% and 23.9% in the respective treatment MUs are exceptionally high. The transformation of smoothing values from default to X=70, Y=60 saved around 390 MU (nasopharynx) and 290 MU (lung) per fraction. This will result in a reduction of approximately 32 and 21 minutes respectively, in the total radiation-beam-on time for the entire course of a patient treatment. Thus, this smoothing level can replace the default level without significant deviations in the plan quality, but with a considerable decrease in MU values and in the total "beam-on" time.

The Varian Eclipse TPS uses both a dose-volume optimizer (DVO) algorithm for evaluation of dose for optimization and a more accurate AAA for final volume dose calculation. The fast optimization DVO algorithm introduces an optimization convergence error [27] when the dose calculation is in the build-up region or is due to the calculation of lateral scatter. Therefore, the final AAA-based dose calculation DVH may differ from the optimized DVO-based DVH for the IMRT plans with a PTV in the head and neck or lung region. This error can be minimized by performing a large number of iterations within the DVO, followed by a periodic correction [28] to the final dose calculation. The standard practice of optimization in our institution is the use of a relatively larger number of iterations for nasopharynx and lung plans where the PTVs are not in the vicinity of electronic equilibrium. It is understood that a large number of iterations often results in increasing MUs and a smaller MLC gap width. We also studied the impact of smoothing on MUs for a small number of iterations (50) and found a slight and less marked, but statistically significant, decrease in MUs with increasing smoothing. However, this study was done by use of 100 iterations matching with our clinical cases that yields a minimum cost function for the nasopharynx and lung plans. Also, this study was restricted to a particular plan setting which influences the total objective function. The iterative method for reaching a minimum cost function is influenced by many variables, such as

the optimization priority, user-defined dose volume constraints, and smoothing. The relative contribution of smoothing penalty and the structure-dose penalty were varied and found to have little effect on plan quality [12]. Further work is required for finding the effect of smoothing in the user-defined dose-volume constraints for different disease sites.

2.5 Conclusion

The study of nasopharynx and lung IMRT treatment plans with different scenarios of fluence levels helped us to understand the effect of user-interfaced fluence smoothing with the Eclipse TPS in detail. This scientific endeavor clearly showed a significant reduction in treatment MUs without any considerable variations in OAR sparing. The estimated biological outcome and DVH analysis do not recommend the rejection of any combinations of smoothing from vendor-recommended levels to the maximum values of this study. However, the observed efficiency of plan deliverability in terms of the gamma index toward higher smoothing levels promotes the idea of advancing the smoothing levels from X=40, Y=30 to X=70, Y=60. In addition, an appreciable reduction in MUs without critical deviations in the plan quality powerfully supports the recommendation of using smoothing levels up to X=70 and Y=60, at least for the anatomic regions studied.

References

[1] Delaney, G., Jacob, S., Featherstone, C. and Barton, M. The role of radiotherapy in cancer treatment. Cancer 2005, 104:1129-1137.

[2] External Beam Planing Reference Guide Eclipse. u. o.: Varian medical systems. 2007, ss.465-466.

[3] Dobler, Barbara, et al. Direct machine parameter optimization for intensity modulated radiationtherapy (IMRT) of oropharyngeal cancera planning study. Journal of Applied Clinical Medical Physics 2009,10(4):3066.

[4] Broderick, Maria, Michelle Leech, and Mary Coffey. Direct aperture optimization as a means of reducing the complexity of Intensity Modulated Radiation Therapy plans. Radiat Oncol 2009,4(8):1-7.

[5] Mohan R, Arnfield M, Tong S, Wu Q, Siebers J. The impact of fluctuations in intensity patterns on the number of monitor units and the quality and accuracy of intensity modulated radiotherapy. Med Phys 2000,27:1226-1237.

[6] Hall EJ, Wu C. Radiation induced second cancers: The impact of 3DCRT and IMRT. Int J Radiat Oncol Biol Phys 2003,56:83-88.

[7] Spirou SV, Fournier-Bidoz N, Yang J, Chui CS, Ling CC. Smoothing intensity modulated beam profiles to improve the efficiency of delivery. Med Phys 2001, 28:2105-2112.

[8] Sun X, Xia P. A new smoothing procedure to reduce delivery segments for static MLC-based IMRT planning. Med Phys 2004, 31:1158-1165.

[9] Webb S, Convery DJ, Evans PM. Inverse planning with constraints to generate smoothed intensity modulated beams. Phys Med Biol. 1998,43(10): 2785-2794.

[10] Matuszak MM, Larsen EW, Fraass BA. Reduction of IMRT beam complexity through the use of beam modulation penalties in the objective function. Med Phys. 2007,34(2):507-520.

[11] Matuszak MM, Larsen EW, Jee K, McShan DL, Fraass BA. Adaptive diffusion smoothing: a diffusion-based method to reduce IMRT field complexity. Med Phys. 2008,35(4):1532-1546.

[12] Anker CJ, Wang B, Tobler M, Chapek J et al. Evaluation of fluence smoothing feature for three IMRT planning systems. J Appl Clin Med Phys 2010,11:3035.

[13] Varian Medical Systems. 1. Reference Guide for Eclipse Algorithms: Vision Eclipse- External Beam Planning v6.5. Palo Alto, CA: Varian Medical Systems,2004.

[14] Nicolini G, Fogliata A, Vanetti et al. What is an acceptably smoothed fluence? Dosimetric and delivery considerations for dynamic sliding window IMRT. Radiation Oncology 2007,2:42, doi:10.1186/1748-717X-242.

[15] Mayo C, Urie M. Eclipse IMRT- A practical Treatment Planning Guide. Las Vagas, NV. Varian Medical Systems, 2004:24-27.

[16] Armoogum, K. S. Effect of smoothing on treatment plan efficiency in IMRT:eclipse Helios dose optimisation. Journal of Radiotherapy in Practice 2012,11(4):229-238.

[17] Mayo C, Yorke E, Merchant TE. Radiation associated brainstem injury. Int J Radiat Oncol Biol Phys.2010,76:S36-S41.

[18] Mayo C, Martel MK , Marks LB , Flickinger J , Nam J , Kirkpatrick J. Radiation dose-volume effects of optic nerves and chiasm. Int J Radiat Oncol Biol Phys. 2010,76:S28-S35.

[19] Kirkpatrick JP, van der Kogel AJ, Schultheiss TE. Radiation dose-volume effects in the spinal cord. Int J Radiat Oncol Biol Phys. 2010,76:S42-S49.

[20] Marks LB, Bentzen SM, Deasy JO. et al. Radiation dose-volume effects in the lung. Int J Radiat Oncol Biol Phys. 2010,76:70-76.

[21] Matzinger O, Gerber E, Bernstein Z, et al. EORTC-ROG expert opinion. Radiotherapy volume and treatment guidelines for neo-adjuvant radiation of adenocarcinomas of the gastroesophageal junction and the stomach. Radiother Oncol 2009,92:164-175.

[22] Anbumani S, Arunai Nambi Raj N, S Prabhakar G, et al. Quantification of uncertainties in conventional plan evaluation methods in Intensity Modulated Radiation Therapy. J BUON. 2014,19(1):297303.

[23] Gay HA, Niemierko A. A free program for calculating EUD-based NTCP and TCP in external beam radiotherapy. Phys Med 2007,23 (3-4):115-125.

[24] Niemierko, Andrzej. A generalized concept of equivalent uniform dose (EUD). Med Phys.1999,26(6):1100.

[25] Low, D. A., Harms, W. B., Mutic, S., Purdy, J. A. A technique for the quantitative evaluation of dose distributions. Medical physics 1998,25(5):656-661.

[26] Nelms, B. E., Simon, J. A. A survey on IMRT QA analysis. Journal of applied clinical medical physics 2007,8(3):76-90.

[27] Jeraj Robert, Paul J. Keall, and Jeffrey V. Siebers. The effect of dose calculation accuracy on inverse treatment planning. Physics in medicine and biology 2002,47(3):391.

[28] Zacarias Albert S., and Michael D. Mills. Algorithm for correcting optimization convergence errors in Eclipse. Journal of Applied Clinical Medical Physics. 2009,10(4):3061.

Chapter 3

Treatment plan evaluation by radiobiological methods

3.1 Introduction

The modern technological developments have introduced remarkable improvements in planning and execution of radiation therapy. The IMRT ensures a highly conformal dose distribution to the target and is very beneficial when the target and the critical structures are situated near or overlapping each other [1]. The conformal treatment plans are produced by an inverse planning optimization algorithm associated with a TPS. Depending on the number of beams, their directions and given dose constraints, the iterative optimization algorithm generates a solution in the form of treatment plans. Thus, the optimization engine of IMRT planning allows the planner to produce multiple number of treatment plans. Out of these, the best plan is selected by performing a detailed plan comparison.

In the routine clinical practice, different tools are available for the selection of the most suitable treatment plans. A commonly used method for evaluation of treatment plan is by judging physical quantities such as dose and dose-volume parameters. This plan assessment process includes 1) viewing the two-dimensional

dose distributions calculated on CT images and 2) examining DVH for the maximum, mean and / different clinically relevant volume doses for each OARs or tumour. In addition to this, there is another method of evaluation which is based on radiobiological dose-response models. In this assessment, acceptance or rejection of a plan is done by the use of radiobiological indices such as TCP and NTCP. It has been studied that the treatment plans with identical mean, maximum or minimum doses may have significantly different clinical outcomes [2]. This necessitates the use of an additional plan evaluation tool such as radiobiological estimates along with the conventional dosimetric-based evaluation.

In contrast to the three dimensional conformal radiotherapy plans, the dose distribution of IMRT plans is more heterogeneous and complex in nature [3-5]. In order to select an optimum plan, the clinician needs an effective plan comparison method to grade the plans in terms of relevant dosimetric quantities. A detailed investigation of the dose distributions, DVHs and radiobiological estimation will be required for finding the most suitable treatment plan. However, in the current clinical practice, the execution of whole plan assessment methods is a time-consuming task and hence a visual inspection of the dose distribution and DVHs are carried out. In the present study, we have performed the radiobiological methods of evaluation along with the routine physical dose evaluation for a number of patients who were treated in our radiation therapy center. The main purpose of this study was to re-check the comparison of multiple treatment plans obtained for a particular patient by the use of radiobiological response evaluation. We have estimated the TCP and NTCP in both IMRT and VMAT plans and correlated the radiobiological estimations with the physical dose quantities.

3.2 Materials and Methods

3.2.1 Patient plans

A total of 30 patients representing typical cases of Head and Neck (HN), prostate and brain tumours were used in this retrospective planning study. All the plans

were designed on Eclipse TPS (Varian Medical Systems, Palo Alto, CA, USA), Version 10.0, using Anisotropic Analytical dose calculation Algorithm. These treatment plans were selected at random from the cohort of patients with different carcinomas, who had already completed their treatments with use of a Varian Clinac-iX LINAC with a 120 leaf millennium multi leaf collimator (Varian Medical Systems, Palo Alto, CA). Three sets of plans (namely: plan 1, plan 2 and plan 3) along with a clinically approved and verified plan (final plan) were studied for each patient. These competing plans were generated by using slightly different objective functions, which may be considered acceptable. All four plans of one patient were prepared in the same type of technique (IMRT/VMAT). Our 10 cases of each group consisted of 5 patients with IMRT technique and 5 patients with VMAT technique. Thus, a total of 120 treatment plans from 30 patients were selected for analysis, which contained both IMRT and VMAT plans in equal number. The IMRT plans generally consisted of either seven or nine static beams, where as the most of VMAT plans were created by using two arcs (either full or partial) rotating in opposite directions. All of the investigated prostate cases were treated with a dose of 250 cGy / fraction, giving a total dose of 7000 cGy. The HN patients were treated with 212.1 cGy / fraction (total dose = 7000 cGy). The prescription dose for brain cases was 5000 cGy delivered in 25 fractions (phase 1) followed by 1000 cGy in another 5 fractions (phase 2). Figure 3.1 depicts the typical dose distributions of the HN, prostate and brain treatment plans.

3.2.2 Plan analysis

Plans in each group were compared against their final plan by DVH analysis. The PTV of each site included its primary tumour. Other high and low risk lymph nodes were also delineated, but were not included in the present dosimetric study. For target coverage, at least 95% of the PTV should receive at least 95% of the prescribed dose. We have analyzed the dose to 95% of the volume ($D_{95\%}$) for all PTVs and the D_{max} or mean dose (D_{mean}) / dose to volumes of different

Table 3.1: Normal tissue tolerance doses used in the study.

Organs	Dose values [cGy]		References
Brainstem	D_{max}	5400	[6]
Optic chiasm	D_{max}	5500	[7]
optic nerve	D_{max}	5500	[7]
Spinal cord	D_{max}	5000	[8]
Cochlea	D_{mean}	4500	[9]
Mandible	D_{max}	7000	[10]
Lens	D_{max}	1200	[11]
Parotid	D_{mean}	2500	[12]
Small bowel	D_{max}	5200	[13]
Bladder	V_{50}	6500	[14]
Rectum	V_{50}	5000	[15]
Femoral head	D_{max}	5200	[10]

OARs. During the treatment planning process, various OAR dose constraints were used as per RTOG and Quantitative Analysis of Normal Tissue Effects in the Clinic (QUANTEC) protocols. These constraints included no more than 50% of bladder volume to receive a dose greater than 6500 cGy ($V_{50} \leq 65\%$), no more than 50% of rectum to receive a dose of 5000 cGy ($V_{50} < 50\%$) and different D_{max}/D_{mean} for rest of the OARs. All these figures are summarized in Table 3.1 [6-15].

For the comparison of treatment plans, a radiobiological based plan evaluation was also carried out. There are different models available in literature for the prediction of tumor cure and normal tissue complication probabilities [16-20]. In the present study, we have used EUD based radiobiological modelling, which is very effective in predicting the effect of more heterogeneous dose distributions [21]. The EUD is the uniform dose that gives the same radiobiological effect, if delivered over the same number of fractions as does the non-uniform dose distribution of interest. According to Niemierko's model, the EUD is given by [21-22]

$$EUD = \left(\sum_{i=1} (v_i D_i^a) \right)^{\frac{1}{a}} \tag{3.1}$$
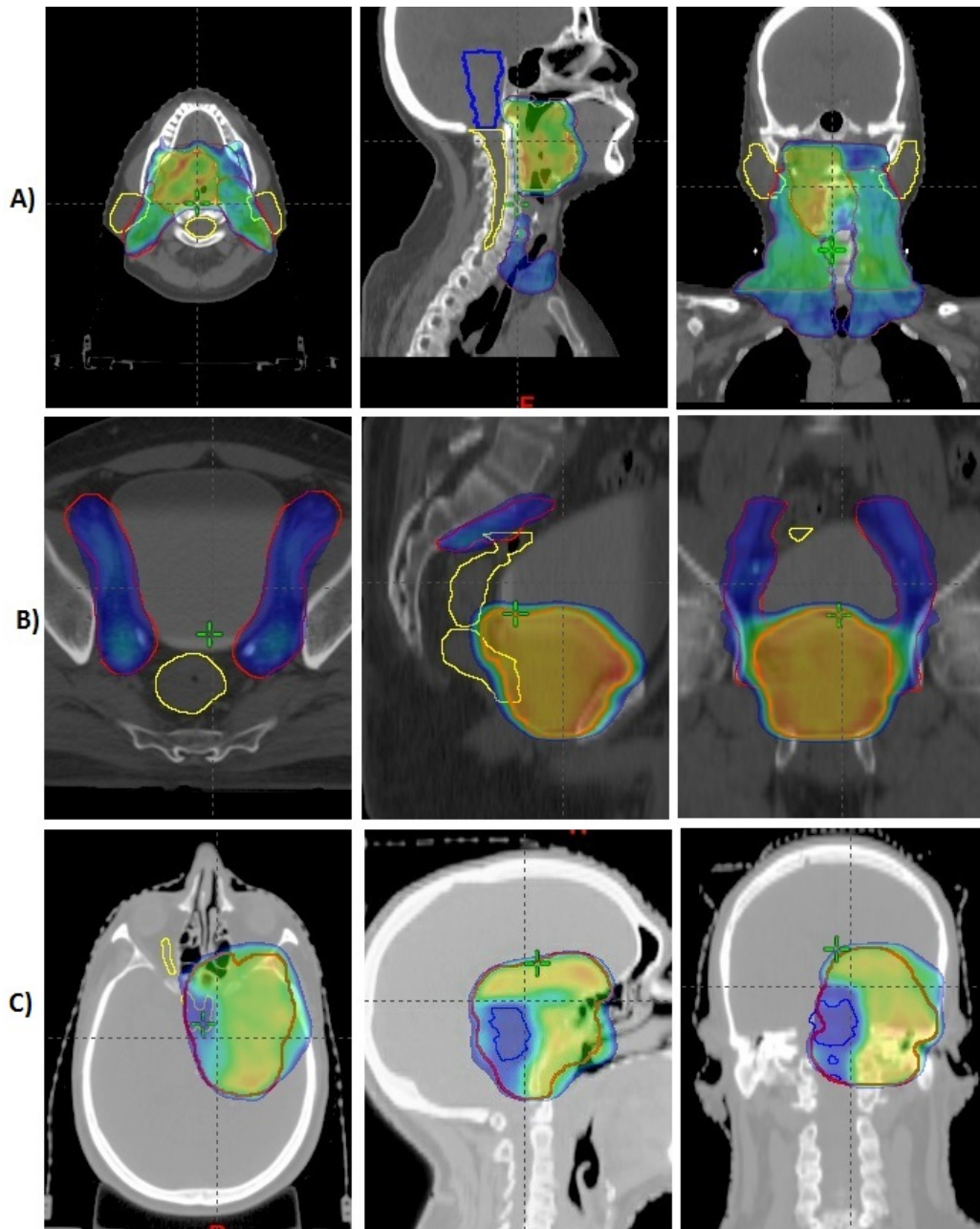
Figure 3.1: Axial, sagittal and coronal views (from left to right) of color washed isodose distributions of A) HN, B) prostate and C) brain treatment plan.

where a is a unitless tissue-specific parameter, whose value is negative for tumors and positive for normal structures. If a = 1, the EUD is the mean dose. v_i is also unitless and represents the ith partial volume receiving a dose D_i in Gy. The TCP and NTCP are calculated from the EUD as follows [21]:

$$TCP = \frac{1}{1 + \left(\frac{TCD_{50}}{EUD} \right)^{4\gamma_{50}}} \tag{3.2}$$

$$NTCP = \frac{1}{1 + \left(\frac{TD_{50}}{EUD} \right)^{4\gamma_{50}}} \tag{3.3}$$

The TCD_{50} is the tumor dose required for control of 50% of the tumor, and TD_{50} is the tolerance dose for a 50% complication rate at a specific time interval when the whole organ of interest (tumor or normal tissues) is homogeneously irradiated. γ_{50} is a dimensionless (%/%) parameter that describes the slope of the dose-response curve. It is also specific to both normal tissues and tumors. The parameters TCD_{50} and γ_{50} are obtained by fitting the clinical dose-response data to the EUD-based models.

The EUD-based TCP and NTCP were calculated by the use of a MATLAB program (The MathWorks, Inc., Natick, MA, USA) [21]. This program requires cumulative DVH data along with various radiobiological factors such as TCD_{50}, TD_{50}, a, and γ_{50}. The values of these factors used in this study are summarized in Table 3.2 (Values of radiobiological parameters were obtained from various publications [23 - 27]).

3.2.3   Statistical analysis

For examining the significance of the results obtained during plan comparison, statistical tests have been carried out. The variations in both target coverage

Table 3.2: List of parameters used for calculation of EUD-based TCP and NTCP.

Structure set	Volume type	End point	a	TCD_{50}/ TD_{50}	γ_{50}	α/β	References
HN-PTV	Tumor	-	-13	51.77	2.28	10	[23]
Prostate-PTV	Tumor	-	-10	28.34	1	1.2	[24]
Brain-PTV	Tumor	-	-8	27.04	0.75	10	[25]
Brainstem	Normal	Necrosis	7	65	3	2.1	[21,26]
Spinal cord	Normal	Myelitis	13	66.5	4	2	[21,27]
Parotid	Normal	Xerostomia	0.5	46	4	2	[23]
Mandible	Normal	Reduced joint junction	10	72	4	3.5	[23]
Bladder	Normal	Volume loss	2	80	4	8	[24]
Rectum	Normal	Necrosis	8.33	80	4	3.9	[24]
Femoral head	Normal	Necrosis	4	65	4	0.85	[24]
Small bowel	Normal	Obstruction	6	55	4	3	[23]
Optic chiasm	Normal	Blindness	25	65	3	3	[21,26]
Optic nerve	Normal	Blindness	25	65	3	3	[21,26]
Lens	Normal	Cataracts	3	18	1	1.2	[21]
Cochlea	Normal	Chronic serous otitis	31	65	3	3	[23]

and OAR doses across four plans were statistically studied by using one way ANOVA. The differences between data were considered statistically significant, if denoted by small p values (< 0.05). Also, the correlation between physical and radiobiological dose indices was calculated by parametric Pearson tests and the correlation coefficients were found statistically significant for p-value less than 0.05.

3.3 Results

The treatment plan DVHs are compared for all the investigated plans. The detailed analysis of DVH data results in the following dosimetric information. Figure 3.2 compares the target coverage of different plans in terms of both the $D_{95\%}$ and EUD of the PTVs for all treatment sites. It is observed that, the values of $D_{95\%}$ and EUD increased in the final plan while comparing with that of other plans. The observed maximum differences in the average values of $D_{95\%}$ between final plan and a plan in the same group were 0.85 %, 2.11 % and 3.14
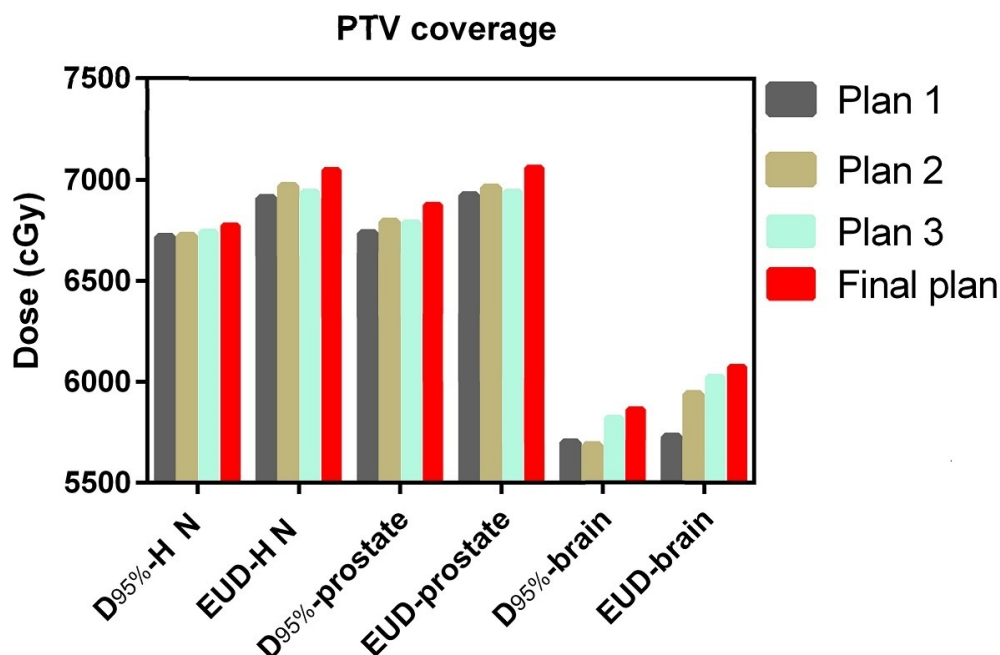
Figure 3.2: PTV coverage in terms of $D_{95\%}$ and EUD for different plans in each study group.

% for the HN, prostate and brain plans respectively. The corresponding EUD values of PTV were 1.99 %, 1.97 % and 6.04 % for the above study groups. The comparison results of physical and biological dose indices of various OARs were shown in Table 3.3 in terms of average $\pm$ standard deviation dose values. The study is also extended between IMRT and VMAT plans of each group of patient. The maximum percentage differences of $D_{95\%}$ of PTV in VMAT plans were 2.1 %, 2.5 % and 2.3 % for HN, prostate and brain cases respectively. However, the corresponding deviations of IMRT plans were 0.86 %, 0.85 % and 0.91 % only. The radiobiological estimation of EUD and TCP showed a similar behaviour. The estimated maximum percentage variations in EUD (TCP) of VMAT plans were 2.3 % (1.4 %), 2.6 % (0.25 %) and 12.4 % (4.8 %) and those of IMRT plans were 1.9 % (0.9 %), 1.3 % (0.14 %) and 0.52 % (0.13 %) respectively, for the above study groups.

Table 3.3: Detailed report on comparison between different dose values and EUD for various OARs across all 4 plans in each group. Statistical analysis, one way ANOVA was carried out. No statistically significant variations in dose figures were observed (p > 0.05).

Study groups	Structure set	Dose indices	Average ± standard deviation dose values in cGy				p value
			Plan 1	Plan 2	Plan 3	Final plan	
HN	Brainstem	D_{max}	4975.8±289.8	4929.1±381.7	4946.6±359.9	5010.0±228.9	0.6739
		EUD	2733.4±406.9	2705.4±409.4	2742.0±348.1	2743.9±371.4	0.6086
	Spinal cord	D_{max}	4233.3±305.1	4283.0±327.2	4200.5±357.0	4239.8±297.8	0.3053
		EUD	2735.5±280.5	2689.5±270.6	2659.5±308.4	2733.6±306.6	0.1829
	Right parotid	D_{mean}	3632.3±836.2	3667.6±315.0	3688.1±816.4	3537.0±845.9	0.1859
		EUD	2714.3±946.1	2733.2±926.3	2754.5±936.2	2762.5±825.1	0.7449
	Left parotid	D_{mean}	3620.5±651.8	3608.6±660.5	579.5±684.3	3564.9±689.7	0.4689
		EUD	2676.0±677.0	2659.0±690.6	2657.8±721.7	2621.7±720.2	0.5694
	Mandible	D_{max}	7426.3±348.2	7498.5±390.7	7502.7±376.3	7372.4±307.0	0.1724
		EUD	5675.2±551.8	5720.0±537.3	5699.5±556.8	5632.7±518.1	0.2658
Prostate	Bladder	V_{50}	4110.2±451.1	4104.7±441.3	4083.2±477.6	4161.8±401.2	0.8434
		EUD	3976.7±433.8	4014.9±426.6	3992.2±431.4	4024.2±416.0	0.6061
	Rectum	V_{50}	4284.7±669.5	4198.0±583.0	4165.2±595.7	4258.5±518.2	0.5301
		EUD	5311.7±367.2	5367.1±386.7	5439.2±322.2	5401.5±276.7	0.1171
	Right femoral head	D_{max}	4607.8±459.3	4703.7±365.2	4658.1±433.2	4708.8±383.9	0.6116
		EUD	1793.2±404.5	1810.8±372.0	1832.0±339.0	1817.5±312.3	0.6234
	Left femoral head	D_{max}	4703.9±417.8	4689.5±434.9	4640.7±577.1	4722.8±439.5	0.7252
		EUD	1763.9±475.1	1817.3±377.3	1798.1±344.8	1787.0±324.6	0.5428
	Small bowel	D_{max}	5495.3±818.9	5632.5±572.8	5525.0±652.1	5634.6±576.7	0.5934
		EUD	3085.6±333.8	3141.4±227.1	3127.1±268.5	3147.9±238.1	0.3561
Brain	Brainstem	D_{max}	5358.1±520.2	5368.6±537.0	5410.6±531.9	5353.2±544.9	0.4714
		EUD	3852.4±1215.1	3838.8±1198.2	3813.8±1002.4	3708.6±1081.8	0.5353
	Optic chiasm	D_{max}	5153.3±522.9	5096.8±494.9	5074.5±452.0	5105.5±432.8	0.5093
		EUD	4335.3±996.0	4384.1±754.4	4353.0±727.6	4392.3±710.8	0.8439
	Right optic nerve	D_{max}	3911.2±1770.9	3838.9±1726.2	3732.8±1739.4	3913.0±1695.9	0.2527
		EUD	3044.4±1737.8	2989.4±1674.7	2857.3±1490.3	2897.8±1461.4	0.2844
	Left optic nerve	D_{max}	4532.1±1888.2	4546.9±1902.8	4137.5±2102	4485.6±1916.3	0.3660
		EUD	3822.9±1864.3	3847.6±1893.2	3637.0±1786.2	3624.3±1779.6	0.1316
	Right lens	D_{max}	765.1±301.5	797.8±351.8	840.7±359.8	796.5±343.8	0.3022
		EUD	295.0±124.2	310.7±160.6	329.6±166.7	301.9±148.1	0.2435
	Left lens	D_{max}	1004.5±551.0	1009.6±547.9	1018.1±531.9	1001.6±538.0	0.8828
		EUD	415.7±285.4	431.8±300.6	431.4±337.7	428.2±333.9	0.7383
	Right cochlea	D_{mean}	3659.7±2424.8	3632.1±2448.2	3602.2±2400.5	3635.0±2433	0.6530
		EUD	2982.5±2292.5	2913.5±2295.3	2789.2±2100.2	2785.2±2138.3	0.2720
	Left cochlea	D_{mean}	4309.1±2657.4	4244.6±2724.6	4207.5±2737.8	4222.5±2732.8	0.1923
		EUD	3916.2±2694.3	3736.6±2625.8	3741.2±2642.0	3708.8±2641.7	0.1970

3.4 Discussion

The overall objective of this retrospective study is to check the acceptability of treatment plans by incorporating the radiobiological evaluation tools. The results of the dosimetric comparison of 120 radiotherapy plans, at various sites support the plan assessment process in the routine practice. Even though all four plans showed passable dose distributions from the dosimetric point of view, the final plan had more acceptable dose distribution when compared to other plans. This study revealed that the final plans showed higher target coverage, which is represented in terms of $D_{95\%}$ and EUD of PTV. The main aspect of this study is the use of radiobiological model for the treatment plan comparison. Radiobiological methods were reported to be effective in the plan evaluation process in comparison to the use of physical dose metrics alone [20]. The estimated TCP, which is in correlation with the target conformity index [20] did not show any considerable variation along different plans as is evident in Fig.3.3. Although the final plan in each group exhibited a slight improvement in PTV coverage, no statistically significant differences were observed. Based on the doses of various OARs shown in Table 3.3, neither of the plans appears significantly different from the final plan. The calculated NTCPs for most of the structures were found to have little or no variation between the plans, which is clearly shown in Fig.3.4. Though relatively larger differences were observed for certain structures such as mandible, rectum, optic nerves and cochlea, none of these variations were statistically significant. The present study also reported the comparison of treatment plans for both IMRT and VMAT techniques. Figure 3.5 illustrates the maximum % variation of both EUD and physical dose indices of final plan from other plans in IMRT and VMAT techniques. A minute deviation of the dosimetric parameters from final plan to any other plan was noticed for IMRT, whereas the final plans in VMAT technique showed relatively larger deviation from the rest of the plans.

In the current retrospective planning study, we have performed a direct comparison between radiobiological and physical dose indices. The dose coverage of
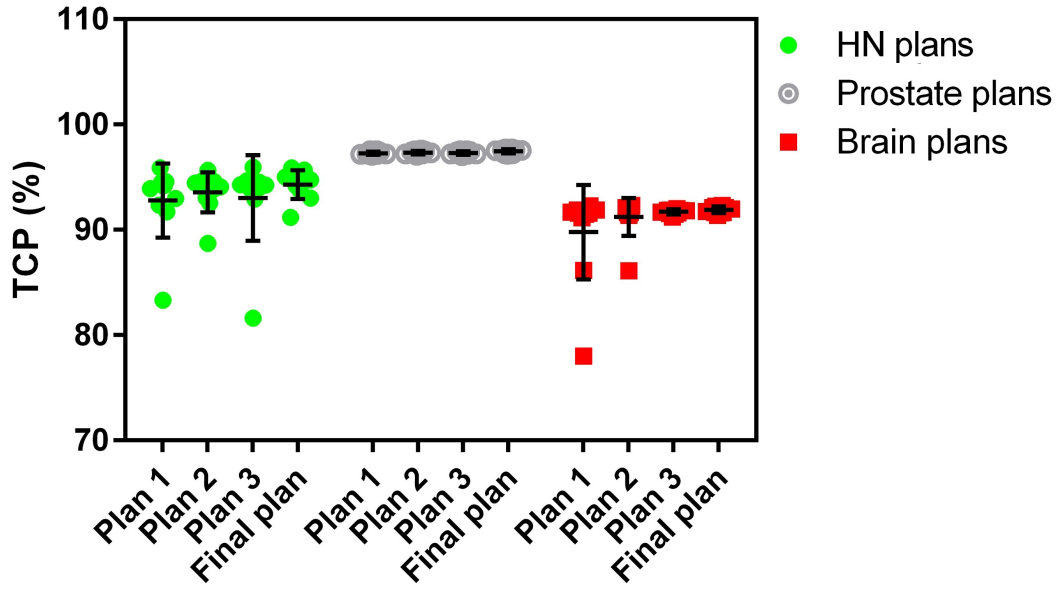
Figure 3.3: Variations in TCP along different plans. No major deviations were observed.

PTVs, in terms of $D_{95\%}$, of all plans was found to be correlated with the estimated TCPs of the corresponding plans, represented by the Pearson correlation coefficients (r). The diagonal elements of Table 3.4 represent a higher correlation between physical and biological dose values of every corresponding plans of each of the patient group. However, the off-diagonal elements denote the correlation of physical dose index of any plan with respect to the biological dose index of every other plan. A relatively lower correlation was noticed in most of these figures, which also confirmed the use of biological index, TCP for dose coverage of PTVs in plan comparison process. Table 3.5 conveys the correlation between physical doses and NTCP of various OARs for final plans. The complication probabilities for different organs such as spinal cord, parotids, mandible, bladder, rectum, small bowel, optic chiasm, right optic nerve, lenses and left cochlea were correlated well with their physical dose indices ($p < 0.05$). However, the correlations of D_{max} received by brainstem in H&N plans and that of femoral head, left optic nerve and the D_{mean} of right cochlea in other plans were deviated more with the radiobiological complication probabilities. The TCP or NTCP values depend on the radiobiological parameters and the dose distribu-
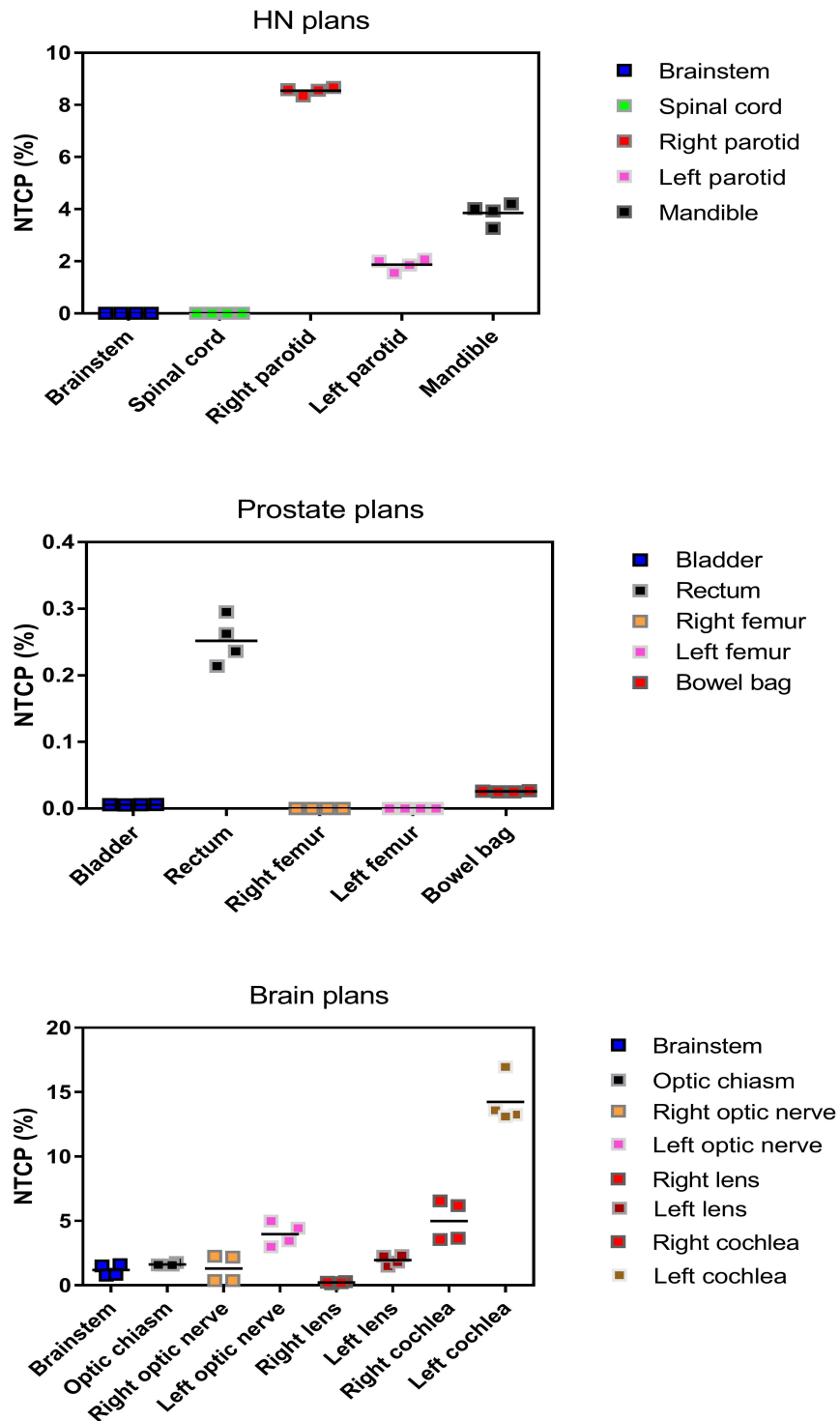
Figure 3.4: Estimated NTCP (%) values of the various OARs were studied and average values for each set of plans were plotted.
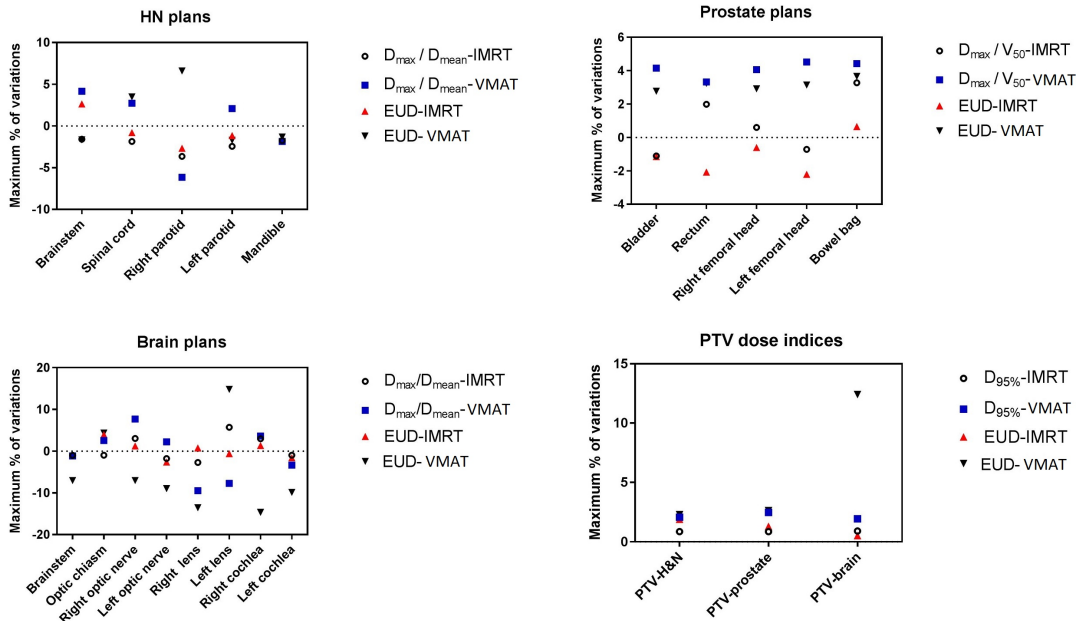
Figure 3.5: Deviation of final plan from other plans of IMRT and VMAT cases in terms of biological and physical dose indices. More discrepancies of target and OAR doses for VMAT plans than for IMRT were observed.

tion of the target or OARs. In this study, the same radiobiological parameters were used for all the plans of a particular group and the varying factor is the dose distribution of individual plans. The normal tissue structures located near or overlapping to the PTV were probably subjected to a significantly increased D_{max}. In some of our investigated plans, the stated structures were found to be adjacent with the PTV and therefore their dose values deviated more with the radiobiological complication probabilities.

Conventional plan evaluation is based on single or multiple dose-volume constraints and one of its limitations is the requirement of more than one dose-volume point for evaluating the complication of a particular organ. During the plan evaluation, the clinician needs to consider the priorities of various dose-volume constraints when some of the constraints pass and other fails. However, radiobiological plan evaluation uses full three dimensional dose distributions, take account of different dose-volume criteria and outputs a comprehensible estimate of biological outcome. Also, the plan assessment by using dose-volume criteria tells that an effect occur or do not occur with respect to certain dose

Table 3.4: Pearson correlation coefficient (r) between TCP and $D_{95\%}$ of different PTVs.

Study groups	TCP→ ↓ $D_{95\%}$	Plan 1	Plan 2	Plan 3	Final
HN-PTV	Plan 1	**0.891**	-0.007	-0.106	-0.185
	Plan 2	0.258	**0.869**	0.063	-0.010
	Plan 3	0.367	0.270	**0.935**	0.161
	Final	0.103	0.200	0.212	**0.921**
Prostate-PTV	Plan 1	**0.575**	0.444	-0.031	-0.124
	Plan 2	0.217	**0.797**	0.242	0.112
	Plan 3	0.582	0.757	**0.538**	0.331
	Final	0.575	0.766	0.460	**0.866**
Brain-PTV	Plan 1	**0.895**	0.769	0.089	-0.014
	Plan 2	0.842	**0.829**	0.234	0.074
	Plan 3	0.116	-0.195	**0.725**	0.668
	Final	0.101	-0.084	0.889	**0.807**

limit. But the biological evaluation gives continuous estimates of tumor cure and organ complication probabilities rather than considering threshold levels in DVHs. Hence, a properly calibrated radiobiological model is recommended as a tool to complement the conventional dosimetric analysis by predicting the radiobiological outcome. It is particularly useful when a clinician needs to select the best plan from competing plans.

The comparison and ranking of treatment plans is of great significance as there are many cases in radiotherapy where multiple treatment plans need to be compared. There are few studies which have reported some ranking methods for plan evaluation and comparison. A study conducted by Miften et al. [5] developed an IMRT plan evaluation and ranking tool based on uncomplicated target conformity index (TCI+). The dose-volume-based indices sum up complex dose distributions to a single index, which can be used to choose the optimal plan. Another study performed by Akpati et al. [28] formulated a Unified Dosimetry Index (UDI) that reckons the deviations between treatment plans. This method uses an equation which is developed by combining different dosimetric objectives such as dose coverage, conformity, homogeneity and dose gradient. However, in this particular study, we have performed a comprehensive radiobiological response evaluation for the comparison of treatment plans whereby it validated

Table 3.5: The correlation between complication probabilities and physical dose values of various OARs. Majority of the above figures are statistically significant.

Study groups	Structure set	Pearson coefficient (r)	p-value
HN	Brainstem	0.542	0.1059
	Spinal cord	0.875	0.0021
	Right parotid	0.889	0.0006
	Left parotid	0.731	0.0163
	Mandible	0.656	0.0393
Prostate	Bladder	0.846	0.0039
	Rectum	0.794	0.0061
	Right femoral head	-0.440	0.1106
	Left femoral head	-0.561	0.0784
	Small bowel	0.938	0.0001
Brain	Brainstem	0.824	0.0034
	Optic chiasm	0.708	0.0328
	Right optic nerve	0.643	0.0449
	Left optic nerve	0.447	0.1954
	Right lens	0.879	0.0307
	Left lens	0.834	0.0027
	Right cochlea	0.496	0.1446
	Left cochlea	0.692	0.0267

the method of selection of competing plans for the treatment. Also, this work is completed on three particular sites, with two treatment techniques, and by using larger set of data that constitute 120 plans.

3.5 Conclusion

This retrospective dosimetric study of IMRT and VMAT plans performed on different groups of patients, validated the use of radiobiological method for treatment plan comparison. The comprehensive radiobiological response study endorses the routine plan evaluation by analysis of isodose distribution and DVHs. For the examined patient cohort, a better target coverage is noticed for final plans in each group, where as no statistically significant differences in physical and biological dose indices of OARs were observed. The estimated biological outcome and DVH analysis indicated that the iterative optimization produces least differences between plans for IMRT when compared to VMAT. The tumor

cure or normal tissue complication probabilities were found to be well correlated with the corresponding physical dose indices.

References

[1] Yu CX. Intensity modulated arc therapy: A new method for delivering conformal radiation therapy. The theory & practice of intensity modulated radiation therapy. Madison, WI: Advanced Medical Publishing. 1997,107-120.

[2] Mavroidis P, Lind BK, Brahme A. Biologically effective uniform dose (D) for specification, report and comparison of dose response relations and treatment plans. Physics in medicine and biology. 2001,46(10):2607-2630.

[3] Mohan R, Wang X, Jackson A, Bortfeld T, Boyer AL, Kutcher GJ, Leibel SA, Fuks Z, Ling CC. The potential and limitations of the inverse radiotherapy technique. Radiotherapy and Oncology. 1994,32(3):232-248.

[4] Vineberg KA, Eisbruch A, Coselmon MM, McShan DL, Kessler ML, Fraass BA. Is uniform target dose possible in IMRT plans in the head and neck? International Journal of Radiation Oncology* Biology* Physics. 2002, 52(5):1159-1172.

[5] Miften MM, Das SK, Su M, Marks LB. A dose-volume based tool for evaluating and ranking IMRT treatment plans. Journal of Applied Clinical Medical Physics. 2004,5(4):1-14.

[6] Mayo C, Yorke E, Merchant TE. Radiation associated brainstem injury. International Journal of Radiation Oncology* Biology* Physics. 2010,76(3Suppl):S36-S41.

[7] Mayo C, Martel MK, Marks LB, Flickinger J, Nam J, Kirkpatrick J. Radiation dose-volume effects of optic nerves and chiasm. International Journal of Radiation Oncology* Biology* Physics. 2010,76(3Suppl):S28-S35.

[8] Kirkpatrick JP, van der Kogel AJ, Schultheiss TE. Radiation dose-volume effects in the spinal cord. International Journal of Radiation Oncology* Biology* Physics. 2010,76(3Suppl):S42-S49.

[9] Bhandare N, Jackson A, Eisbruch A, Pan CC, Flickinger JC, Antonelli P, Mendenhall WM. Radiation therapy and hearing loss. International Journal of Radiation Oncology* Biology* Physics. 2010, 76(3Suppl):S50-S57.

[10] Emami B, Lyman J, Brown A, Cola L, Goitein M, Munzenrider JE, Shank B, Solin LJ, Wesson M. Tolerance of normal tissue to therapeutic irradiation. International Journal of Radiation Oncology* Biology* Physics. 1991, 21(1):109-122.

[11] Rubin P. Law and order of radiation sensitivity: absolute versus relative. In: Vaeth JM, Meyer JL, eds. Frontiers of radiation therapy and oncology. Basel: Karger.1989,7-40.

[12] Deasy JO, Moiseenko V, Marks L, Chao KC, Nam J, Eisbruch A. Radiotherapy dose-volume effects on salivary gland function. International Journal of Radiation Oncology* Biology* Physics. 2010,76(3Suppl):S58-S63.

[13] Lawton CA, Michalski J, El-Naqa I, Buyyounouski MK, Lee WR, Menard C, O'Meara E, Rosenthal SA, Ritter M, Seider M. RTOG GU Radiation oncology specialists reach consensus on pelvic lymph node volumes for high-risk prostate cancer. International Journal of Radiation Oncology* Biology* Physics. 2009,74(2):383-387.

[14] Viswanathan AN, Yorke ED, Marks LB, Eifel PJ, Shipley WU. Radiation dose-volume effects of the urinary bladder. International Journal of Radiation Oncology* Biology* Physics. 2010, 76(3Suppl):S116-S122.

[15] Michalski JM, Gay H, Jackson A, Tucker SL, Deasy JO. Radiation dose-volume effects in radiation-induced rectal injury. International Journal of Radiation Oncology* Biology* Physics. 2010, 76(3Suppl):S123-S129.

[16] Niemierko A. Reporting and analyzing dose distributions: a concept of equivalent uniform dose. Medical physics. 1997,24(1):103-110.

[17] Thames HD, Zhang M, Tucker SL, Liu HH, Dong L, Mohan R. Cluster models of dose-volume effects. International Journal of Radiation Oncology* Biology* Physics. 2004, 59(5):1491-1504.

[18] Lyman JT. Complication probability as assessed from dose-volume histograms. Radiation Research. 1985,8:S13-S19.

[19] Niemierko A, Goitein M. Modeling of normal tissue response to radiation: the critical volume model. International Journal of Radiation Oncology* Biology* Physics. 1993,25(1):135-145.

[20] Anbumani S, Raj NA, Prabhakar GS, Anchineyan P, Bilimagga RS, Palled SR, Chairmadhurai A. Quantification of uncertainties in conventional plan evaluation methods in Intensity Modulated Radiation Therapy. Journal of BU ON.: official journal of the Balkan Union of Oncology. 2014,19(1):297-303.

[21] Gay HA, Niemierko A. A free program for calculating EUD-based NTCP and TCP in external beam radiotherapy. Physica Medica. 2007,23(3):115-125.

[22] Niemierko A. A generalized concept of equivalent uniform dose (EUD). Med Phys. 1999,26(6):1100.

[23] Oinam AS, Singh L, Shukla A, Ghoshal S, Kapoor R, Sharma SC. Dose volume histogram analysis and comparison of different radiobiological models using in-house developed software. Journal of Medical Physics. 2011,36(4):220-229.

[24] Rana S, Cheng CY. Radiobiological impact of planning techniques for prostate cancer in terms of tumor control probability and normal tissue complication probability. Annals of medical and health sciences research. 2015,4(2):167-172.

[25] Jaganathan A, Tiwari M, Phansekar R, Panta R, Huilgol N. Intensity-modulated radiation to spare neural stem cells in brain tumors: a computational platform for evaluation of physical and biological dose metrics. Journal of cancer research and therapeutics. 2011,7(1):58-63.

[26] Kehwar T. S. Analytical approach to estimate normal tissue complication probability using best fit of normal tissue tolerance doses into the NTCP equation of the linear quadratic model. Journal of cancer research and therapeutics. 2005,1(3):168-179.

[27] Rana S, Rogers K. Radiobiological evaluation of dose calculation algorithms in Rapid Arc planning of esophageal cancer treatment plans. Journal of Solid Tumors. 2013,3(3):44-52.

[28] Akpati HC, Kim C, Kim B, Park T, Meek A. Unified dosimetry index (UDI): a figure of merit for ranking treatment plans. Journal of Applied Clinical Medical Physics. 2008,9(3):99-108.

Chapter 4

Quality Assurance of Linear Accelerator using Electronic Portal Imaging Device

4.1 Introduction

Radiation therapy has been carried out in our institution since 2011 with a medical LINAC capable of treating patients by use of different treatment techniques. In addition to 3D conformal techniques, IMRT and VMAT are the standard modalities of treatment in the radiation therapy centre of the institution. The higher complexity in planning and delivery of radiation therapy require more rigorous QA for the machine and treatment plan. There are various recommendations for dosimetric, mechanical and radiation safety QA tests pertaining to the machine. The AAPM - Task Groups reports, TG 40 and TG 142 describe various QA tests and their tolerances according to the periodicity such as daily, monthly and annually [1-2]. These reports also provide directions to the physicist for customizing the QA program and designing an institutional protocol. The QA protocol followed by our institution is summarized in the Table 4.1. Pre-treatment QA is also recommended for treatment fields per individual pa-

tient plans [3-4]. Traditionally, various radiation detectors such as ionization chamber, film and different commercially available array detectors are used for the QA checks. These QA methods are time consuming, expensive and require excess resources. Moreover, in all of these methods, the analysis reports may not be made readily available with the patient treatment chart.

Amorphous silicon EPID replaces radiographic film images for patient treatment verification. Its role in 2D dosimetry is quite significant for the last ten years. Several studies have reported the use of portal dosimetry in the verification of treatment fields [5-9]. Being a real-time dosimeter having good resolution and requiring only minimum set-up time, EPID is preferable for periodic machine QA tests [10-12]. A study performed by Elmpt [13] reviewed information provided in various publications including the characteristics of EPIDs of different vendors, their calibrations, EPID 2D dosimetry, etc. Despite its capability for wide range of QA applications, there is still an uncommonness of clinical use due to the shortage of commercially available EPID dosimetry solutions. This can be resolved by developing codes in MATLAB program (The MathWorks, Inc., Natick, MA, USA), even if the dosimetry software is not available in the institution.

The present study aims to assess the feasibility of using EPID for various QA tests in radiation therapy. The analysis was carried out on three years of QA data of IMRT patients and the machine (Clinac-iX) through indigenously developed MATLAB programs.

4.2 Materials and Methods

The measurements were performed using Varian Clinac-iX LINAC (Varian Medical Systems, Palo Alto, CA, USA), having 6 MV and 15 MV photon energy modes. The machine was equipped with 60 leaf pairs MLC having widths 0.5 cm for the inner 40 pairs and 1.0 cm for the outer 20 pairs at the iso-centre of the LINAC. IMRT and VMAT treatments were performed by using 6 MV photons

with a maximum dose rate of 600 MU/Min. The LINAC was calibrated to deliver 1 cGy corresponds to 1 MU at depth of maximum dose, field size of 10 x 10 cm^2 and source to surface distance of 100 cm. Portal Vision aS1000 (Varian Medical Systems, Palo Alto, CA, USA) is an amorphous silicon flat panel detector with an active imaging area of 40 x 30 cm^2 and with resolution of 1024 x 768 pixels. The EPID was attached to a retractable arm and calibrated according to the vendors specifications. The response corresponds to 100 MU delivered by a 10 x 10 cm^2 radiation field at 100 cm Source to Detector Distance (SDD) was defined as 1 calibrated unit. The centre of the detecting surface of the EPID was aligned to the LINAC cross-wire and all images were acquired at SDD of 100 cm without any additional build up. Portal dosimetry software enables image acquisition mode for recording fluence patterns of IMRT and VMAT fields, image viewing and analysis.

4.2.1 Software tools

This study was performed by using different software tools developed in our department with the help of MATLAB for image analysis. They are 1) dailyqa_prof.m, 2) fwhm_cal.m and 3) fluence_comparison.m. These programs are capable of determining flatness, symmetry, output constancy, Field Width at Half Maximum (FWHM) and fluence comparison in a simple fashion. The programs require images from TPS and portal dosimetry in .jpg format. MLC shaper software (Varian Medical Systems, Palo Alto, CA, USA) was used to edit and create customized MLC patterns. Treatment and QA plans were generated on Eclipse (Varian Medical Systems, Palo Alto, CA, USA) TPS. For the scientific interpretation of results, statistical tests have been carried out. We have used Pearson correlation coefficient (r) for checking the correlation of the data sets using GraphPad prism (Graphpad software, San Diego, CA, USA, version 6.07) and the equivalence was considered significant for p values < 0.05.

4.2.2 Comprehensive Quality Assurance program

The periodic QA checks are conducted to ensure that the machine characteristics do not deviate significantly from baseline values, obtained at the time of commissioning of LINAC. Out of various checks described in Table 4.1, the measurements and analysing methods of the QA tests in our study was as follows.

4.2.3 Profile and output constancy

A quick measurement of output of photon beam was taken daily using EPID before patient treatment begins. This QA procedure involves checks on X and Y profiles of 6 MV photon beam. A field of 20 x 20 cm^2 with uniform fluence was prepared by using MLC shaper and was imported as MLC file into a TPS plan prepared with a single field. This plan was delivered on EPID and the measured fluence map was saved in portal dosimetry in .jpg format. This measured fluence was used for the calculation of flatness, symmetry and central axis dose variations of the beam by the use of the program, dailyqa_prof.m. The input of the MATLAB program is an image of fluence measured by EPID. One point each in four corners of the measured fluence map was defined by the user in order to draw multiple profiles of 0.5 cm apart along X and Y directions on the fluence plane. Flatness and symmetry were calculated along each and every line by using the following equations [14-15] and the average value was displayed.

$$Flatness = \frac{R_{max} - R_{min}}{R_{max} + R_{min}} \times 100\% \tag{4.1}$$

$$Symmetry = \frac{R_L - R_R}{R_L + R_R} \times 200\% \tag{4.2}$$

Where R_{max} and R_{min} are the maximum and minimum readings along the profile within 80% of the field size. R_L and R_R denote readings at two symmetric points left and right or inferior and superior of X and Y profiles respectively. Flatness and symmetry calculations were done as per recommendations of International Electro Technical Commission (IEC) 60976. The given program is

also able to write the results in to Excel spread sheet every day. These steps are shown in Figures 4.1 & 4.2. The daily measured flatness and symmetry were compared with the standard readings, measured after tuning the machine. Output constancy was measured from the central reading of the above fluence map and was compared with the standard value. A more accurate investigation on output constancy of photon beam was performed in every week with a calibrated farmer type ionization chamber (FC65-G) and solid plate phantom (IBA Dosimetry, Schwarzenbruck, Germany). Output constancy was measured with a fixed set up (SSD=100 cm, depth=5 cm, field size = 10x10 cm^2) every Saturday and compared against the daily constancy of the average readings from Monday to Friday.

4.2.4 Quality Assurance of Multi-leaf Collimator

Extensive monthly QA protocol of the institution mainly consists of different MLC checks along with a few mechanical tests. There are several methods available in literature to verify the performance of dynamic MLC (dMLC) [16-18]. The modulation characteristics of intensity modulated beam is determined by position and the speed of MLC leaves. As an initial check of above parameters, MLC patterns were produced by delivery of radiation through arbitrary MLC shapes with varying width and modulation. We have randomly created different shapes with the help of MLC shaper tool and stored in TPS as MLC QA plans. These patterns are shown in Figure 4.3, which include the shapes of alphabets such as L, T, N, Z, S, O, H and projections such as star, triangle and arrow. The accuracy of dMLC in producing complex intensity modulated fluence in different plans was verified with above patterns. Delivered fluence was captured by portal dosimetry software and was studied with corresponding TPS fluence. Field widths at different arms of above patterns were compared with those between planned coordinates (from MLC shaper), computed dose maps (from TPS) and measured fluence maps (from EPID). In-house developed stand-alone MATLAB code, fwhm_cal.m was used for the analysis. Two positions outside the width of

Figure 4.1: Daily analysis of flatness and symmetry along X and Y profiles using MATLAB program.

Sl. No.	Date	X-flatness	X-symmetry	Y-flatness	Y-symmetry
1	01-11-2016	0.4270	0.2948	1.1949	0.2143
2	02-11-2016	0.3947	0.1429	0.4665	0.2588
3	03-11-2016	0.3759	0.2859	1.0542	0.0714
4	04-11-2016	0.4301	0.0714	0.4738	0.1572
5	07-11-2016	1.3008	0.1638	1.3618	0.1311
6	08-11-2016	1.8541	0.1429	1.8119	0.2358
7	09-11-2016	1.2372	0.3066	0.4380	0.1748
8	10-11-2016	1.7798	0.0786	0.4820	0.2185
9	11-11-2016	0.3760	0.1429	0.5997	0.2859
10	14-11-2016	1.1629	0.1572	0.3954	0.2143

Figure 4.2: Results of daily analysis of flatness and symmetry along X and Y profiles.

the fields were needed to be inputted by the user to define the required fields. The comparison process is illustrated in Figure 4.4. Apart from this, other MLC QA such as picket fence, garden fence and leaf speed stability tests were carried out using films to assure the leaf position accuracy and reproducibility of the gap between leaves. These QA checks were not included in the present dosimetric study.

4.2.5 Patient-specific Quality Assurance

Patient-specific QA have been performed for all IMRT and VMAT patients by using either EPID or 2D array detectors. MatriXX 2-D (IBA Dosimetry, Schwarzenbruck, Germany) ionization chamber array system consisting of 1020 vented chambers was used for all pre-treatment QA till the end of 2013. The volume of each detector was 0.08 cm^3. The spatial resolution of the detector array was 7.6 mm and inherent water equivalent build-up thickness was 3.2 mm. The QA plan was calculated with a solid phantom in Eclipse TPS and was transferred to the OmniPro IMRT (IBA Dosimetry, Schwarzenbruck, Germany) verification tool. These plans were delivered to the detector and the measured dose maps were compared with the corresponding TPS computed dose maps.
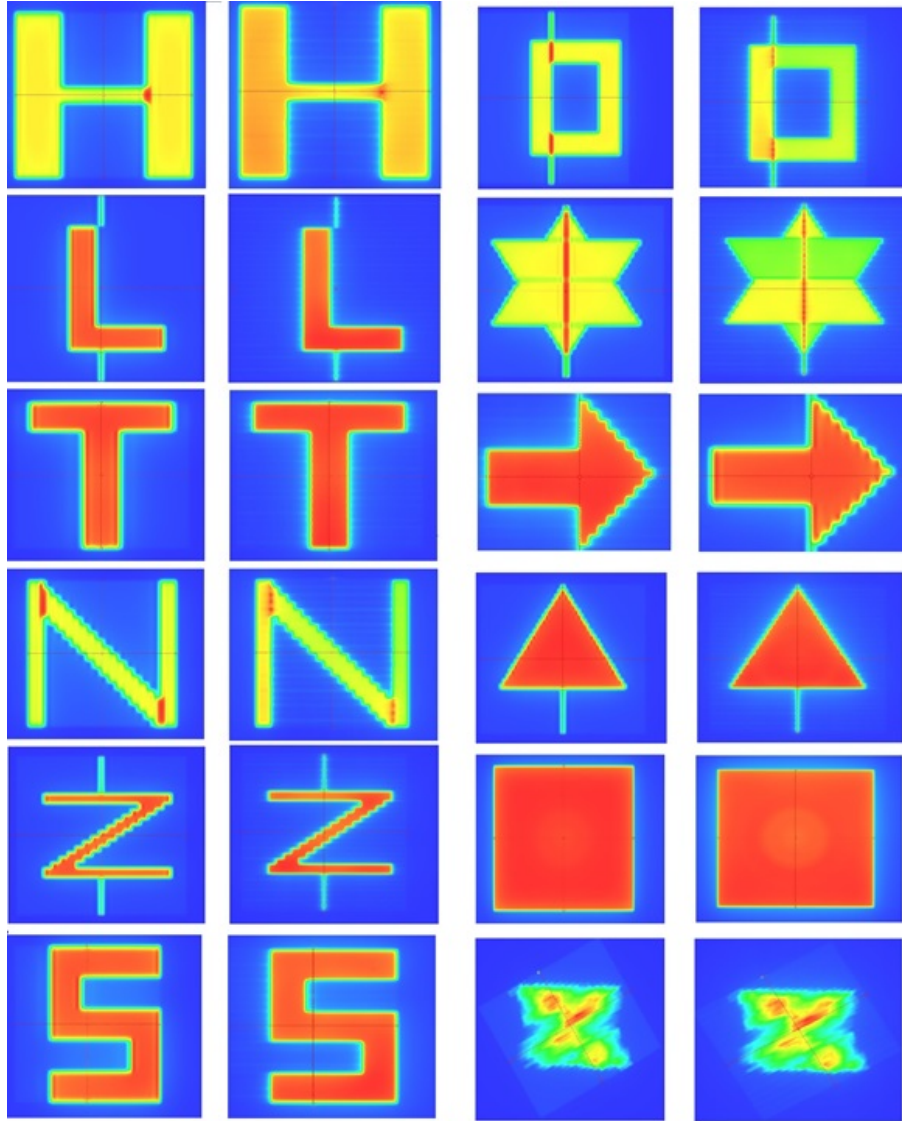
Figure 4.3: Fluence maps of different MLC shapes created with the help of MLC shaper. First and third columns represent the fluence maps from TPS and second and fourth columns represent fluences measured by EPID.
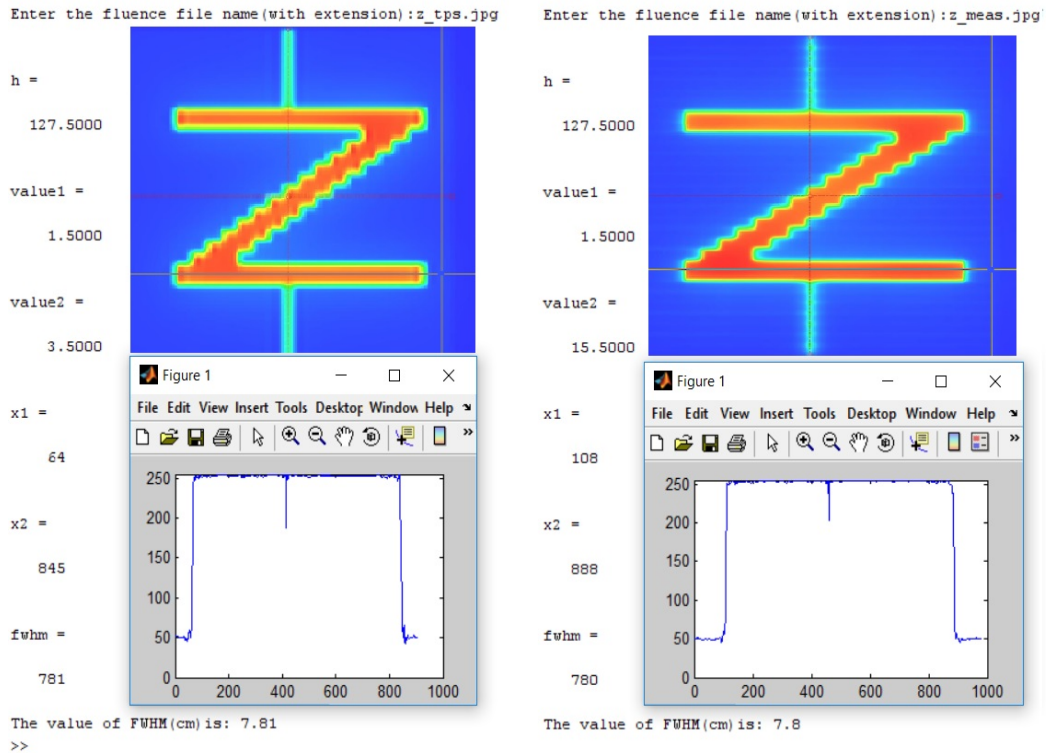
Figure 4.4: Comparison of TPS computed and EPID measured fluences of an MLC pattern (Z shape). FWHM is calculated and displayed.

The MatriXX 2D array detector demands more human resource and time in the large patient specific QA workload. In such a case, EPID is an efficient option for patient-specific QA [6-9], because of its least set-up time and better spatial resolution compared to 2D array detectors [8]. Most of the patient QA was done with EPID and selective cases were re-measured with MatriXX 2D array. Three years of QA data from four anatomic regions, pelvis, thoracic and abdomen, HN and brain was studied. EPID based QA of these 80 IMRT plans consisted of 20 patients in each group were also measured and studied retrospectively by using 2D array detector. The quantitative evaluation was performed in terms of the gamma index [19] of the measured against the TPS-calculated fluence. Percentage value of gamma with a value less than one was calculated for all points in the fluence map. The standard passing criterion of 3 % for dose difference and the 3 mm for distance to agreement (3 % / 3 mm) were used for analysis [20]. The minimum, 25% percentile, median, 75% percentile, maximum, mean

and standard deviation for the gamma values were calculated and tabulated. The correlation of measured data between EPID and 2D array was analysed by Pearson test and correlation coefficients were calculated. The measured EPID fluence of some of these patients was also checked by using indigenously developed image comparison tool, fluence_comparison.m. This program required two images, 1) TPS calculated and 2) EPID measured with user defined origin for both images. Difference of two images was taken and percentage pixel differences were calculated, as shown in Figure 4.5.

4.3   Results

4.3.1   Profile and output constancy

The average values of flatness and symmetry along X axis were 0.8481 ± 0.0895 and 1.148 ± 0.1813 and those along Y axis were 0.9700 ± 0.1503 and 1.2155 ± 0.3141. The institutional data is plotted over three years which is illustrated in Figure 4.6. Daily output of 6 MV photon beam was found to be correlated with the weekend value obtained through solid phantom measurements. The data drift is plotted in the consecutive weeks for all three years and a good correlation was observed which is plotted in Figure 4.7. Pearson correlation coefficient (r) is 0.941 (p=0.0001), 0.888 (p=0.0188) and 0.917 (p = 0.0007) for the years of 2014, 2015 and 2016 respectively.

4.3.2   Quality Assurance of Multi-leaf Collimator

The accuracy of dMLC while shaping the complex IMRT fields was studied and verified. The comparison data in terms of FWHM at different portions of various fields showed good agreement between TPS generated and EPID measured MLC positions. Maximum deviation was 2.9%, obtained for triangle shape. The width of fields planned by MLC shaper was also compared with EPID measured FWHM and found in correlation with each other. A slightly higher variation is observed
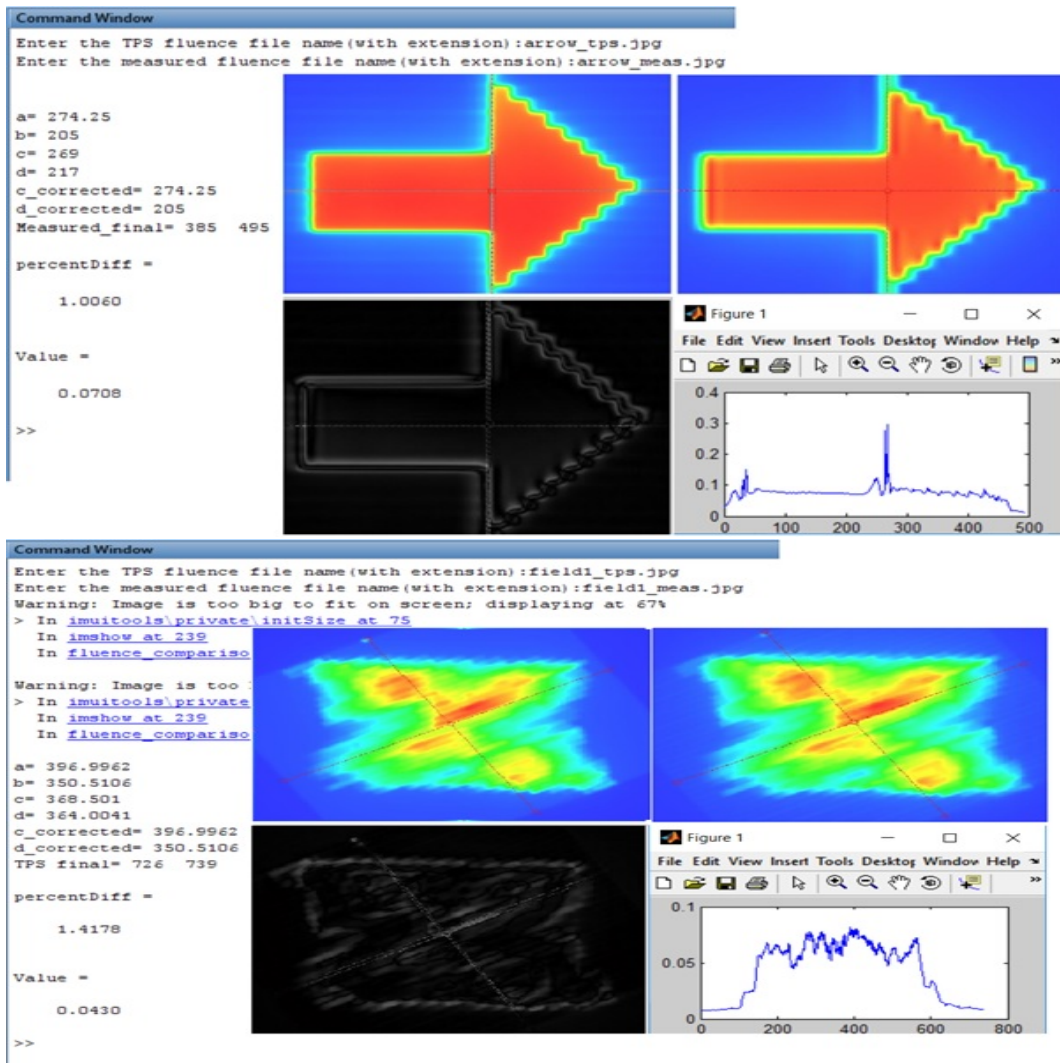
Figure 4.5: Image comparison between TPS generated and EPID measured 2D fluences of an MLC shape and a patient specific QA plan. Percentage difference and root mean square error are also calculated by using MATLAB program.

Table 4.1: Customized QA protocol.

Frequency	Procedure	Tolerance
Daily	Dosimetry	
	Photon beam output and profile constancy	3%
	Mechanical	
	Laser localization and optical distance	
	indicator	1.5 mm /2 mm
	Safety	
	Door interlock, Audiovisual monitor and	
	Beam on indicator	Functional
Weekly	Dosimetry	
	Photon and electron beam output constancy	3%
	Mechanical	
	Collimator size indicator and Jaw position	
	indicators (symmetric and asymmetric)	2 mm
Monthly	MLC QA	
	MLC transmission factor measurement	
	Picket fence, garden fence tests	
	Leaf position accuracy tests in producing complex fields	
	Leaf speed stability	
	Mechanical	
	Light/radiation field coincidence	1 mm / 1% on a side
	Localizing lasers, Gantry / collimator angle	
	indicators and couch position indicators	1 mm /1 deg
Annual	Dosimetry	
	Photon and electron beam flatness and symmetry	
	changes from baseline	1%
	Photon / electron calibration (TRS-398)	$\pm 1\%$
	Photon beam quality (TPR20/10)	
	and electron beam quality ($R_5 0$)	$\pm 1\%$
	Photon output constancy Vs dose rate	$\pm 2\%$
	Photon and electron beam output	
	constancy Vs gantry angle	$\pm 1\%$
	Mechanical	
	Gantry / collimator /couch rotation isocenter	± 1 mm
	Coincidence of radiation and mechanical isocenter	± 2 mm
	Table top sag	2 mm
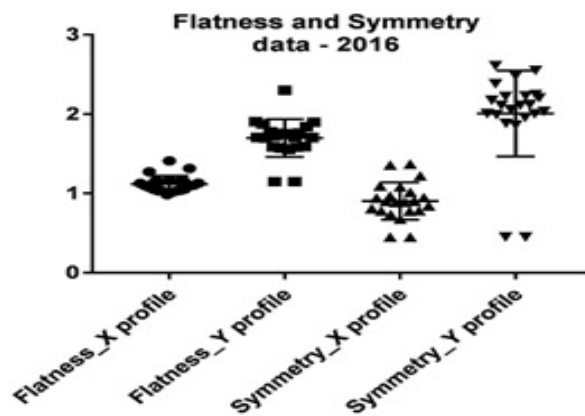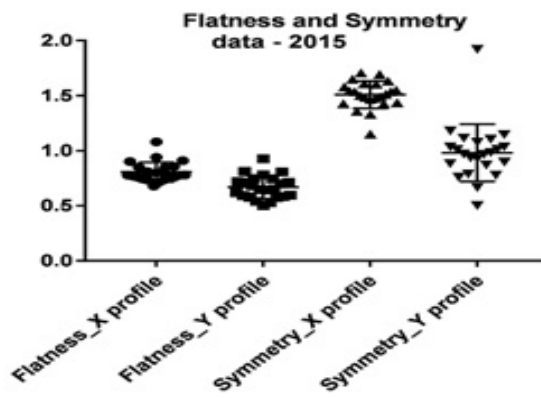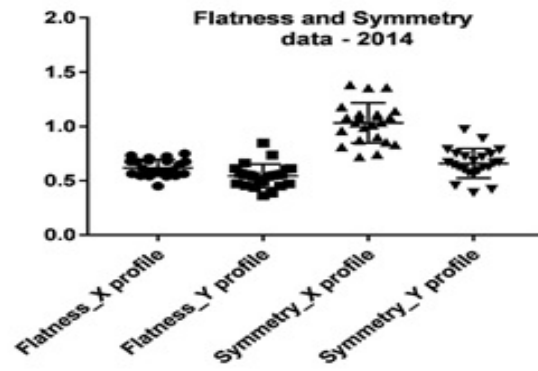
Figure 4.6: Three years institutional data of flatness and symmetry along X and Y profiles.
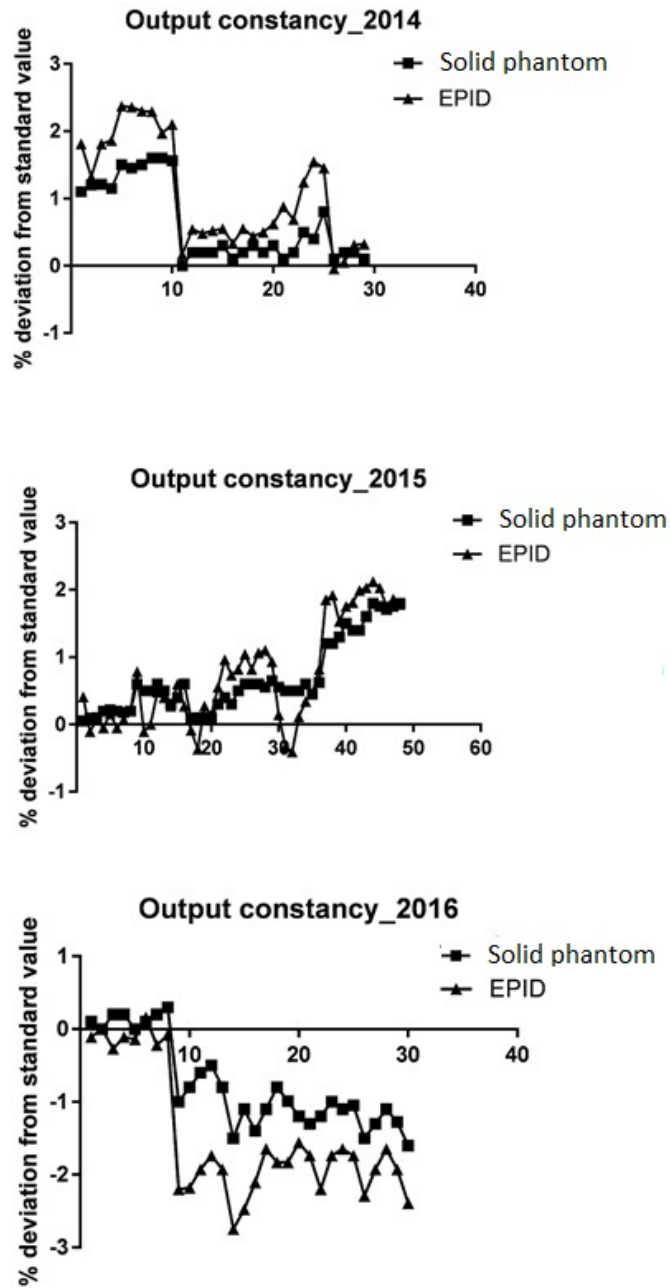
Figure 4.7: The comparison of 6 MV photon beam output constancy between daily EPID and weekly solid phantom measurement.

Table 4.2: Detailed comparison report of field widths planned by MLC shaper, FWHM computed and measured by TPS and EPID for various MLC shapes at different locations.

FWHM(cm)	Field Shapes	Z	L	T	N	S	H	O	Arrow	Triangle
Location 1	MLC shaper	2.5	1.5	2.2	1.0	7.8	7.7	1.5	6.5	8.5
	TPS	2.54	1.44	2.16	0.93	7.82	7.85	1.37	6.41	8.36
	EPID	2.52	1.41	2.13	0.91	7.77	7.78	1.38	6.40	8.41
%	TPS Vs EPID	0.79	2.13	1.41	2.20	0.64	0.90	-0.72	0.16	-0.59
variation	MLC shaper vs EPID	-0.79	6.38	3.29	9.89	0.39	-1.03	8.70	1.56	1.07
Location 2	MLC shaper	10.0	5.5	2.2	1.0	7.5	2.0	6.0	2.0	6.0
	TPS	10.36	5.29	2.16	0.94	7.81	2.15	6.26	1.85	5.98
	EPID	10.27	5.27	2.14	0.95	7.78	2.1	6.2	1.9	5.9
%	TPS Vs EPID	0.88	0.38	0.93	-1.05	0.39	2.38	0.97	-2.63	-1.34
variation	MLC shaper vs EPID	-2.63	4.36	2.80	5.26	-3.60	-4.76	-3.23	5.26	1.69
Location 3	MLC shaper	2.5	1.5	8.5	2.0	1.5	7.5	6.0	5.5	1.5
	TPS	2.54	1.44	8.42	1.98	1.43	7.85	6.26	5.64	1.36
	EPID	2.55	1.46	8.41	1.95	1.42	7.8	6.22	5.66	1.40
%	TPS Vs EPID	-0.39	-1.37	0.12	1.54	0.70	0.64	0.64	-0.35	2.94
variation	MLC shaper vs EPID	-1.96	2.74	1.07	2.56	5.63	-3.85	-3.54	-2.83	7.14

for small field comparison and all the data are given in Table 4.2. The calculated correlation coefficient (r) for TPS vs EPID and MLC shaper vs EPID images are 0.999 (p < 0.0001) and 0.998 (p < 0.0001) respectively.

4.3.3 Patient-specific Quality Assurance

The overall gamma passing rate during the mentioned period of three years for all IMRT plans measured using EPID and compared with respect to their TPS plans was studied. The percentage of points within the gamma passing range (3 % - 3 mm) is 97.6 ± 5.898, 98.3 ± 1.657, 97.4 ± 5.372 and 98.1 ± 2.004 for pelvis, thoracic and abdomen, HN and brain patients respectively. The comparison statistics of total 80 patients along with retrospective study of the same patients with an independent detector is given in Table 4.3. Percentage difference of pixels in fluence comparison for selected patients using MATLAB code fluence_comparison.m exhibited maximum difference of 8.6%.

Table 4.3: Gamma results of fluence comparison between TPS computed vs MatriXX 2D measured for four different anatomic regions. % difference of pixels (TPS vs EPID) computed by MATLAB code is also tabulated.

Site	Statistics	% of pixels passed ($\gamma < 1$)		Correlation coefficient	% difference of pixels computed by MATLAB program
		TPS Vs MatriXX 2D	TPS Vs EPID		TPS Vs EPID
Pelvis	Minimum	94.9	95.79	Pearson,	6.4%
	25% Percentile	98.3	96.58	r=0.582	
	Median	98.75	97.25		
	75% Percentile	99.08	98.19	p value	
	Maximum	99.7	99.52	=0.0025	
	Mean	98.47	97.4		
	Std. deviation	1.151	1.024		
Thoracic &Abdomen	Minimum	93.94	91.8	Pearson,	8.6%
	25% Percentile	98.36	96.05	r=0.605	
	Median	98.78	97.04		
	75% Percentile	99.2	98.13	p value	
	Maximum	99.8	99.52	=0.0020	
	Mean	98.47	96.7		
	Std. deviation	1.274	2.015		
Head &Neck	Minimum	94.3	94.41	Pearson,	5.2%
	25% Percentile	97.1	96.31	r=0.755	
	Median	98.4	97.19		
	75% Percentile	99.0	98.05	p value	
	Maximum	99.7	99.57	=0.0294	
	Mean	98.01	97.14		
	Std. deviation	1.435	1.432		
Brain	Minimum	95.2	93.5	Pearson,	4.9%
	25% Percentile	97.5	95.25	r=0.504	
	Median	98.7	97.15		
	75% Percentile	99.1	98.47	p value	
	Maximum	99.7	99.52	=0.0022	
	Mean	98.29	96.97		
	Std. deviation	1.212	1.748		

4.4 Discussion

The EPID is widely used in recent years owing to its fastness, simplicity and flexibility. This retrospective study on patient specific QA for a period of three years including 350 IMRT plans revealed our experience with EPID as an efficient dosimeter. In the present study, we have investigated the feasibility of EPID as an alternative to the 2D array in routine quality checks. The QA checks on daily beam measurements yield the status of beam profile quickly. The measurements also indicate that the output constancy of machine did not show any major variation from corresponding solid phantom data. The mentioned MLC QA verified: 1) the agreement between TPS computation of a field width and the user-defined width used in MLC shaper and

2) capability of MLC for delivering the complex fields. Patient specific QA exhibited the agreement between planned and delivered fluence, which validated the deliverability of IMRT plans. The study also performed comparison of two measurement systems, EPID and MatriXX 2D array, in IMRT verification of number of patients who had completed treatment in our radiation therapy centre. The results of 2D fluence comparison between these two detectors showed good agreement in fluence matching and statistically significant correlation was obtained. The stated comparison tool using MATLAB also showed deviation of less than 10% for the analysed cases. However, these data did not show any significant correlation with any of other two comparison data.

There are different means to measure 2D dose distributions. Film and multi-dimensional array detector are normally used for checking the MLC characteristics, beam profile and 2D dose maps. Film dosimetry has the advantages of high spatial resolution, but lacks an accurate reading system [21-22]. It is an offline dosimetry system with a short dynamic range and an energy dependent dose response. The 2D array can be connected to a computer and provides real-time measurement which can easily be read out. Even though resolution is limited, it has the advantage of storage and post processing capability of the measured data [23-25]. However, in current clinical practice, the setting up of both the

above detectors is a time-consuming task. The total machine time and human resource for whole QA procedure is always a concern. At the same time, EPID is directly measurable with minimum uncertainty in the set-up and gives images with greater spatial resolution. The detector is independent of position of laser, couch and optical distance reading and hence the measurement set up is very easy. Increased detecting surface, high density detector, high contrast and linear response to exposure made EPID an accurate dosimeter. Hence, EPID is recommendable for maximum number of QA tests in routine checks.

In the present study, we have developed three MATLAB programs for EPID image analysis. These programs are written by use of image handling codes, used for image reading, analysis and comparison of multiple images. The elementary idea of calculation of flatness, symmetry, FWHM and pixel comparison of two images were taken and expanded with MATLAB codes. The software programs permit the user to import image files and these simple programs could easily be used in practice for the QA analysis. All these MATLAB programs were validated independently. The set of images generated by TPS and its corresponding images measured by EPID were compared in three different ways and the results are tabulated in Table 4.4. Percentage difference between same images, corresponding images (TPS vs EPID of same fluence) and different set of images were calculated. Figure 4.8 illustrates the comparison of fluence images between two MLC shapes. The observed difference (% value) and Root Mean Square Error (RMSE) are (0.0%, 0.0), (-0.7%, 0.04) and (48.6%, 0.34), when the comparison were done between TPS fluences of an image and its copy, between TPS and measured fluence and between two different fluence (L and H shapes) respectively. The comparison of data corresponds to different fluence shapes are shown in Table 4.4, validates the accuracy of the program.

Various literatures explain the limitations of EPID dosimetry [13,26]. More prominent are the over sensitivity in lower energies when the beam is scattered by bulk layer of the detector, ghosting and image lag due to the trapping of charges within the photodiode layer. EPID is unable to measure large radiation
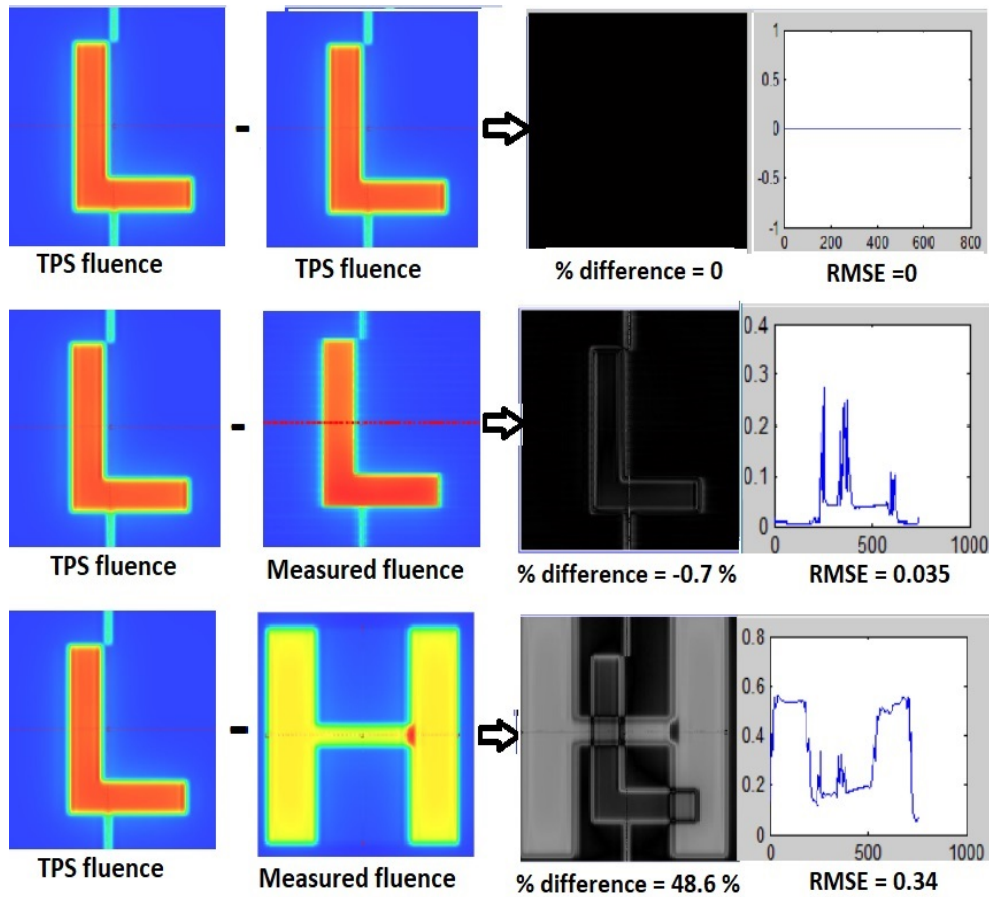
Figure 4.8: Validation of image comparison MATLAB code by comparing three sets of images. From top to bottom row: TPS fluence of an MLC shape (L) and its own copy, TPS vs EPID measured fluences of an MLC shape (L) and TPS vs EPID measured fluences of two different MLC shapes (L and H).

Table 4.4: Comparison results (% difference and RMSE) of different fluence shapes, calculated using MATLAB code. Large disagreement is observed in the comparison of unmatched images.

Fluence shapes	Comparison of corresponding MLC shapes(TPS Vs EPID)		Comparison of different MLC shapes (TPS Vs TPS (H shape))	
	% difference	RMSE	% difference	RMSE
Z	-0.30	0.081	41.5	0.310
L	-0.70	0.035	48.6	0.344
T	-0.13	0.046	34.7	0.308
N	-2.30	0.039	13.5	0.226
S	-0.25	0.059	19.9	0.266
O	-0.90	0.078	24.1	0.341
H	-2.80	0.078	0.00	0.000
Arrow	1.06	0.071	28.6	0.275
Triangle	3.10	0.047	41.9	0.296
Star	-1.80	0.080	17.3	0.393

fields because of the smaller sensitive area and lower spatial resolution compared to that of film dosimetry. Also, the high Z materials of the detector deviate EPID away from the water equivalent characteristics. There are different algorithms and dosimetry solution available now for correcting the EPID measured response. These softwares modified EPID technology more versatile in both imaging and dosimetry. The further advancement in the development of softwares empowered EPID as an efficient tool for in-vivo dosimetry [27-28]. The indigenously developed MATLAB based image comparison tool is not a fully-fledged program as there is no quantitative index other than the percentage difference and standard deviation for fluence comparison. The frequent irradiation of EPID may cause deterioration of its signal and a consequent periodic calibration. The present study is limited to the photon beams for establishing the routine checks of flatness, symmetry and constancy of profile, whereas it is not extended to the case of electron beams. Further work is needed to develop certain indices for effective comparison of fluence by taking care of dose difference and distance to agreement.

Data acquired from QA checks and analysed in the present study establishes a pivotal role of EPID in the various QA programs. Usage of EPID in the daily

QA checks ensures a quick measurement of profile and output constancy of photon beam. Also, EPID guarantees that, no more than 5 minutes are taken to carry out the daily QA tests in the LINAC room. MATLAB based MLC pattern comparison enables a quick and consistent method for MLC QA checks. These tests are added to the monthly QA protocol in addition to the film based MLC checks. Though it may not be possible to replace the currently available 2D comparison tool in patient specific QA, we have used the MATLAB based image comparison method as a quick check of delivered fluence. Moreover, it will be more beneficial for those who do not have any commercial EPID dosimetry software packages. Hence, the EPID dosimetry in combination with the indigenously developed MATLAB program has a potential use in many of the routine QA.

4.5 Conclusion

EPID, at present is a versatile, fast and effective tool for the Quality Assurance of LINAC. Three years of institutional data analysed in the present study establishes the reliability and consistency of portal detector in the dosimetry. A comprehensive QA protocol developed in the study is more suitable for frequent daily measurements, patients specific QA and MLC checks. Using the protocol, EPID based measurements can be performed without much time requirement in LINAC room.

References

[1] Kutcher GJ, Coia L, Gillin M et al. Comprehensive QA for radiation oncology: report of AAPM Radiation Therapy Committee Task Group 40. Med Phys. 1994, 21(4): 581-618

[2] Klein EE, Hanley J, Bayouth J et al. Task Group 142 report: quality assurance of medical accelerators. Med Phys. 2009, 36(9): 4197-4212

[3] Fraass B, Doppke K, Hunt M, Kutcher G, Starkschall G, Stern R, et al. American Association of Physicists in Medicine Radiation Therapy Committee Task Group 53: quality assurance for clinical radiotherapy treatment planning. Med Phys. 1998, 25:1773-1829.

[4] McKenzie, E. M., Balter, P. A., Stingo, F. C., Jones, J., Followill, D. S., & Kry, S. F. Toward optimizing patient-specific IMRT QA techniques in the accurate detection of dosimetrically acceptable and unacceptable patient plans. Medical Physics. 2014, 41(12): 121702.

[5] Pasma, K. L., Dirkx, M. L. P., Kroonwijk, M., Visser, A. G. and Heijmen, B. J. M. Dosimetric verification of intensity modulated beams produced with dynamic multileaf collimation using an electronic portal imaging device. Med. Phys. 1999, 26: 2373-2378.

[6] Talamonti, C., Casati, M. and Bucciolini, M. Pretreatment verification of IMRT absolute dose distributions using a commercial a Si-EPID. Med. Phys. 2006, 33: 4367-4378.

[7] Lee, C., Menk, F., Cadman, P. and Greer, P. B. A simple approach to using an amorphous silicon EPID to verify IMRT planar dose maps. Med. Phys. 2009, 36: 984-992.

[8] Esch, A. V., Huyskens, D. P., Hirschi, L., Scheib, S. and Baltes, C. Optimized Varian a Si portal dosimetry: development of datasets for collective use. Journal of Applied Clinical Medical Physics. 2013, 14:82-99.

[9] Sandra C Vieira, Ren A. Bolt, Maarten L.P. Dirkx, Andries G. Visser, Ben J.M. Heijmen, Fast, daily linac verification for segmented IMRT using electronic portal imaging. Radiotherapy and Oncology. 2006, 80(1): 86-92.

[10] Yang, Y., Xing, L. Quantitative measurement of MLC leaf displacements using an electronic portal image device. Phys. Med. Biol. 2004, 49: 1521-1533.

[11] Parent, L., Seco, J., Evans, P. M., Dance, D. R. and Fielding, A. Evaluation of two methods of predicting MLC leaf positions using EPID measurements. Med. Phys.2006, 33: 3174-3182

[12] Chang, J., Obcemea, C. H., Sillanpaa, J., Mechalakos, J. and Burman, C. Use of EPID for leaf position accuracy QA of dynamic multi-leaf collimator (DMLC) treatment. Med. Phys. 2004, 31: 2091-2096

[13] Van Elmpt, W., McDermott, L., Nijsten, S., Wendling, M., Lambin, P., Mijnheer, B. A literature review of electronic portal imaging for radiotherapy dosimetry. Radiother Oncol. 2008, 88:289-309

[14] Hossain M, Rhoades J. On beam quality and flatness of radiotherapy megavoltage photon beams. Australasian physical & engineering sciences in medicine. 2016, 39(1):135-145.

[15] Nath, R., Biggs, P. J., Bova, F. J., Ling, C. C., Purdy, J. A., van de Geijn, J. and Weinhous, M. S. AAPM code of practice for radiotherapy accelerators:

Report of AAPM Radiation Therapy Task Group No. 45. Med. Phys. 1994, 21: 1093-1121.

[16] Rangel, A. and Dunscombe, P. Tolerances on MLC leaf position accuracy for IMRT delivery with a dynamic MLC. Med. Phys.2009, 36: 3304-3309

[17] Mamalui-Hunter, M., Li, H. and Low, D. A., MLC quality assurance using EPID: A fitting technique with sub pixel precision. Med. Phys.2008, 35: 2347-2355

[18] B. Anup Kumar, S. Suresh Chander, R. Bhupendra, S. Arvind. Study of 2D ion chamber array for angular response and QA of dynamic MLC and pretreatment IMRT plans, Pract Oncol Radiother 2009, 14(3): 89-94

[19] Niyas, P., Abdullah, K., Noufal, M. et al. Effect of fluence smoothing on the quality of intensity-modulated radiation treatment plans, Radiol Phys Technol. 2016, 9: 202.

[20] Nelms BE, Simon JA. A survey on IMRT QA analysis. J App Clin Med Phys. 2007, 8(3):76-90

[21] Bucciolini M, Bounamici FB, Casati M. Verification of IMRT fields by film dosimetry. Med Phys. 2004, 31(1):161-168.

[22] Ju SG, Ahn YC, Huh SJ, Yeo IJ. Film dosimetry for intensity modulated radiotherapy: dosimetric evaluation. Med Phys. 2002, 29(3):315-325.

[23] Tyler M, Vial P, Metcalfe P and Downes S. Clinical validation of an in-house EPID dosimetry system for IMRT QA at the Prince of Wales Hospital.2013. J. Phys.: Conf. Ser. 444 012043

[24] Heilemann G, Poppe B, Laub W. On the sensitivity of common gamma-index evaluation methods to MLC misalignments in Rapidarc quality assurance. Med Phys. 2013, 40(3):031702.

[25] Saminathan, S., Manickan, R., Chandraraj, V. and Supe, Sanjay. S. Dosi-
metric study of 2D ion chamber array matrix for the modern radiotherapy
treatment verification. Journal of Applied Clinical Medical Physics. 2010,
11: 116-127

[26] Bailey DW, Kumaraswamy L, Bakhtiari M, Malhotra HK, Podgorsak MB.
EPID dosimetry for pretreatment quality assurance with two commercial
systems. Journal of Applied Clinical Medical Physics. 2012, 13(4):82-99.

[27] McDermott LN, Wendling M, Sonke J-J, van Herk M, Mijnheer BJ. Re-
placing pretreatment verification with in-vivo EPID dosimetry for prostate
IMRT. Int J Radiat Oncol Biol Phys. 2007, 67(5):1568-1577

[28] Mans A, Wendling M, McDermott LN, et al. Catching errors with in vivo
EPID dosimetry. Med Phys. 2010, 37(6):2638-2644.

Chapter 5

Dolphin dosimetry in three dimensional patient-specific Quality Assurance program

5.1 Introduction

The advanced techniques of radiation therapy stand in need of an accurate patient-specific QA program for verifying the treatment plans. AAPM-TG report-82 recommends verification of IMRT plans before the treatment delivery [1]. Currently available dosimetry system for pre-treatment patient-specific QA are ionization chamber, film dosimeter, 2D array and EPID. All of these detectors have been proven beneficial but also limited with some of their drawbacks [2-6]. Treatment plan verification can be performed by an independent dose calculation, direct dose measurement, or a combination of both. Traditionally, point dose measurements were performed by using a small volume ionization chamber and compared with the treatment plan dose. However, a single point dose is insufficient for dose verification of complex dose distribution of IMRT plans. Radiographic film dosimetry was used for 2D dose verification in a single plane with good resolution, but were limited with the readout system. There

96

are number of commercially available 2D array detectors, which is capable of recording the measured fluence and analysing the treatment plan immediately after the delivery. The major limitation of the 2D array is their low resolution and most of them are not able to display the 3D dose values. EPID is an efficient real time dosimeter, which requires minimum set-up time. But, it shows energy dependent radiation response and also not commonly used in 3D dosimetry. For 3D dose verification, 3D dosimetry using gel and plastic dosimeter has been developed [7-9]. This technique enables a full 3D dose verification, but requires intensive human resource and time.

At present, IMRT is used as a standard technique in different treatment modalities such as VMAT, SBRT and SRS. The highly complex and conformal dose distribution of these modalities demands critical evaluation of doses to the target as well as to various OARs, in addition to the evaluation based on gamma index [10]. A study performed by Nelms et al. [11] discussed lack of correlation between gamma passing rates from 2D array system and OAR dose differences. Hence, an alternate QA technique is required to verify the 3D dose distribution by measuring fluence at various treatment gantry angles. Dolphin-Compass system (IBA Dosimetry, Schwarzenbruck, Germany) is a commercially available dosimetry solution, capable of reconstructing 3D doses in phantom or CT images of patient. The dose calculation can be performed either without or with the help of measurement. The Compass facilitates the comparison of 3D dose distributions and DVH between planned and computed doses.

The dosimetry using Compass software has been reported by several authors [12-14]. These studies were based on Compass-MatriXX 2D array system. The Compass-Dolphin system is a novel 3D dosimetry technique with a transmission detector of increased spatial resolution, improved measurement performance and a high set-up efficiency. Thoelking, et al. [15] published the characteristics of the new transmission detector and its influence on surface dose, dose at depth and in various IMRT plans. Another study by Nakaguchi, et al. [16] evaluated a method for in-vivo 3D dose reconstruction in SBRT using the Dolphin detector. This

study also validated the capability of the dosimeter for detecting the positional errors of MLC leaves. In the present study, we aimed to describe the whole process of commissioning and validation of Dolphin-Compass dosimetry as a patient-specific QA device. The accuracy of beam modelling was tested with the help of various fields, MLC patterns and complex treatment plans. The study was carried out to evaluate the efficiency of above detector system for the QA of treatment plans, which were generated with complex treatment techniques of VMAT and SBRT.

5.2   Materials and Methods

The measurements were done on Versa-HD (Elekta, Stockholm, Sweeden) LINAC, having 6, 10 and 15 MV photon energy radiation beams. The machine is equipped with Agility (Elekta, Stockholm, Sweeden) beam shaping treatment head, which has 160 leaves with 0.5 cm width at isocentre. The intensity modulated radiation treatments were performed by using 6 MV photon beams. All the treatment plans were generated in Monaco TPS, version 5.11 (Elekta, Stockholm, Sweeden). Dose computation engine based on X-ray Voxel Monte Carlo (XVMC) was used for dose calculation with a grid size of 2.5 mm.

5.2.1   Dolphin-Compass system

The Dolphin-Compass system consists of a 2D array detector and a commercially available DVH-based evaluation tool for patient-specific QA. Dolphin detector is made up of pixel-segmented ionization chamber, which is an array of 1513 air-vented parallel plate chambers. Active measurement area of the detector is 24 cm x 24 cm. The diameter, height and volume of the individual ionization chamber are 3.2 mm, 2 mm and 0.016 cm^3 respectively. The spatial resolution of the detector is 5 mm for field size up to 14 cm x 14 cm and 10 mm for outside the 14 cm x 14 cm field. The Dolphin detector is mounted on the treatment head of LINAC as shown in Figure 5.1, and is also capable of measuring the dose online

Figure 5.1: Set-up photograph of Dolphin detector.

with the patient treatment. The Compass system is a software solution based
on collapsed cone convolution/super position dose computation algorithm [17],
which required modelling of LINAC head similar to any other TPS. It provides
both model-based dose computation and measurement-based dose reconstruction
in 3D anatomical volume. For the latter part, a measuring device form IBA
dosimetry is required which can be either MatriXX-2D array or more advanced
Dolphin detector. The combination of Dolphin and Compass is used in this
study. Treatment plans generated by using Monaco TPS were compared with
Compass computed dose and also with reconstructed dose measured by Dolphin
detector.

5.2.2 Commissioning and validation of dosimetry

The Compass software was installed and the dosimetry system was modelled.
To commission the beam model, specifications of LINAC and MLC, details of
detector used for measurement and a set of measured beam data were required.

Table 5.1: List of measurements of depth dose curves and output factors for Compass commissioning. Abbreviations: meas. = measurement.

Type of meas.	Field size at SAD(cm x cm)	Depth of meas.(cm)	Detector used for meas.
	2 x 2		Razor diode
Depth dose curves	3 x 3 5 x 5 10 x 10 15 x 15 20 x 20 30 x 30 40 x 40	-0.5 to 35	CC13-ionization chamber
	2 x 2		Razor diode
Output factors	3 x 3 5 x 5 10 x 10 15 x 15 20 x 20 30 x 30 40 x 40	10	CC13-ionization chamber

The measured data consisted of Percentage Depth Dose (PDD) curves, Crossline (X-axis) and Inline (Y-axis) radiation beam profiles, O.F and absolute output of the LINAC. Measurements were performed in water phantom, $BluePhantom^2$ - radiation field analyser (IBA Dosimetry, Schwarzenbruck, Germany) by using an ionization chamber (CC13) and a diode detector (Razor diode). All the measurements were done at a fixed Source to Surface Distance (SSD) of 90 cm and for the same set of field sizes. The Field sizes are defined at Source to Axis Distance (SAD) of 100 cm. Tables 5.1 & 5.2 show the list of measurements required for commissioning the Compass dosimetry system.

Validation of compass computation algorithm was performed by comparison of treatment plans generated in TPS against the measurement data. Two different types of radiation fields were used; 1) simple and complex fields prepared in phantom and 2) IMRT and VMAT treatment fields planned on patient CT data. A homogeneous water phantom of size 30 x 30 x 30 cm^3 was created in the TPS and open fields of various sizes from 2 x 2 cm^2 to 40 x 40 cm^2 were generated.

100

Table 5.2: List of measurements of beam profiles for Compass commissioning. Abbreviations: meas. = measurement.

Field size at SAD(cm x cm)	Depth of meas.(cm)	Detector used for meas.
2 x 2	1.6	Razor diode
	5	
	10	
	15	
3 x 3	1.6	Razor diode
	5	
	10	
	15	
5 x 5	1.6	Razor diode
	5	
	10	
	15	
10 x 10	1.6	CC13
	5	ionization
	10	chamber
	15	
15 x 15	1.6	CC13
	5	ionization
	10	chamber
	15	
20 x 20	1.6	CC13
	5	ionization
	10	chamber
	15	
30 x 30	1.6	CC13
	5	ionization
	10	chamber
	15	
40 x 40	1.6	CC13
	5	ionization
	10	chamber
	15	

During the planning, the SSD was 95 cm and a dose of 200 cGy is prescribed at a depth of 5 cm in phantom. Six user-defined points were created in phantom, which are described as A, B, C, D, E and F. Position of these points and their descriptions are depicted in Figure 5.2. The doses calculated by TPS at each of these points were compared against the corresponding doses obtained as a result of measurement as well as the computation of Dolphin dosimetry. The dosimetry was also validated in complex segmented intensity modulated radiation fields for capturing MLC movement error during the radiation delivery. These static and dynamic fields were prepared with various MLC shapes, include MLC files such as FOURL, 7SEGA, 3ABUT, HDMLC, HIMRT and DMLC. Clinically approved and verified treatment plans from a group of patients, who were completed their treatment by either VMAT or IMRT technique, were also considered for the evaluation. All the above plans were delivered to both Dolphin detector mounted on gantry head and MatriXX 2D array detector in a fixed set-up with solid water phantom. The reconstructed dose after the fluence measurement by Dolphin and MatriXX 2D array was independently compared against the corresponding TPS generated values.

5.2.3   Dosimeter for patient-specific Quality Assurance

Compass computes 3D dose by using modelled data of photon beam from LINAC and patient treatment data from TPS. During the process of treatment planning, certain files such as RTStruct, RTPlan and RTDose were generated and stored in the Monaco TPS under the respective patient folder. These files along with CT images of the patient were imported into Compass. The RTPlan file is subdivided in to number of control points and each control point is defined with respective collimator opening and MU. These parameters along with the commissioned beam data help to calculate the number and energy of photons passing through an area perpendicular to the beam, which is represented as energy fluence. Using this, Compass performs an independent dose computation on CT images without any measurement. A total of 30 cases were considered
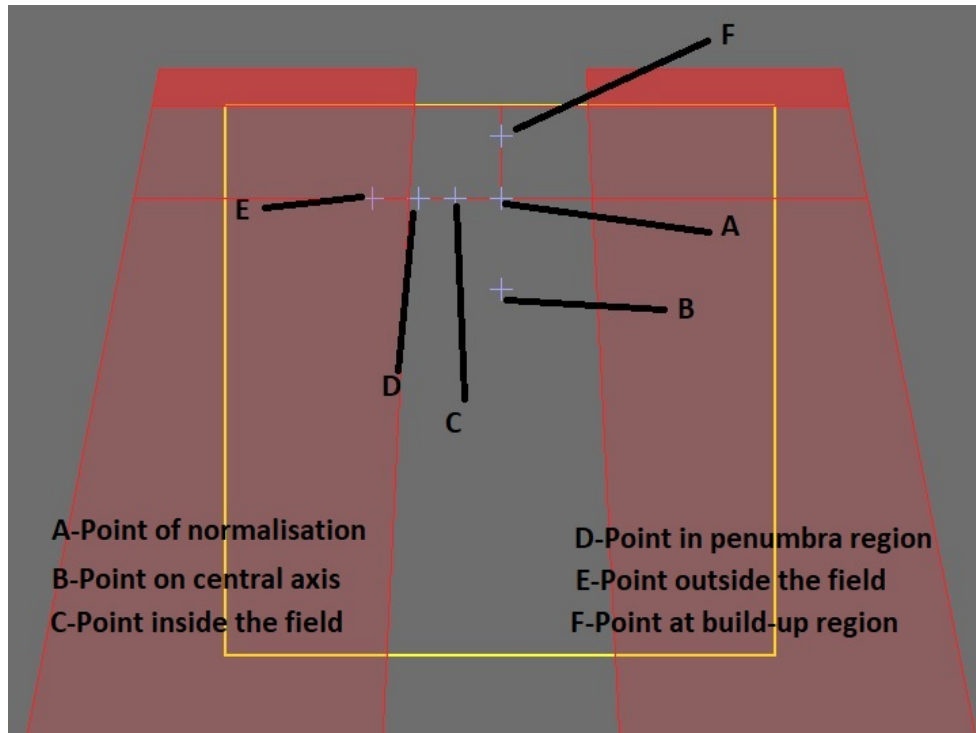
Figure 5.2: Diagram showing various dose points in the phantom.

for this study, which included patients with carcinoma of lung, liver and HN. These patients had already completed their treatments with different treatment techniques such as IMRT, SBRT and VMAT, respectively. The highest dose prescription of SBRT cases was 5500 cGy in 5 fractions. Lung cases were treated with a total dose of 6000 cGy (200 cGy/fraction) and the HN patients were prescribed for a total dose of 7000 cGy (212.1 cGy/fraction). Treatment plans were generated with seven or nine static beam angles for IMRT. The SBRT and VMAT plans have maximum of four full / partial arcs. TPS generated plans were imported, re-calculated with the model based compass dose calculation algorithm. This Compass computed plans were compared and verified with the TPS plans.

The deliverability of treatment plans was verified with the help of measurement-based dose reconstruction of Dolphin-Compass system. Compass predicts a response in the detector measurement plane based on input TPS-fluence, LINAC model and Monte Carlo (MC) derived high resolution detector

response model [18]. However, this prediction may not be so accurate due to small errors in the delivery of plans. A measurement based correction factor is applied on predicted response so that the residual differences between predicted and measured response will be minimized. Once a treatment plan is imported in to Compass, it identifies the nominal fluence from Dicom RTplan and a response is predicted with the Compass beam model and the detector response function. The predicted response is compared with the measured response and response difference is divided into two components. The first component is a scaling factor, which is applied to nominal fluence to obtain weighted fluence and the second element is a residual response, which is converted in to residual fluence with the help of a deconvolution kernel. The reconstructed fluence is obtained by addition of residual fluence and weighted fluence. Thus the measured response from the Dolphin detector array is converted in to delivered fluence with the help of a MC generated ion chamber correction kernel and residual response function. TPS-generated treatment plans were compared, evaluated, and verified against the measurement based dose reconstruction in patient CT images.

The visual comparison of reconstructed and measured dose values was executed by viewing the 2D and 3D dose distributions on CT images. The quantitative 3D evaluation in terms of gamma index was performed for the delivered and Compass computed fluence against the TPS-calculated fluence. The percentage volume of patient and planning target on CT with a gamma value less than one ($\gamma < 1$) was obtained and analysed. The standard passing criterion of 3 % - 3 mm (3 % for dose difference and the 3 mm for DTA analysis) and a tighter criterion of 2 % - 2 mm were evaluated in this study. DVH data was compared for evaluating the doses to PTV and OAR. The near-maximum dose ($D_{2\%}$) and the dose to 95 % of the volume ($D_{95\%}$) were calculated for PTV, whereas the D_{max} or mean dose (D_{mean}) / dose to different volumes were studied for OARs.

5.3 Results

5.3.1 Validation of Dolphin dosimetry

Measurements were performed as per Tables 5.1 & 5.2 and the data were used for commissioning of Dolphin-Compass dosimetry. As a first step of the validation of dosimetry, the point doses between TPS calculated, Compass computed and Dolphin measured were compared. Table 5.3 represents the doses at various points for different square shaped fields of sizes from 2 x 2 cm^2 to 30 x 30 cm^2. For all field sizes, compass computed doses of points were in good agreement with the corresponding TPS calculated values except in certain regions such as penumbra, outside the field and at build-up depth. The comparison of dolphin measured against TPS calculated doses also showed similar behaviour. The average percentage variations of point doses between compass computation and TPS calculation were 4.2 ± 4.9, 9.7 ± 6.5 and 3.0 ± 1.1 for points in penumbra, out of field and build-up region respectively. In the case of comparison between dolphin measurement and TPS calculation, the corresponding figures were 4.3 ± 1.5, 0.2 ± 0.2 and 2.4 ± 3.0. The percentage variations of all dose points across various fields are plotted in Figure 5.3. The results of gamma passing rate of the TPS calculated complex segmented radiation fields with respect to their compass computed and dolphin measured are summarized in Table 5.4. The gamma passing rate of square fields and five number of patient plans are also shown in Table 5.4. The TPS calculated fluences were also compared with those measured by using another array detector, MatriXX 2D ionization chamber array. This array detector can directly calculate dose from measurements without the need of beam modelling.

5.3.2 Patient-specific Quality Assurance

The results of patient-specific QA in terms of percentage of gamma failing are depicted in Figure 5.4. The measured and compass computed plans were compared with respect to their TPS plans for three different treatment sites. In the

Table 5.3: Comparison of doses of different points for various square fields. * No dose calculation is possible at these points.

Dose Points	Methods	Dose (cGy) for different square fields (cm x cm)									
		2 x 2	3 x 3	4 x 4	6 x 6	8 x 8	10 x 10	15 x 15	20 x 20	25 x 25	30 x 30
Point A	TPS	200.1	200.3	200.1	200.2	199.7	200.2	199.8	199.8	200.9	200.0
	Compass	202.1	200.9	201.1	202.2	200.4	201.2	200.8	201.4	202.8	201.3
	Dolphin	182.2	195.2	196.4	198.4	199.5	199.8	200.3	200.8	201.8	201.7
Point B	TPS	145.8	147.2	148.6	150.7	153.5	155.6	158.4	159.0	160.6	160.8
	Compass	148.4	148.2	149.8	153.0	156.0	158.4	161.0	161.6	163.6	164.1
	Dolphin	133.2	144.1	145.7	153.2	153.7	155.5	158.7	160.7	162.7	163.7
Point C	TPS	177.4	189.5	196.5	200.2	200.0	201.8	202.6	203.5	203.9	205.2
	Compass	177.8	186.7	198.2	202.6	202.6	205.0	205.3	206.1	206.3	207.7
	Dolphin	164.2	183.8	191.4	194.8	196.5	198.0	200.5	201.7	202.9	204.5
Pointt D	TPS	67.1	75.2	98.8	116.5	144.2	175.6	185.8	164.8	170.7	175.4
	Compass	61.5	69.7	93.6	111.5	141.8	170.6	199.0	166.7	173.5	180.0
	Dolphin	63.2	70.0	93.8	110.2	138.9	167.9	178.9	160.3	166.7	169.8
Point E	TPS	2.3	3.3	4.6	6.9	9.1	10.5	13.4	15.8	20.4	*
	Compass	1.5	1.9	3.3	4.7	6.1	6.9	8.9	10.5	22.0	*
	Dolphin	4.0	5.1	3.2	7.3	10.9	12.0	15.1	17.2	22.1	*
Point F	TPS	242.9	232.5	233.5	229.6	229.2	228.6	230.1	228.5	227.0	225.2
	Compass	244.5	242.2	241.8	238.0	238.6	236.4	234.2	233.6	233.9	233.3
	Dolphin	225.5	230.5	235.5	232.9	233.6	233.3	233.5	232.8	233.0	232.6
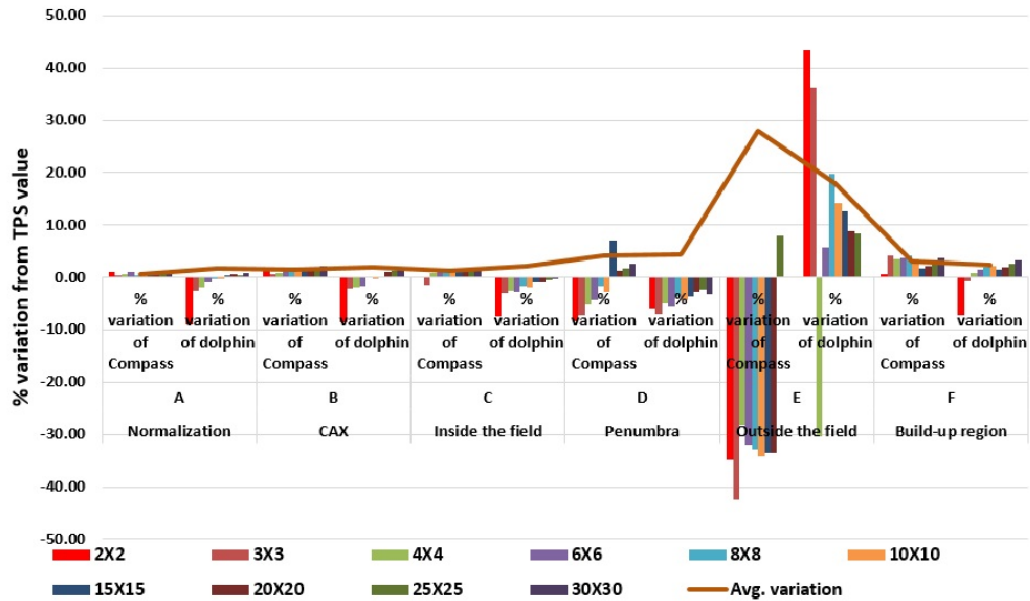
Figure 5.3: Percentage variation in doses of various points in phantom.

Table 5.4: Comparison of gamma passing values of complex segmented MLC fields, square fields and patient-specific QA plans.

Radiation Fields	% of points passing the γ (3 mm - 3 %) criterion	
	Compass v_s TPS	Dolphin v_s TPS
FOURL	100	99.2
7SEGA	99.5	97.5
3ABUT	99.5	96.6
HDMLC	100	100.0
HIMRT	100	99.6
DMLC	100	99.2
2 x 2 cm^2	100	99.5
3 x 3 cm^2	100	99.0
4 x 4 cm^2	100	99.3
6 x 6 cm^2	100	99.5
8 x 8 cm^2	100	99.8
10 x 10 cm^2	99.8	99.7
15 x 15 cm^2	100	99.5
20 x 20 cm^2	100	99.3
Patient 1	97.8	96.7
Patient 2	98.2	95.4
Patient 3	96.5	94.5
Patient 4	98.0	98.7
Patient 5	99.8	99.2

case of lung plans, the percentage of failed points in standard gamma criterion (3 % - 3 mm) is 0.43 ± 0.6 and 3.94 ± 1.6 in patient and PTV respectively, when comparing the compass computed and TPS calculated fluence. The corresponding values are 1.33 ± 0.8 and 9.95 ± 1.5 during the comparison of measured and TPS fluence. Similarly, the percentage of gamma failing points are 0.23 ± 0.2, 4.11 ± 3.1, 2.88 ± 3.2 and 13.26 ± 3.1 for liver plans and 0.38 ± 0.2, 3.54 ± 3.3, 1.49 ± 0.6 and 8.75 ± 3.2 for HN plans. Gamma failing points calculated by using stricter gamma criterion (2 % - 2 mm) were also evaluated and these values showed similar behaviour in different cases. In all these cases, measured plans showed relatively larger number of failure points in PTV in comparison with patient volume.

Target coverage was estimated in terms of $D_{95\%}$ and maximum dose was obtained as $D_{2\%}$ for the PTV. The DVH comparison data of $D_{95\%}$ of the PTV between Compass-computed, Dolphin-measured and TPS-calculated are shown in Figure 5.5. The D_{max}, D_{mean} and volume dose for various OARs were also studied and the correlation of these data between three systems are plotted in Figure 5.6.

5.4   Discussion

In the present study, we have extensively described the commissioning and validation of Dolphin-Compass dosimetry and the patient-specific QA by using this dosimetry. Unlike other 2D dosimetry for IMRT QA, Compass required a beam modelling for its commissioning. It is necessary to measure the required beam data accurately to ensure the correct beam modelling of Compass. Figure 5.7 represents the (a) PDD of 6 MV beam for different field sizes, (b) and (c) crossline and inline profiles for selective field sizes at four different depths of 1.6 cm, 5.0 cm, 10.0 cm and 20.0 cm. O.F and output of the beam is shown in Table 5.5. All the above data are in good agreement with the baseline values, measured at the time of commissioning of LINAC. The method of validation of new dosime-
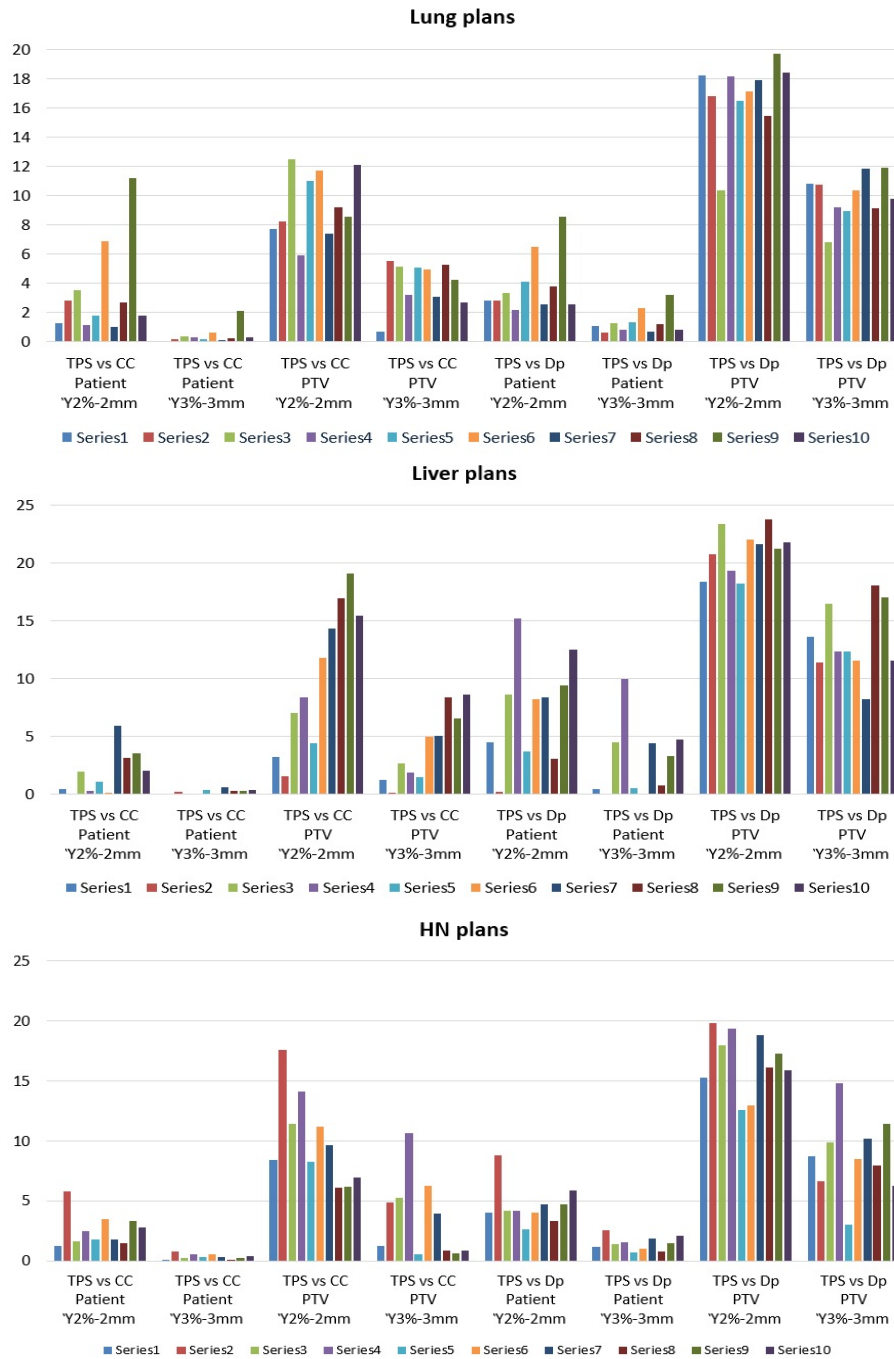
Figure 5.4: Percentage of gamma failing points in patient-specific QA.

Figure 5.5: Comparison of $D_{95\%}$ of PTV between TPS, Compass and Dolphin generated data.
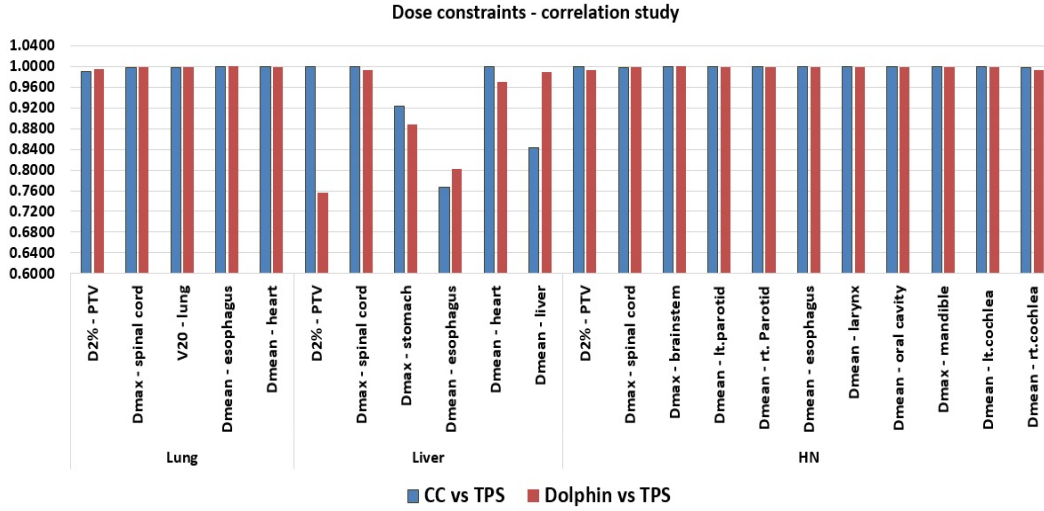
110

Figure 5.6: Correlation of OAR doses between three systems.

try involved measurement of uniform and non-uniform fluences obtained from different square shaped fields and from static or dynamic MLC patterns. The agreement in point doses at various locations in and around the square fields verified the accuracy of Dolphin-Compass dosimetry. However, the disagreement in doses of three different points (D, E and F in Figure 5.2) in phantom showed the limitation of this dosimetry for predicting low intensity, more of scattered component and near-surface dose. Dolphin accurately measured doses inside the field size of 3 x 3 cm^2 and above. In the case of extremely small field (2 x 2 cm^2), the observed variation was -8.9%, -8.6% and -7.4% for points A, B and C (Figure 5.2) respectively, which appeared due to the limitation of small-field dosimetry. The measurements by using different MLC patterns and complex IMRT fluence also revealed the efficiency of Dolphin dosimetry for IMRT verification. Moreover, we were able to confirm the accuracy of the Dolphin dosimetry by using MatriXX 2D ionization chamber detector. The comparison data are depicted in Figure 5.8. The results obtained from MatriXX 2D array is found to be closer to those from Dolphin detector for square fields and IMRT plans. The average differences of gamma (3 % - 3 mm) values were 3.27 % and 1.94 % for these fields and the maximum variation was observed for MLC patterns such as FOURL, 3ABUT and DMLC, as is evident from Figure 5.8. The more number of failure

111

Table 5.5: Output factors of 6 MV beam for various field sizes.

Field size at SAD (cm x cm)	Output Factor
2 x 2	0.789
3 x 3	0.846
5 x 5	0.906
10 x 10	1.000
15 x 15	1.056
20 x 20	1.092
30 x 30	1.136
40 x 40	1.153

points are observed at the edges of these complex intensity fields. This caused the MatriXX- 2D array measurement to deviate slightly far from the results of Dolphin. Thus, the results of open-field, MLC patterns and patient-specific QA suggested that the dosimetry system can provide adequate accuracy for clinical use and also confirmed that the beam model was set appropriately.

Dolphin-Compass dosimetry is superior over many other QA systems because of its capability of calculating 3D dose on patient CT scan using beam modeling, array detector measurement and treatment plan. We have measured a total of 30 treatment plans, which consisted of IMRT, SBRT and VMAT techniques. The TPS plans were compared with corresponding Dolphin-measured and the Compass-computed plans. Most of our gamma comparison results are well within the clinically acceptable tolerance level of 5% [19]. The results of 3D comparison show that more than 95% of pixels are passing in both PTV and patient volume within 3 % - 3 mm gamma criterion during the comparison of Compass vs TPS. In the case of verification by measurement, percentage of pixels in the patient volume are well agreed with the TPS for all studied plans. However, there are a few failure points in PTVs of lung, liver and HN plans. Out of these, liver plans showed more failure (13.26 ± 3.1) points in gamma values, which is due to the higher complexity and conformity of SBRT plans. The higher deviation of fluence over very small distances results into failure in gamma, which is due to the reconstruction inaccuracies of Compass and limited resolution of Dolphin. However, SBRT requires a QA tool with least dependency on high
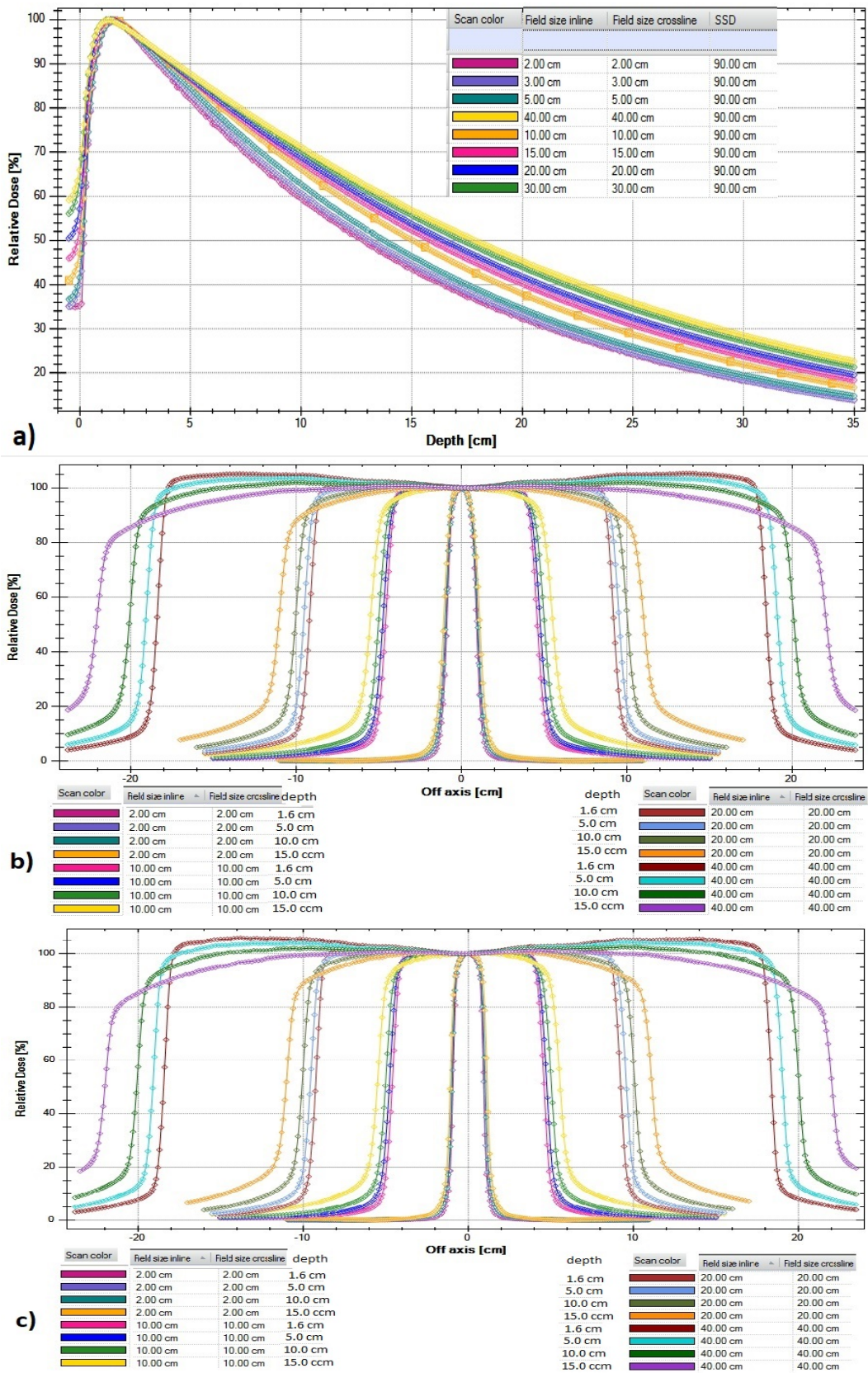
Figure 5.7: Beam data measurements: a) PDD for different field sizes, b)crossline beam profile for selective fields and c) inline beam profile for selective fields.
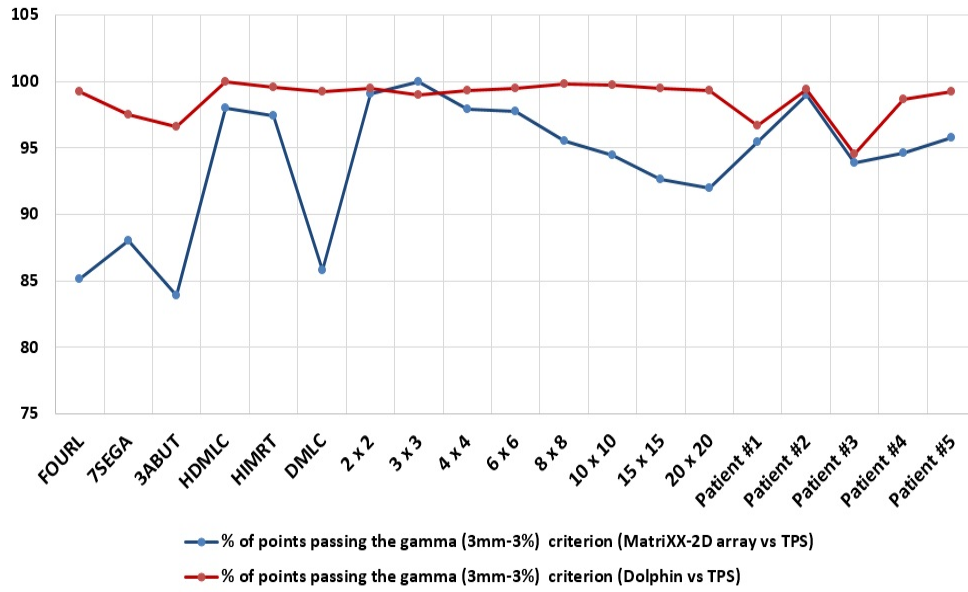
Figure 5.8: Results of gamma comparison between Dolphin and Matrixx 2D array.

dose and dose rate [16]. The Dolphin detector consists of ionization chamber, which is least dependent on the above factors. Another important aspect of this study is the 3D dose comparison with the help of DVH. By using collapsed cone convolution/super position algorithm, Compass performs an independent dose computation and also reconstructs the 3D dose distribution from measured fluence. The TPS calculated $D_{95\%}$ of the PTV is found to be correlated with the measured as well as the reconstructed values. Also, the TPS calculated various OAR dose values are in well agreement with the other two systems. As it is evident from Figure 5.6, the maximum variations of OAR dose values are within 1.0 % for lung and HN cases, whereas certain OAR of SBRT cases shows relatively larger disagreement between measured, Compass-computed and TPS-calculated values. The Dolphin-Compass dosimetry fails to reproduce a steeper dose-fall because of the stringent dose volume criteria used in SBRT treatment planning. The overall results of the patient specific-QA from three different complex sites are satisfactory.

For 3D dosimetry, a few other techniques such as film, EPID and LINAC log file based dose reconstructions are also available now. The major drawback of

fluence reconstruction by using film is the large time-requirement for the measurement and analysis. Also, this relative dosimetry method cannot provide information during the course of an irradiation. However, a 2D detector array is able to measure the fluence during the delivery causing the analysis of the results are easier and hence it is simple to integrate in a clinical practice. EPID dosimetry is comparable with this, but neither its implementation is easier nor it has the energy dependent response. Reconstruction based on log file is not an independent dosimetry check and it always shows delay in analysis. The 3D dosimetry using Dolphin detector is an emerging solution in patient-specific QA. Ionization chamber array always raises concern of limited resolution. However, Dolphin-Compass system can detect small changes of dose profiles and DVH in comparison to other 2D array detectors. This is because the system is based on a reconstruction method by combining sensitive ionization chambers and accurate beam modeling [20]. Also, the Compass 3D dosimetry uses a sufficiently accurate algorithm for the dose determination which is independent from the TPS. Therefore, it can be used for a TPS QA to check the commissioning data and routine dose calculation of TPS. Three dimensional DVH analysis along with the conventional 2D gamma passing rates provides extra confidence for assuring the accuracy in delivery of treatment plans. Dolphin is designed for ease of use, can be made available for measurement within 2 minutes by simply attaching to the gantry and is operated wirelessly. This dosimetry offers instant verification and confirmation of each delivered beam segments and is able to display the results automatically.

5.5 Conclusion

Traditional patient-specific QA methods are performed in phantom and it is not possible to quantify the QA results in patient anatomy. The capability of Dolphin-Compass dosimetry to reconstruct the 3D dose on patient CT was studied in detail. The dosimetry system was installed by using modelled beam

data of LINAC head. The accuracy of beam modelling was validated and a comprehensive 3D dose comparison was performed. The efficiency of the detector system for the patient-specific QA of complex treatment plans using modern techniques such as IMRT, VMAT and SBRT were investigated.

References

[1] Ezzell GA, Galvin JM, Low D, et al. Guidance document on delivery, treatment planning, and clinical implementation of IMRT: report of the IMRT Subcommittee of the AAPM Radiation Therapy Committee. Med Phys. 2003, 30: 2089-2115.

[2] Low DA, Moran JM, Dempsey JF, Dong L, Oldham M. Dosimetry tools and techniques for IMRT. Med Phys. 2011, 38: 13131338.

[3] Dong L, Antolak J, Salehpour M, et al. Patient-specific point dose measurement for IMRT monitor unit verification. I nt J Radiat Oncol Biol Phys. 2003, 56: 867-377.

[4] Masi L, Casamassima F, Doro R, Francescon P. Quality assurance of volumetric modulated arc therapy: Evaluation and comparison of different dosimetric systems. Med Phys. 2011, 38: 612-622.

[5] Fenoglietto P, Laliberte B, Ailleres N, et al. Eight years of IMRT quality assurance with ionization chambers and film dosimetry: experience of the Montpellier Comprehensive Cancer Centre. Radiat Oncol. 2011, 6: 85.

[6] Howell RM, Smith IP, Jarrio CS. Establishing action levels for EPID-based QA for IMRT. J Appl Clin Med Phys. 2008, 9:16- 2721.

[7] Vandecasteele J, De Deene Y. Evaluation of radiochromic gel dosimetry and polymer gel dosimetry in a clinical dose verification. Phys Med Biol. 2013, 58: 6241 6262.

[8] Oldham M, Sakhalkar H, Guo P, Adamovics J. An investigation of the accuracy of an IMRT dose distribution using two- and three-dimensional dosimetry techniques. Med Phys. 2008, 35: 20722080.

[9] Adamovics J, Maryanski MJ. Characterisation of PRESAGE: A new 3-D radiochromic solid polymer dosemeter for ionising radiation. Radiat Prot Dosimetry. 2006, 120: 107112.

[10] Nelms BE, Simon JA. A survey on IMRT QA analysis. J App Clin Med Phys. 2007, 8(3):7690

[11] Nelms BE, Zhen H, Tom WA. Per-beam, planar IMRT QA passing rates do not predict clinically relevant patient dose errors. Med Phys. 2011, 38: 1037-1044.

[12] Boggula R, Jahnke L, Wertz H, et al. Patient-specific 3D pre-treatment and potential 3D online dose verification of Monte Carlo-calculated IMRT prostate treatment plans. Int J Radiat Oncol Biol Phys. 2011; 81: 116875.

[13] Boggula R, Lorenz F, Mueller L, et al. Experimental validation of a commercial 3D dose verification system for intensity-modulated arc therapies. Phys Med Biol. 2010, 55: 56195633.

[14] Korevaar EW, Wauben DJ, van der Hulst PC, et al. Clinical introduction of a linac head-mounted 2D detector array based quality assurance system in head and neck IMRT. Radiother Oncol. 2011, 100: 446452.

[15] Thoelking J, Sekar Y, Fleckenstein J, Lohr F, Wenz F, Wertz H. Characterization of a new transmission detector for patient individualized online plan verification and its influence on 6 MV x-ray beam characteristics. Z Med Phys. 2015, 26:200208.

[16] Nakaguchi Y, Ono T, Maruyama T, et al. Validation of a method for in vivo 3D dose reconstruction in SBRT using a new transmission detector. J Appl Clin Med Phys. 2017, 18:6975.

[17] Vikraman S, Manigandan D, Karrthick KP, et al. Quantitative evaluation of 3D dosimetry for stereotactic volumetric-modulated arc delivery using COMPASS. J Appl Clin Med Phys. 2014, 16(1): 5128.

[18] Godart J, Korevaar EW, Visser R, Wauben DJ, Van't Veld AA. Reconstruction of high-resolution 3D dose from matrix measurements: error detection capability of the COMPASS correction kernel method. Phys Med Biol. 2011, 56(15): 5029-5043.

[19] Thwaites D. Accuracy required and achievable in radiotherapy dosimetry: have modern technology and techniques changed our views? J Phys. 2013, 444: 012006.

[20] Godart J, Korevaar EW, Visser R, Wauben DJ, Vant Veld AA. Reconstruction of high-resolution 3D dose from matrix measurements: error detection capability of the COMPASS correction kernel method. Phys Med Biol. 2011, 56: 5029-5043.

Chapter 6

Electron Monte Carlo algorithm in electron beam treatment planning

6.1 Introduction

Modern radiation therapy has been facilitated by multiple energy LINAC. High energy radiation from LINAC is capable of producing irreparable damages to the cells and thereby is used for cancer treatment. The mostly used types of radiation in the treatment of cancer are photons and electrons of energy in the order of MeV. In conventional LINAC, commonly available photon beams have maximum energies of 6, 10 and 15 MeV and electron beams have energy ranges from 6 to 18 MeV. Depending on the size and location of the tumour, photon or electron beams are used in radiation therapy. The selection of modality is related to the mechanism of deposition of energy per unit mass in tissue. Figure 6.1 shows the PDD as a function of depth for both 6 MV photon and 6 MeV electron beams in a water phantom. Photon beams exhibit a relatively lower surface dose, rapid increase of dose beyond the surface up to a d_{max} and an exponential fall of dose beyond the d_{max}. Whereas in the case of electron beam, a higher

surface dose, relatively smaller raise in dose from surface to the d_{max} and a very sharp decrease of dose beyond d_{max} are observed. Therefore, electrons provide distinctive advantages over photons in delivering dose in the target volume while minimising dose to deeper tissues. In general, photons are used to treat the deep seated tumors and electrons are used for superficial lesions [1]. More advanced treatment technics like IMRT and VMAT uses low or medium energy photon beams. The common treatment sites of electron beam include skin, lip, chest wall and certain head and neck region.

Like photon beam radiation therapy, electron beam therapy also starts with a CT simulation. The CT scan is then imported into a computerized TPS and is used to produce a treatment plan of the patient. Once a suitable plan has been determined and approved, patients are positioned at the treatment unit and the planned radiation fields are delivered. TPS generates individual patient plan by using 1) Radiation beam data and 2) Patient scan data. Different treatment planning algorithms are available specifically for both photons and electrons. The dose calculation algorithms are the complex pieces of software in the TPS. It consist of a sequence of instructions, which operate on CT data by taking input from the radiation beam characteristics and calculate the dose distribution and MU. Initially the electron beam dose calculations were based on empirical methods, which utilized ray line geometries and assumed broad beam dose distributions in homogeneous media [2]. After that, Pencil Beam algorithm was introduced with the capability of predicting the effects of contour irregularity and beam obliquity. This was based on Gaussian pencil beam distributions obtained from multiple scattering theories [3]. However, both the above algorithms failed for field sizes smaller than the extent of lateral scatter equilibrium [4] because of their inefficiency to predict PDD and to calculate the MU accurately. The MC based algorithms are currently the most accurate methods for dose calculations [5-7].

There are different MC codes available for radiation therapy planning; EGS4, PENELOPE and EGSnrc [8-10]. They face the challenge of computation speed
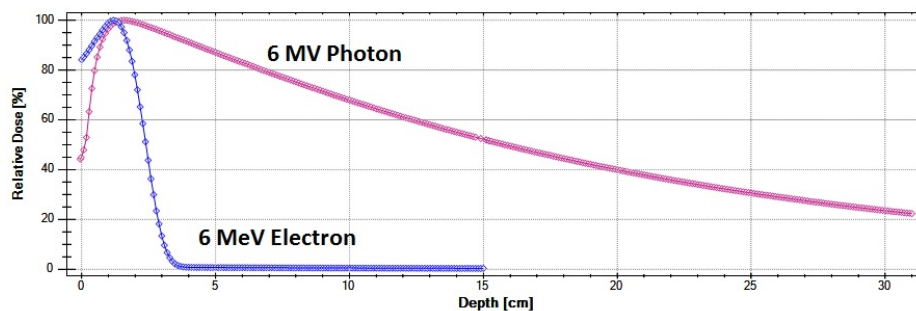
Figure 6.1: Percentage depth dose as a function of depth for 6 MV photon and 6 MeV electron beams.

in the practical treatment planning. This lead to the development of the fast MC codes [11-13], which have increased efficiency but with loss of some accuracy in the dose calculation. The eMC algorithm is an MC based dose calculation algorithm available in Eclipse (Varian Medical Systems, Palo Alto, CA) TPS. The eMC can produce treatment plans quickly when compared to other commercially available MC algorithms. The accuracy and acceptability of this algorithm have been evaluated in several studies [14-18]. In the present study, we have aimed to investigate the performance of this algorithm in MU calculations of various regular and irregular shaped electron beams. A simple and direct measurement based method was developed for validating the treatment MU calculated by eMC.

6.2   Materials and Methods

The eMC algorithm is a fast implementation of the MC method for dose calculation of electron beam [15]. The algorithm consists of 1) electron transport/dose deposition model that performs the transport and dose deposition caused by the electrons in the patient and 2) electron beam phase-space model which describes the electrons that come out of the treatment head of LINAC. The measurement required for commissioning of pencil beam algorithm of electron beam planning is the relative O.F for different field sizes and various SSD. Whereas, eMC uses energy dependent dose kernel libraries which are pre-calculated with the EGS4 MC code and therefore minimal amount of measured beam data is required for

122

the commissioning [15].

Measurements were performed by using clinac-iX (Varian Medical Systems, Palo Alto, CA) LINAC with 120 leaf millennium MLC. The LINAC is capable of delivering both photon and electron beams of multiple energies. The electron energies available in our machine are 6, 9, 12 and 15 MeV. LINAC is also equipped with different electron beam applicators with sizes of 6 cm x 6 cm, 10 cm x 10 cm, 15 x 15 cm, 20 cm x 20 cm and 25 cm x 25 cm. An applicator is used to collimate the beam and is attached to the treatment unit head such that the electron field is defined at a closest distance from the patient. A photograph of applicator is shown in Figure 6.2. The LINAC was calibrated for all energies using the primary calibration protocol TRS-398 [19]. The electron beam calibration had performed prior to this study so that an electron beam of 200 MU with an applicator 10 cm x 10 cm gave an absorbed dose of 200 cGy at d_{max} in water for an SSD of 100 cm. This is interpreted as the reference dose rate of the machine which is equal to 1 cGy / MU. The above calibration was performed in water phantom, whereas the rest of the measurements were done in plastic water phantom [20]. An ionization chamber-CC13 (IBA Dosimetry, Schwarzenbruck, Germany), a thimble chamber from IBA was used for the measurement. Figure 6.3 depicts the experimental set up of LINAC along with plastic phantom.

The present study consisted of two different sets of measurements of O.F and cutout factors. The first set was to measure relative O.F for all electron energies with available applicators and three distinct SSDs of 100 cm, 105 cm and 110 cm. All the measurements were carried out in the respective d_{max} of every beam. The d_{max} of all beams were measured at the time of commissioning of the machine and the data are tabulated in Table 6.1. In the second part of this study, cutout correction factors were measured and compared with the corresponding eMC calculated data. For this part, a simple and measurement based dosimetric method was developed.

Figure 6.2: Photograph of electron applicator.

Figure 6.3: Experimental setup using plastic water phantom in LINAC.

Table 6.1: Depth of maximum dose (d_{max}) for various electron beams.

Eneregy (MeV)	d_{max} (mm)
6	14.0
9	20.0
12	27.0
15	30

6.2.1 Relative output factor

Relative O.F is defined as the ratio of beam output for a particular applicator to the beam output at reference applicator (10 cm x 10 cm) measured at respective d_{max} of any energy. It depends on various beam parameters such as electron energy, applicator size, beam shaping inserts and SSD. For all electron beams the O.F are measured in plastic phantom by delivering a fixed number of MUs for different SSD. This measured relative O.F is compared with that generated in TPS by eMC algorithm. QA plans were created in Eclipse TPS using plastic water phantom for all available combinations of energy, applicators and selected SSDs. Dose of 200 cGy was prescribed at d_{max} of all beams and MU were calculated. In the electron beam dosimetry, the number of MU required to deliver a prescribed dose (D) in cGy to the calibration depth can be calculated as

$$MU = \frac{D}{(k \times O.F)} \tag{6.1}$$

Where k is the reference dose rate (=1 cGy/MU) of the LINAC at Source Calibration Distance. From the known values of D and MU, eMC calculated relative O.F values were derived and compared with the measured values.

6.2.2 Cutout factor

A cutout is an insert made up of an alloy cerrobend which is placed on the applicator to produce customized shape for radiation beam in different clinical use. Figure 6.4 represents the photographs of two irregular shaped cutouts used for electron treatment. The cerrobend is a low-temperature melting alloy containing bismuth, lead, tin, and cadmium in 50.0%, 26.7%, 13.3% and 10.0% by weight respectively. The shielding thickness of the cutouts are approximately equal to the maximum range of the highest electron energy beam passing through it [21]. Cutout factor is defined as the ratio of beam output for a particular cutout to the

beam output at reference applicator (10 cm x 10 cm). Different square cutouts of sizes from 10 cm x 10 cm to 3 cm x 3 cm were prepared for this study. The irregular cutouts were obtained from 10 patients who had already completed their treatments. QA plans for all these cutouts were prepared in Eclipse TPS using eMC algorithm and the corresponding MUs were obtained. The MU of these plans were calculated manually also by using initially measured O.F. During this calculation, the effect of applicator on dosimetry were considered, but not the cutout correction factor. However, the cutout correction factor were derived from the measurements. The measurements were carried out by delivering above calculated MU on the phantom using corresponding cutouts (both regular and irregular) and from the measured data, the cutout correction factors were calculated as shown in the following steps.

Deliver the calculated MU using treatment cutout. If nC_1 is the charges collected by ionization chamber, then

$$D_{cor} \propto nC_1 \tag{6.2}$$

where D_{cor} = corrected dose. Deliver 200 MU (= 200 cGy) at d_{max} with 10 cm x 10 cm applicator (without cutout). Let nC_2 is the collected charges for this MU. Then,

$$200 \propto nC_2. \tag{6.3}$$

From equations (6.2) and (6.3),

$$D_{cor} = \frac{nC_1}{nC_2} \times 200 \tag{6.4}$$

Ratio of prescribed dose to corrected dose (due to the effect of cutout), D / D_{cor} represents the fraction of MU_{cor} to the initial MU. The correction factor (D / D_{cor}) was applied to the manually calculated MU to get the corrected MU

Figure 6.4: Photographs of irregular shaped cutouts.

(MU_{cor}), which is shown below in equation (6.5).

$$MU_{cor} = \frac{D}{D_{cor}} \times MU. \tag{6.5}$$

The above computed MU_{cor} was compared with the eMC calculated MU.

6.3 Results

The relative O.F was measured in plastic phantom for all electron beams with different combinations of applicator and SSD. The measured and corresponding eMC calculated relative O.F values are given in Table 6.2. It was observed that, the eMC calculated values agree with the measurement for all cases of the present study. Average and standard deviation of the ratio of O.F are 0.984 ± 0.0175, 0.989 ± 0.0089, 0.985 ± 0.0077 and 0.986 ± 0.0070 for 6, 9, 12 and 15 MeV electron beams respectively. The detailed results of cutout factor measurements are shown in Tables 6.3 & 6.4. In the case of square cutouts, the eMC calculated cutout factors agreed with those of measured values within 3% for cutout sizes of 4 cm x 4 cm or larger. However, the eMC calculated value was found to vary 4.4% from measured value in the cutout of size 3 cm x 3 cm. In irregular clinical electron cutouts with different energies and SSDs, eMC calculated MU was correlated with corrected MU (actual measurement) within 4.0%. A discrepancy of more than 4% was observed for three cutouts.

127

Table 6.2: Detailed list of eMC calculated and measured relative O.F for different energies and SSDs. Abbreviations: eMC = electron Monte Carlo, Meas. = measured, O.F = output factor, SSD = source to surface distance.

	Energy	6 MeV		9 MeV		12 MeV		15 MeV	
SSD	Applicator	eMC	Meas.	eMC	Meas.	eMC	Meas.	eMC	Meas.
	cm x cm	O.F	O.F	O.F	O.F	O.F	O.F	O.F	O.F
	6X6	0.957	0.963	0.994	0.976	0.977	0.998	0.966	0.971
	10X10	0.973	1.000	0.973	0.985	1.000	0.985	0.985	1.000
100 cm	15X15	0.976	1.000	0.976	0.980	0.996	0.984	0.980	0.994
	20X20	0.990	1.014	0.976	0.980	0.985	0.995	0.962	0.981
	25X25	0.990	1.014	0.977	0.957	0.964	0.993	0.939	0.953
	6X6	0.858	0.842	1.019	0.870	0.867	1.003	0.866	0.866
	10X10	0.870	0.893	0.973	0.881	0.895	0.985	0.877	0.896
105 cm	15X15	0.881	0.895	0.984	0.877	0.896	0.979	0.877	0.896
	20X20	0.889	0.912	0.974	0.881	0.889	0.991	0.866	0.886
	25X25	0.886	0.913	0.970	0.855	0.870	0.982	0.851	0.861
	6X6	0.756	0.736	1.027	0.781	0.776	1.007	0.778	0.779
	10X10	0.791	0.800	0.988	0.794	0.808	0.982	0.787	0.808
110 cm	15X15	0.794	0.808	0.982	0.797	0.811	0.983	0.794	0.808
	20X20	0.803	0.827	0.971	0.791	0.805	0.982	0.787	0.803
	25X25	0.803	0.828	0.970	0.772	0.789	0.979	0.772	0.781

Table 6.3: Agreement of eMC calculated correction factor with measured data for square cutouts. Abbreviations: MU_{cal} = manually calculated MU, MU_{cor} = MU corrected by measurement, MU_{TPS} = eMC calculated MU.

Energy (MeV)	SSD (cm)	Applicators (cm x cm)	O.F	MU_{cal}	Cutout size (cm x cm)	MU_{cor}	MU_{TPS}	$MU_{TPS}/$ MU_{cor}
6	100	10X10	1.000	200.0	3 x 3	202.1	211.0	1.044
6	100	6X6	0.963	207.7	4 x 4	208.0	214.0	1.029
6	100	10X10	1.000	200.0	5 x 5	201.3	207.0	1.028
9	100	10X10	1.000	200.0	6 x 6	202.9	201.0	0.991
9	100	10X10	1.000	200.0	7 x 7	200.6	203.0	1.012
12	100	10X10	1.000	200.0	8 x 8	201.0	200.0	0.995
15	100	10X10	1.000	200.0	9 x 9	200.0	200.0	1.000
6	100	10X10	1.000	200.0	10 x 10	200.0	201.0	1.005

128

Table 6.4: Comparison between eMC calculated cutout factor and measured data for 10 irregular clinical electron cutouts of different shapes and sizes. Abbreviations: MU_{cal} = manually calculated MU, MU_{cor} = MU corrected by measurement, MU_{TPS} = eMC calculated MU.

Energy (MeV)	SSD (cm)	Applicators (cm x cm)	O.F	MU_{cal}	Cutout shape	MU_{cor}	MU_{TPS}	MU_{TPS}/MU_{cor}
6	100	15X15	0.999	200.2	shape1	204.0	203.0	0.995
6	100	15X15	0.999	200.2	shape2	200.0	204.0	1.020
12	110	15X15	0.808	618.7	shape3	672.5	694.0	1.032
6	110	15X15	0.808	618.8	shape4	696.5	723.0	1.038
6	100	15X15	1.000	200.0	shape5	214.2	220.0	1.027
12	100	15X15	0.994	201.3	shape6	217.0	212.0	0.977
9	105	10X10	0.895	223.5	shape7	242.1	251.0	1.037
9	110	10X10	0.808	247.5	shape8	269.6	285.0	1.057
6	110	20X20	0.827	241.8	shape9	252.8	273.0	1.080
6	110	15X15	0.808	247.5	shape10	259.3	276.0	1.064

6.4 Discussion

In the present study, we have investigated the accuracy of eMC in predicting the actual electron beam transport in phantom. A significant component of the resultant of interaction is amount of scatter, which is expressed in terms of O.F. The measured O.F of total 80 different electron fields showed good agreement with the corresponding eMC calculated values. The comparison between measured and eMC calculated O.F were studied and theses values were found within the value of 3% (mostly within 2%). There is significant correlation between two data sets, which is clearly shown in Figure 6.5. The ratio of O.F with respect to SSD for all applicators were also studied. Figure 6.6 depicts the variations in O.F obtained for different SSDs, which did not show any trend or reproducibility. Hence the statistical column analysis was performed using GraphPad prism (Graphpad software, San Diego, CA, USA, version 6.07). One way ANOVA, in which the mean of each column (O.F ratio for each SSD) has been compared with the mean of every other column and found that the observed variations in O.F with SSD are not statistically significant.

Another aspect of the present study is the stated method for evaluating the performance of eMC in the MU calculations of clinical cutouts. The method
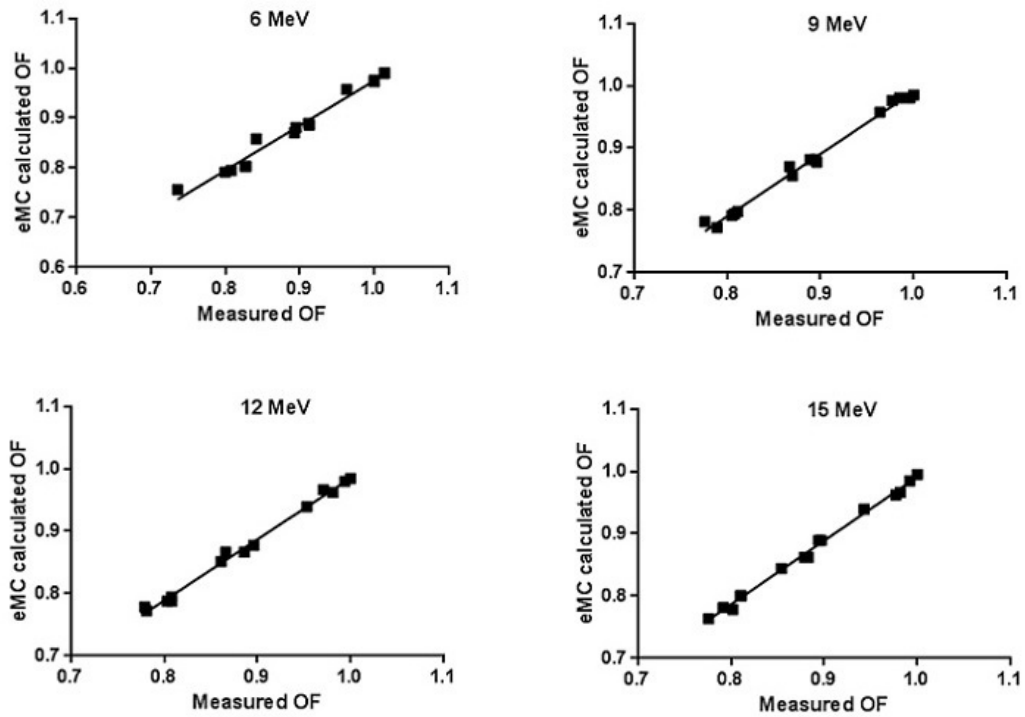
Figure 6.5: Comparison of eMC calculated and measured O.F for different energies.
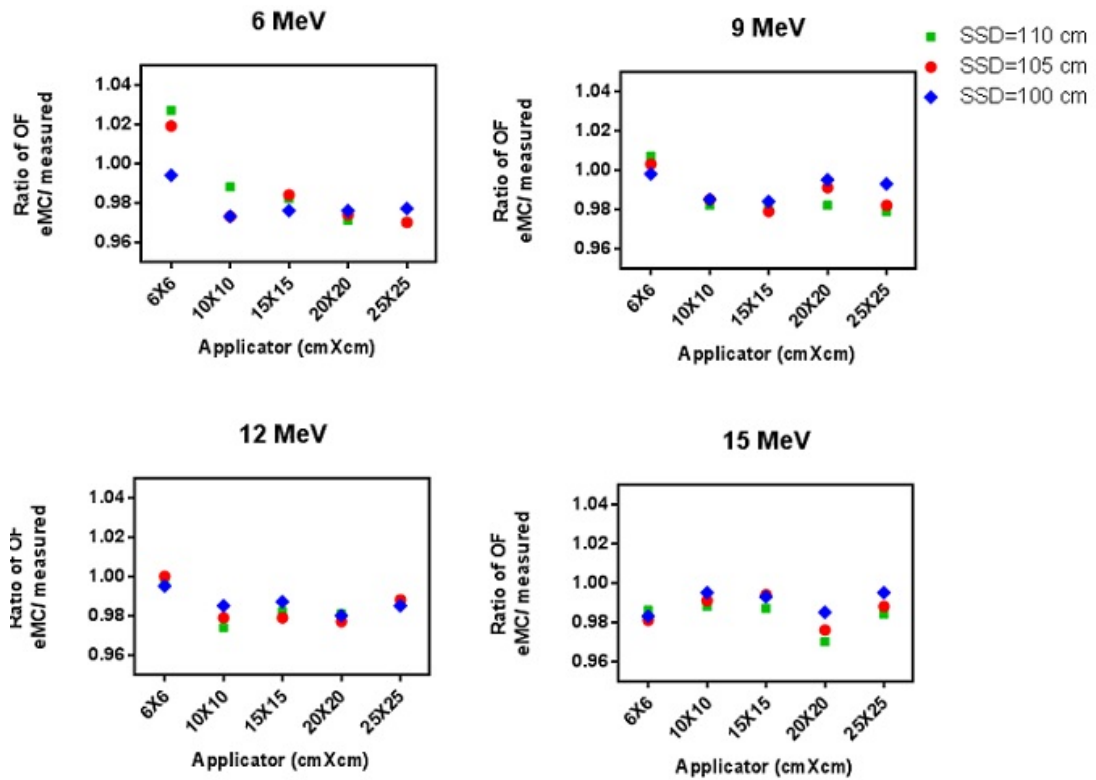

Figure 6.6: Ratio of O.F with respect to variation in SSD.

based on actual measurement is a simplified way of measuring the cutout correction factor and can be used in both regular and irregular shaped cutouts. In the case of regular shaped cutouts, correction factors of all measured fields except 3 cm x 3 cm were found good agreement with the eMC calculated values. The developed method is able to correct the treatment MU in different shaped clinical cutouts. Also, this study necessitates the need of MU correction when a cutout is introduced for shaping the clinical beam. In the present study, we have also compared the eMC calculated MU against uncorrected and corrected MU separately. Uncorrected MU represents the calculated MU without applying cutout correction factor. The eMC calculated MU were found to deviate large from the uncorrected MU when compared to corrected MU. The maximum variation was 20% and out of ten measured cutouts, seven were observed with variations of more than 10%. The observations are plotted in Figure 6.7.

Our results of cutout factor measurements are well agreed with the reported works of Popple RA, et al.[16], Hu Y.A., et al.[17] and Xu Z, et al.[18]. Ratio of eMC calculated MU and measured MU represents relation of eMC generated cutout factors with measured values. Another important feature of this study is the direct measurements in irregular cutouts. The clinically used cutouts for various sites (head and neck, chest wall and inguinal region) hold different sizes and shapes. The treatment MUs calculated by eMC algorithm for selected combinations of energy, applicator and SSD were found to be in reasonably good agreement with the measurement except for few. The larger variation was observed for three cutouts, which were highly irregular, relatively smaller in size, with lower energy and of SSD = 110 cm. Large discrepancies in cutout factors for 3 cm x 3 cm or other small irregular cutouts is influenced by measurement uncertainty [22] and statistical variations of eMC calculations.

The present study evaluates the performance of eMC algorithm for electron beam treatment planning. Various dosimetric parameters such as O.F, cutout correction factor and treatment MU are checked and validated. However, the dose distribution calculated by eMC has not been compared with another system.
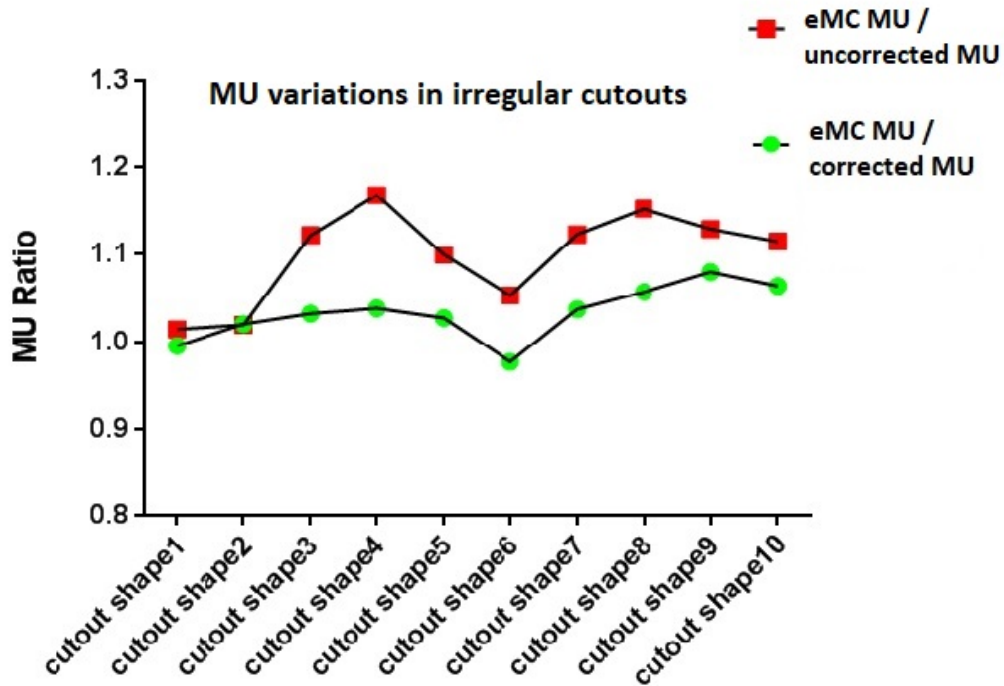
Figure 6.7: Ratio of eMC calculated MU to corrected and uncorrected MU.

Another limitation is that, the MC simulated depth dose fall is not validated, though it is not relevant for the calculation of MU at d_{max}. The ionization chamber used in the measurement is inherently limited in collecting the charges in small field dosimetry [22]. Because of this stochastic nature of MC calculation, it is very important to do an independent performance check of this algorithm in the respective clinical set up. The simple and direct method that we have performed in our radiation therapy centre, validated the eMC algorithm for clinical use.

6.5 Conclusion

Our new approach with simple and direct measurements resulted in the good performance of eMC algorithm in Eclipse TPS. The results of comparison of relative O.F and cutout factor are appreciable with the given measuring system. The observed agreement of eMC with the measurement in different scenario validates its clinical use.

References

[1] Khan, F.M., The Physics of radiation therapy , 3rd Ed., 2003, Lippincott Williams Wilkins, Philadelphia.

[2] Sternick E. Algorithms for computerized treatment planning. In: Orton CG, Baagne F, editors. Proceedings of the Practical Aspects of Electron Beam Treatment Planning Symposium 1977; Cincinnati, Ohio. New York: American Institute of Physics. 1978:52.

[3] Hogstrom KR, Starkschall G, Shiu AS. Dose calculation algorithms for electron beams. In: Purdy JA, editor. Advances in radiation oncology physics: Dosimetry, Treatment Planning and Brachytherapy. American Institute of Physics Monograph 19. New York: American Institute of Physics. 1992, 900.

[4] Lax I, Brahme A. Collimation of high energy electron beams. Acta Radiol Oncol. 1980, 19(3):199-207.

[5] Bielajew, A.F., Monte Carlo dose calculation: why gamble with anything else? Proc. 1st Int. Workshop on EGS4. 1997 (Tsukuba City, Japan: Laboratory for High Energy Physics) 310-323.

[6] Ma, C.M., et al., Clinical implementation of a Monte Carlo treatment planning system Med. Phys. 1999, 26: 2133-2143.

[7] Ma, C.M. and Jiang S.B. Monte Carlo modelling of electron beams from medical accelerators. Phys. Med. Biol. 1999, 4, R157-89.

[8] Nelson WR, Hirayama H, Rogers DW. Stanford Linear Accelerator Center Report SLAC-265. Stanford, CA. 1985, 94: 305-398.

[9] Bar, J., et al., PENELOPE: an algorithm for Monte Carlo simulation of the penetration and energy loss of electrons and positrons in matter, Nucl. Instrum. Methods B, 1995, 100: 31-46.

[10] Kawrakow, I., Accurate condensed history Monte Carlo simulation of electron transport, I. EGSnrc, the new EGS4 version , Med. Phys. 2000, 27: 485-498.

[11] Neuenschwander, H., Mackie, T.R., and Reckwerdt, P.J., MMC: a high performance Monte Carlo code for electron beam treatment planning Phys. Med. Biol. 1995, 40: 543-574.

[12] Keall, P.J. and Hoban, P.W., Super-Monte Carlo: a 3D electron beam dose calculation algorithm, Med. Phys. 1996, 23: 2023-2034.

[13] Kawrakow, I., Fippel, M., and Friedrich, K., 3D electron dose calculation using a voxel based Monte Carlo algorithm (VMC), Med. Phys. 1996, 23: 445-457.

[14] Ding GX, Duggan DM, Coffey CW, Shokrani P, Cygler JE. First macro Monte Carlo based commercial dose calculation module for electron beam treatment planning new issues for clinical consideration. Phys Med Biol. 2006, 51(11):2781-2799.

[15] Neuenschwander H, Mackie TR, Reckwerdt PJ. MMC-a high-performance Monte Carlo code for electron beam treatment planning. Phys Med Biol. 1995, 40(4):543-574.

[16] Popple RA, Weinber R, Antolak JA, et al. Comprehensive evaluation of a commercial macro Monte Carlo electron dose calculation implementation using a standard verification data set. Med Phys. 2006, 33(6):1540-1551.

[17] Hu, Y. A., Song H , Chen Z , Zhou S. and Yin F. Evaluation of an electron Monte Carlo dose calculation algorithm for electron beams. Journal of Appl Clin Med Phys. 2008, 9: 1-15.

[18] Xu Z, Walsh S. E, Telivala T. P, Meek A.G. and Yang G. Evaluation of the eclipse electron Monte Carlo dose calculation for small fields. Journal of Appl Clin Med Phys. 2009, 10: 75-85.

[19] IAEA Technical Reports Series No. 398: Absorbed Dose Determination in External Beam Radiotherapy, International Atomic Energy Agency, Vienna 2000.

[20] McEwen, M. R., and D. Niven. Characterization of the phantom material Virtual Water in high-energy photon and electron beams. Med phys. 2006, 33(4): 876-887.

[21] Khan F. M, Doppke K. P, Hogstrom K. R, Kutcher G. J, Nath R, Prasad S. C, Purdy J. A, Rozenfeld M. and Werner B. L. Clinical electron-beam dosimetry: Report of AAPM Radiation Therapy Committee Task Group No. 25. Med Phys. 1991, 18: 73-109.

[22] Laub W. U and Wong T. The volume effect of detectors in the dosimetry of small fields used in IMRT. Med Phys. 2003, 30: 341-347.